ISSN 0021-3438 (Print)
ISSN 2412-8783 (Online)

IZVESTIYA
NON-FERROUS METALLURGY

Vol. 31, No. 2, 2025

Scientific and Technical Journal
Founded in 1958
4 Issues per year

ИЗВЕСТИЯ ВУЗОВ
ЦВЕТНАЯ МЕТАЛЛУРГИЯ

Том 31, № 2, 2025

Научно-технический журнал
Основан в 1958 г.
Выходит 4 раза в год

ISSN 0021-3438 (Print)
ISSN 2412-8783 (Online)

IZVESTIYA NON-FERROUS METALLURGY

Vol. 31, No. 2
2025

Scientific and Technical Journal
Founded in 1958
4 Issues per year
http://cvmet.misis.ru

Journal is included into the List of the peer-reviewed scientific publications recommended by the Highest Attestation Commission of the Ministry of Education and Science of the Russian Federation for publishing the results of doctoral and candidate dissertations

Abstracting/Indexing: Russian Science Citation Index (RSCI), Chemical Abstracts (Online), INIS, OCLC ArticleFirst, Ulrich's Periodicals Directory, VINITI Database (Abstract Journal)

Founder

National University of Science and Technology "MISIS"
Address: 1 Bld, 4 Leninskiy Prosp., Moscow 119049, Russia
http://www.misis.ru

Editor-in-Chief

Evgeny A. Levashov
Prof., Dr. Sci. (Eng.), Corresponding Member of the RAS,
NUST MISIS, Moscow, Russia

Deputy Editor

Vladislava A. Ignatkina
Prof., Dr. Sci., NUST MISIS, Moscow, Russia

Editorial Board

Abhilash – Dr., Ph.D., CSIR – National Metallurgical Laboratory, Jamshedpur, India
E.V. Ageev – Prof., Dr. Sci. (Eng.), SouthWest State University, Kursk, Russia
M.V. Ananyev – Prof., Dr. Sci. (Chem.), Federal State Research and Development Institute of Rare Metal Industry (JSC "Giredmet"), Moscow, Russia
N.A. Belov – Prof., Dr. Sci. (Eng.), NUST MISIS, Moscow, Russia
E.V. Bogatyreva – Prof., Dr. Sci. (Eng.), NUST MISIS, Moscow, Russia
V.B. Deev – Prof., Dr. Sci. (Eng.), NUST MISIS, Moscow, Russia
V.M. Denisov – Prof., Dr. Sci. (Chem.), Siberian Federal University, Krasnoyarsk, Russia
D.V. Drobot – Prof., Dr. Sci. (Chem.), Russian Technological University (MITHT), Moscow, Russia
F.V. Grechnikov – Prof., Dr. Sci. (Eng.), Acad. of RAS, Samara National Research University n.a. S.P. Korolev (Samara University), Samara, Russia
D.V. Gunderov – Dr. Sci. (Phys.-Math.), Institute of Molecule and Crystal Physics Ufa Research Center of the RAS, Ufa, Russia
B.B. Khina – Dr. Sci. (Phys.-Math.), The Physical-Techical Institute of NAS of Belarus, Minsk, Belarus
D.V. Louzguine – Prof., Dr. Sci., Tohoku University, Sendai, Japan
S.V. Mamyachenkov – Prof., Dr. Sci. (Eng.), Ural Federal University, Yekaterinburg, Russia
Z.A. Mansurov – Dr. Sci. (Chem.), Prof., Institute of Combustion Problems, Almaty, Kazakhstan
N.V. Nemchinova – Prof., Dr. Sci. (Eng.), Irkutsk National Research Technical University, Irkutsk, Russia
K.V. Nikitin – Prof., Dr. Sci. (Eng.), Samara State Technical University, Samara, Russia
P.V. Polyakov – Prof., Dr. Sci. (Chem.), Siberian Federal University, Krasnoyarsk, Russia
E.S. Prusov – Cand. Sci. (Eng.), Vladimir State University, Vladimir, Russia
V.N. Rychkov – Prof., Dr. Sci. (Chem.), Ural Federal University, Ekaterinburg, Russia
D. Sadoway – Prof., Dr., Massachusetts Institute of Technology, Boston, USA
G.A. Salishchev – Prof., Dr. Sci. (Eng.), Belgorod National Research University, Belgorod, Russia
D.V. Shtansky – Prof., Dr. Sci. (Phys.-Math.), NUST MISIS, Moscow, Russia
V.M. Sizyakov – Prof., Dr. Sci. (Eng.), Saint-Petersburg Mining University, St. Petersburg, Russia
Stopic Srecko – Dr.-Ing. habil., RWTH Aachen University, Aachen, Germany
B.B. Straumal – Prof., Dr. Sci. (Phys.-Math.), Institute of Solid State Physics of the RAS, Chernogolovka, Moscow region
O.Yu. Tkacheva – Dr. Sci. (Chem.), Institute of High Temperature Electrochemistry of the Ural Branch of the RAS, Yekaterinburg, Russia
M. Verhaege – Prof., Dr., University of Gent, Belgium
G.M. Vol'dman – Prof., Dr. Sci. (Chem.), Russian Technological University (MITHT), Moscow, Russia
G. Xanthopoulou – Dr., National Center for Scientific Research "Demokritos", Agia Paraskevi, Attica, Greece
A.L. Yerokhin – Prof., Dr., University of Manchester, United Kingdom
Onuralp Yücel – Prof., Dr., Istanbul Technical University, Maslak, Istanbul, Turkey
Yu.P. Zaikov – Prof., Dr. Sci. (Chem.), Corresponding Member of the Institute of High Temperature Electrochemistry of the Ural Branch of the RAS, Yekaterinburg, Russia
R.Kh. Zalavutdinov – Cand. Sci. (Phys.-Math.), A.N. Frumkin Institute of Physical Chemistry and Electrochemistry of the RAS, Moscow, Russia
M. Zinigrad – Prof., Dr., Ariel University, Ariel, Israel
A.I. Zouboulis – Prof., Dr., Aristotle University of Thessaloniki, Greece

Editorial Staff

Address: NUST MISIS, 1 Bld, 4 Leninskiy Prosp.,
Moscow 119049, Russia
Phone: +7 (495) 638-45-35
E-mail: izv.vuz@misis.ru

Certificate of registration No. 015842 (13.03.1997)
Re-registration PI No. ФС77-79229 (25.09.2020)

Subscription: Ural-Press Agency

© NUST MISIS, Moscow, 2025
© Izvestiya. Non-Ferrous Metallurgy, 2025

Leading Editor – O.V. Sosnina
Executive Editor – A.A. Kudinova
Layout Designer – E.A. Legkaya

Signed print 23.06.2025. Format 60×90 1/8.
Offset paper No. 1. Digital printing. Quires 11
Order 22439. Free price

Printed in the printing house of the MISIS Publish House
1 Bld, 4 Leninskiy Prosp., Moscow 119049, Russia. Phone/fax: +7 (499) 236-76-17

Articles are available under Creative Commons Attribution Non-Commercial No Derivatives

ISSN 0021-3438 (Print)
ISSN 2412-8783 (Online)

ИЗВЕСТИЯ ВУЗОВ
ЦВЕТНАЯ МЕТАЛЛУРГИЯ

Том 31, № 2
2025

Научно-технический журнал   Основан в 1958 г.   Выходит 4 раза в год   http://cvmet.misis.ru

Журнал включен в Перечень рецензируемых научных изданий, рекомендованных ВАК Минобрнауки РФ для публикации результатов диссертаций на соискание ученых степеней

Журнал включен в базы данных: Russian Science Citation Index (RSCI), Chemical Abstracts (Online), INIS, OCLC ArticleFirst, Ulrich's Periodicals Directory, РИНЦ, БД/РЖ ВИНИТИ

Учредитель

ФГАОУ ВО Национальный исследовательский технологический университет «МИСИС»
Адрес: 119049, г. Москва, Ленинский пр-т, 4, стр. 1
http://www.misis.ru

Главный редактор

Евгений Александрович Левашов
д.т.н., чл.-корр. РАН, профессор, НИТУ МИСИС, г. Москва

Заместитель главного редактора

Владислава Анатольевна Игнаткина
д.т.н., профессор, НИТУ МИСИС, г. Москва

Редакционная коллегия

Е.В. Агеев – д.т.н., ЮЗГУ, г. Курск
М.В. Ананьев – д.х.н., АО «Гиредмет», г. Москва
Н.А. Белов – д.т.н., проф., НИТУ МИСИС, г. Москва
Е.В. Богатырева – д.т.н., НИТУ МИСИС, г. Москва
Г.М. Вольдман – д.х.н., проф., РТУ (МИТХТ), г. Москва
Ф.В. Гречников – д.т.н., акад. РАН, проф., СНИУ, г. Самара
Д.В. Гундеров – д.ф.-м.н., ИФМК УНЦ РАН, г. Уфа
В.Б. Деев – д.т.н., проф., НИТУ МИСИС, г. Москва
В.М. Денисов – д.х.н., проф., СФУ, г. Красноярск
Д.В. Дробот – д.х.н., проф., РТУ (МИТХТ), г. Москва
Ю.П. Зайков – д.х.н., проф., член-корр. ИВТЭ УрО РАН, г. Екатеринбург
Р.Х. Залавутдинов – к.ф.-м.н., ИФХЭ РАН, г. Москва
С.В. Мамяченков – д.т.н., проф., УрФУ, г. Екатеринбург
З.А. Мансуров – д.х.н., проф., Институт проблем горения, г. Алматы, Казахстан
Н.В. Немчинова – д.т.н., проф., ИРНИТУ, г. Иркутск
К.В. Никитин – д.т.н., проф., СамГТУ, г. Самара
П.В. Поляков – д.х.н., проф., СФУ, г. Красноярск
Е.С. Прусов – к.т.н., доцент, ВлГУ, г. Владимир
В.Н. Рычков – д.х.н., проф., УрФУ, г. Екатеринбург
Г.А. Салищев – д.т.н., проф., НИУ «БелГУ», г. Белгород
В.М. Сизяков – д.т.н., проф., СПГУ, г. Санкт-Петербург
Б.Б. Страумал – д.ф.-м.н., проф., ИФТТ РАН, г. Черноголовка
О.Ю. Ткачева – д.х.н., ИВТЭ УрО РАН, г. Екатеринбург
Б.Б. Хина – д.ф.-м.н., доц., ФТИ НАН Беларуси, г. Минск, Беларусь
Д.В. Штанский – д.ф.-м.н., проф., НИТУ МИСИС, г. Москва
Abhilash – Dr., Ph.D., CSIR – National Metallurgical Laboratory, Jamshedpur, India
D.V. Louzguine – Prof., Dr., Tohoku University, Sendai, Japan
D. Sadoway – Prof., Dr., Massachusetts Institute of Technology, Boston, USA
Stopic Srecko – Dr.-Ing. habil., RWTH Aachen University, Aachen, Germany
M. Verhaege – Prof., Dr., University of Gent, Belgium
G. Xanthopoulou – Dr., National Center for Scientific Research «Demokritos», Agia Paraskevi, Attica, Greece
A.L. Yerokhin – Prof., Dr., University of Manchester, United Kingdom
Yücel Onuralp – Prof., Dr., Istanbul Technical University, Maslak, Istanbul, Turkey
M. Zinigrad – Prof., Dr., Ariel University, Ariel, Israel
A.I. Zouboulis – Prof., Dr., Aristotle University of Thessaloniki, Greece

Редакция журнала

Адрес: 119049, г. Москва, Ленинский пр-т, 4, стр. 1,
НИТУ МИСИС
Тел.: +7 (495) 638-45-35
E-mail: izv.vuz@misis.ru

Свидетельство о регистрации № 015842 от 13.03.1997 г.
Перерегистрация ПИ № ФС77-79229 от 25.09.2020 г.

Подписка: Агентство «Урал-пресс»

© НИТУ МИСИС, Москва, 2025
© «Известия вузов. Цветная металлургия», 2025

Ведущий редактор – О.В. Соснина
Выпускающий редактор – А.А. Кудинова
Дизайн и верстка – Е.А. Легкая

Подписано в печать 23.06.2025. Формат 60×90 1/8.
Бум. офсетная № 1. Печать цифровая. Усл. печ. л. 11
Заказ 22439. Цена свободная

Отпечатано в типографии Издательского Дома МИСИС
119049, г. Москва, Ленинский пр-т, 4, стр. 1. Тел./факс: +7 (499) 236-76-17

Статьи доступны под лицензией Creative Commons Attribution Non-Commercial No Derivatives

CONTENTS

Metallurgy of non-ferrous metals

Metallurgy of Rare and Precious Metals

Foundry

Energy and Resource Saving

СОДЕРЖАНИЕ

Металлургия цветных металлов

Металлургия редких и благородных металлов

Литейное производство

Энерго- и ресурсосбережение

METALLURGY OF NON-FERROUS METALS / МЕТАЛЛУРГИЯ ЦВЕТНЫХ МЕТАЛЛОВ

UDC 669.2, 669.046.584
https://doi.org/10.17073/0021-3438-2025-2-5-18

Research article
Научная статья

Characterization of an atypical intermediate layer formed in Vanyukov furnaces during smelting of charges with a high content of technogenic materials

L.V. Krupnov[1,3], **R.A. Pakhomov**[2], **A.V. Kaverzin**[3], **Ya.I. Kosov**[2], **P.V. Malakhov**[1]

[1] Polar Division of **PJSC "MMC "Norilsk Nickel"**
2 Gvardeyskaya sq., Norilsk 663302, Russia

[2] **LLC Gipronickel Institute**
11 Grazhdansky Prosp., Saint-Petersburg 195220, Russia

[3] **N.M. Fedorovsky Polar State University**
7 50-Let Oktyabrya Str., Norilsk 663310, Russia

✉ Leonid V. Krupnov (KrupnovLV@nornik.ru)

Abstract: The growing need for recycling, along with the depletion of high-grade ore concentrates, has led to the inclusion of previously accumulated technogenic materials — such as metallurgical slags, sludge from settling ponds of recirculating water systems, and similar waste— into the charge of primary smelting units. The share of such feedstock in the furnace charge now reaches approximately 25 %, which has resulted in serious technological disruptions to the stable operation of primary autogenous smelting units. In Vanyukov furnaces, this is manifested by the appearance – alongside the typical smelting products (matte and slag) – of a new atypical phase, the so-called intermediate layer. The formation of this layer leads to adverse effects, including the obstruction of flow paths from the furnace hearth to the slag and matte siphons, ultimately causing a complete shutdown of the unit. A sample of this abnormal product, collected from an industrial furnace during a period of process instability, was analyzed using differential scanning calorimetry (DSC), thermogravimetric analysis (TGA), and differential thermal analysis (DTA). These methods allowed the determination of temperature ranges corresponding to phase transformations of the components comprising the intermediate layer. The results obtained can be used to define optimal parameters for stable smelting operation and to develop technical solutions that prevent conditions favorable for the formation of refractory accretions.

Key words: charge, technogenic feedstock, low-energy-value feedstock, liquid-bath smelting furnace, Vanyukov furnace, matte, slag, smelting products, oxysulfide phase, energy-dispersive *X*-ray microanalysis (EDS), differential thermal analysis (DTA).

Acknowledgments: The authors express their gratitude to the staff of the Norilsk Nickel R&D Center at the Institute of Non-Ferrous Metals, Siberian Federal University, who participated in the study: S.A. Silyanova, B.M. Lobastova, N.V. Nelyubina, A.S. Samoilo.

For citation: Krupnov L.V., Pakhomov R.A., Kaverzin A.V., Kosov Ya.I., Malakhov P.V. Characterization of an atypical intermediate layer formed in Vanyukov furnaces during smelting of charges with a high content of technogenic materials. *Izvestiya. Non-Ferrous Metallurgy.* 2025;31(2):5–18. https://doi.org/10.17073/0021-3438-2025-2-5-18

Изучение свойств атипичного продукта – «промежуточного слоя» печей Ванюкова, при переработке шихты с высоким содержанием техногенных продуктов

Л.В. Крупнов[1,3], **Р.А. Пахомов**[2], **А.В. Каверзин**[3], **Я.И. Косов**[2], **П.В. Малахов**[1]

[1] **Заполярный филиал ПАО «ГМК «Норильский никель»**
663302, Россия, Красноярский кр., г. Норильск, пл. Гвардейская, 2

[2] **ООО «Институт Гипроникель»**
195220, Россия, г. Санкт-Петербург, Гражданский пр-т, 11

[3] **Заполярный университет им. Н.М. Федоровского**
663310, Россия, Красноярский кр., г. Норильск, ул. 50 лет Октября, 7

✉ Леонид Владимирович Крупнов (KrupnovLV@nornik.ru)

Аннотация: Современные требования, определяющие необходимость рециклинга, а также снижение объемов качественных рудных концентратов привели к вовлечению в переработку на головных плавильных агрегатах ранее накопленного техногенного сырья – металлургических шлаков, илов прудов-отстойников систем оборотного водоснабжения и т.п. Доля такого сырья в загрузке плавильных агрегатов достигает уже ~25 %, что обусловило серьезные технологические сбои в устойчивом ведении процесса на головных автогенных плавильных агрегатах. Для печей Ванюкова это появление наряду с типичными продуктами плавки (штейна и шлака) нового атипичного продукта – так называемого промежуточного слоя, образование которого приводит к негативным последствиям, которые выражаются в запечатывании перетоков из горна печи в шлаковый и штейновый сифоны с последующей полной остановкой агрегата. Изучение такого аномального продукта, отобранного на промышленном агрегате в период отклонения от устойчивого ведения технологического процесса, методами дифференциально-сканирующей калориметрии, термогравиметрического и дифференциального термического анализа позволило определить температурные интервалы фазовых преобразований компонентов, входящих в состав промежуточного слоя. Полученные результаты помогут определить желаемые параметры устойчивого ведения процесса плавки и предложить технические решения, препятствующие неблагоприятным условиям настылеобразования.

Ключевые слова: шихта, техногенные продукты, низкоэнергетическое сырье, печь плавки в жидкой ванне, печь Ванюкова, штейн, шлак, продукты плавки, оксисульфидная фаза, рентгеноспектральный микроанализ (РСМА), дифференциальный термический анализ (ДТА).

Благодарности: Авторы благодарят сотрудников R&D Центра «Норникель» Института цветных металлов Сибирского федерального университета, принявших участие в работе: С.А. Сильянова, Б.М. Лобастова, Н.В. Нелюбина, А.С. Самойло.

Для цитирования: Крупнов Л.В., Пахомов Р.А., Каверзин А.В., Косов Я.И., Малахов П.В. Изучение свойств атипичного продукта – «промежуточного слоя» печей Ванюкова, при переработке шихты с высоким содержанием техногенных продуктов. *Известия вузов. Цветная металлургия*. 2025;31(2):5–18. https://doi.org/10.17073/0021-3438-2025-2-5-18

Introduction

At the Polar Division of PJSC “MMC Norilsk Nickel” (PD NN), copper pyrometallurgical operations involve processing of copper sulfide feedstock to produce copper anodes, which are then transferred to the electrorefining stage for the production of cathode copper. One of the feed materials used in the process is technogenic feedstock. Its use is necessitated by the depletion of high-quality ores and the implementation of environmental programs [1]. The production technology includes several sequentially arranged pyrometallurgical units, the primary of which is the Vanyukov furnace, a bath smelting unit. This is one of the modern and high-capacity pyrometallurgical units used to process copper sulfide materials. Global analogues of the Vanyukov furnace include bottom-blown smelting furnaces, Isasmelt (top-submerged lance) reactors, Mitsubishi process furnaces with multiple non-submerged tuyeres, flash smelting furnaces, and others [2—5].

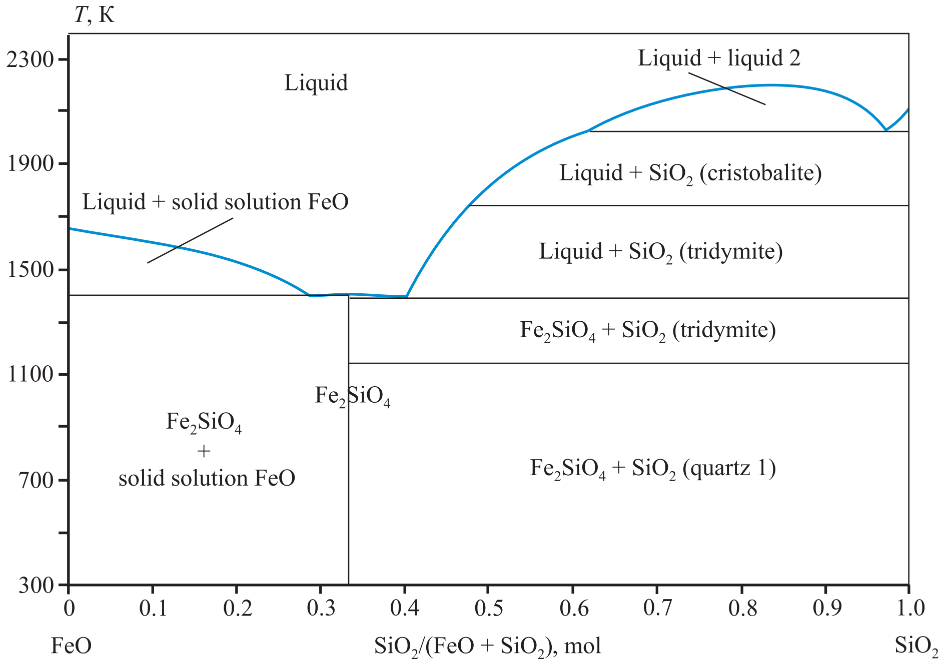

Fig. 1. Binary phase diagram of FeO–SiO$_2$ system

Рис. 1. Диаграмма состояния двойной системы FeO–SiO$_2$

In copper production at PD NN, silica-rich fluxes are used for slag formation. International industrial practice widely employs ferrosilicate slags in the processing of copper and copper-nickel sulfide feedstocks. Examples include the Olympic Dam smelter (Australia), Zhong Tiao Shan's Houma smelter (China), and Konkola Copper Mines (Zambia), among others [6—8]. The use of silica (SiO$_2$) as a fluxing agent significantly facilitates the oxidative blowing of sulfide feedstock by forming slags with relatively low melting points. The binary FeO—SiO$_2$ phase diagram is shown in Fig. 1.

However, variations in feed composition under constant oxidizing potential, disruption of process parameters, increased oxidant supply, natural gas shortages (used to compensate heat losses), and other factors may lead to the formation of high-melting compounds in the furnace atmosphere of pyrometallurgical units. These compounds are represented by spinel-type phases of variable composition containing non-ferrous metals [9; 10].

Since 2019, significant process disruptions have been observed in the operation of the Vanyukov furnace at the Copper Plant of PD NN due to considerable changes in the composition of the processed feedstock [11; 12]. One of the key issues has been impaired melt flow caused by a reduction in the cross-sectional area of the tapping channel. The narrowing of the flow path was attributed to the appearance of a new, atypical product in the smelting output — a so-called intermediate layer. This material forms a separate oxide phase with sulfide inclusions and occupies an interfacial position between the slag and matte phases [13]. The composition of this layer was initially unclear, necessitating further investigation into its origin and formation conditions.

Similar issues have been encountered in the operation of the most widespread technology for processing copper and nickel sulfide concentrates — flash smelting [14—18]. As the intermediate layer became saturated with magnetite, it led to the formation of a solid phase, which eventually settled on the hearth and slag zone of the furnace. To mitigate the risk of accretion formation, a set of technological and engineering measures was implemented, involving modifications to both the equipment and the process parameters. For instance, at the Kalgoorlie Nickel Smelter operated by WMC (Australia), lime was added to the feed mix to lower the slag melting point and improve its fluidity, the smelting temperature was raised to 1360 °C, and smelting and converting operations were integrated within a single unit by installing six electrodes in the settling zone [19—22].

The objective of this study was to determine the mechanism and formation conditions of the intermediate heterogeneous layer during smelting in Vanyukov furnaces at the Copper Plant of PD NN, and to develop recommendations for ensuring stable operation at this production stage.

Research methodology

The study was based on a sample of the intermediate layer collected in October 2023. The formation of this sample during that period was associated with a deterioration in the composition of the processed charge. The sample represented an oxysulfide product (Fig. 2), in which oxide and sulfide regions of the intermediate layer were distinguishe. In this study, the two phases wee examined separately.

The atypical smelting product was studied using thermogravimetric analysis (TGA), differential thermal analysis (DTA), differential scanning calorimetry (DSC), *X*-ray diffraction analysis (XRD) [23—25], scanning electron microscopy (SEM), and energy-dispersive *X*-ray spectroscopy (EDS). It is worth noting that this combination of methods is widely applied in the study of technogenic material recycling and non-ferrous slag processing [26—32].

XRD analysis was performed using a Shimadzu XRD7000 diffractometer (Japan); thermal analysis (DTA and TGA) was carried out using Setsys Evolution-1750 (Setaram) and NETZSCH STA 409 PC/PG (Germany) thermal analyzers; SEM and EDS were performed using a Tescan 5130MM scanning electron microscope equipped with an Oxford Instruments INCA Energy microanalysis system and a YAG crystal as a backscattered electron detector. Analytical chemistry methods were applied using iCAP 6500 Duo SSEA and iCAP 7600 Radial atomic emission spectrometers (Thermo Scientific, USA). Thermodynamic modeling was conducted using the FactSage software package (version 6.4.1, 2012).

The content of major elements in the sulfide and oxide parts of the intermediate layer is presented in Table 1.

Results of sulfide phase analysis

The elemental composition (see Table 1), *X*-ray diffraction analysis (XRD, Fig. 3), scanning electron microscopy (SEM), and energy-dispersive *X*-ray spectroscopy (EDS, Fig. 4) of the sulfide phase indicate that

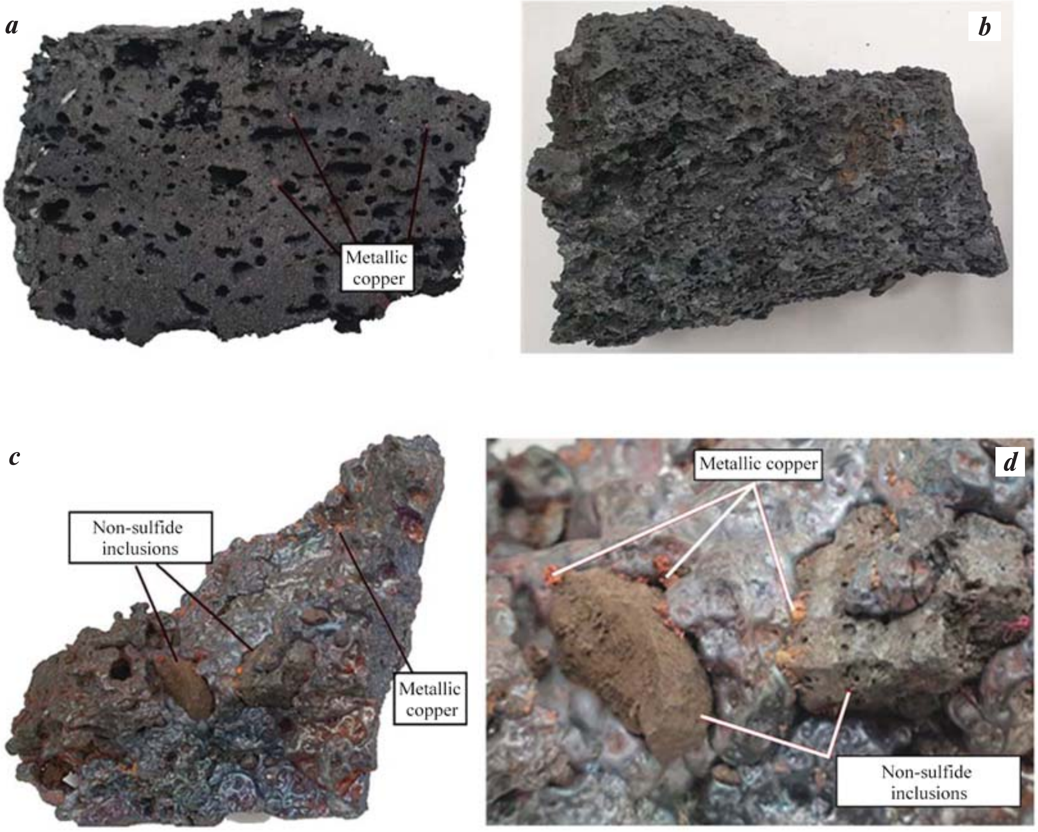

Fig. 2. General view of the atypical smelting product – intermediate layer: oxide phase (***a***, ***b***) and sulfide phase (***c***, ***d***)

Рис. 2. Общий вид атипичного продукта плавки – промежуточного слоя: оксидной (***a***, ***b***) и сульфидной (***c***, ***d***) фаз

Table 1. **Elemental composition of the analyzed samples**

Таблица 1. Элементный состав исследуемых проб

Component	Content of major elements, wt. %												
	Fe	Ni	Si	Cu	Al	Ti	Mg	Zn	Na	Ca	Co	K	S
Oxide phase	31.77	8.87	7.96	3.59	2.38	2.34	2.29	0.79	0.75	0.62	0.54	0.21	0.18
Sulfide phase	0.32	5.19	0.49	59.27	0.29	0.13	0.15	–	0.2	–	–	–	33.74

it is close in composition to typical copper matte. The results of the bulk chemical analysis (Table 1) are consistent with the phase composition data obtained by XRD, SEM, and EDS. The main components of the sulfide portion of the intermediate layer are copper (Cu, 59.27 wt. %) and sulfur (S, 33.74 wt. %), along with a notable nickel (Ni) content of 5.19 wt. %. The contents of other elements do not exceed 0.5 wt. %. According to the XRD data, the dominant phase in the sulfide portion is chalcocite (Cu_2S) (Fig. 3). The SEM and EDS analyses reveal additional mineral phases, including metallic solid solutions based on Cu—Ni alloys (Fig. 4, *c*), skeletal crystals of bunsenite (NiO) (Fig. 4, *c*, *d*), as well as less common olivine-group minerals such as liebenbergite (Ni_2SiO_4) (Fig. 4, *d*) and heazlewoodite (Ni_3S_2) (Fig. 4, *b*).

The conducted study demonstrated that the sulfide portion of the intermediate layer consists of distinct sulfide and metallic phases embedded in a structure of high-melting-point oxide material.

TGA and DTA of the sulfide phase were carried out under an argon atmosphere at a heating rate of 30 °C/min up to a maximum temperature of 1100 °C. The resulting thermogram is shown in Fig. 5. The data indicate that mass loss begins gradually at approximately 400 °C and accelerates above 700 °C. This behavior may

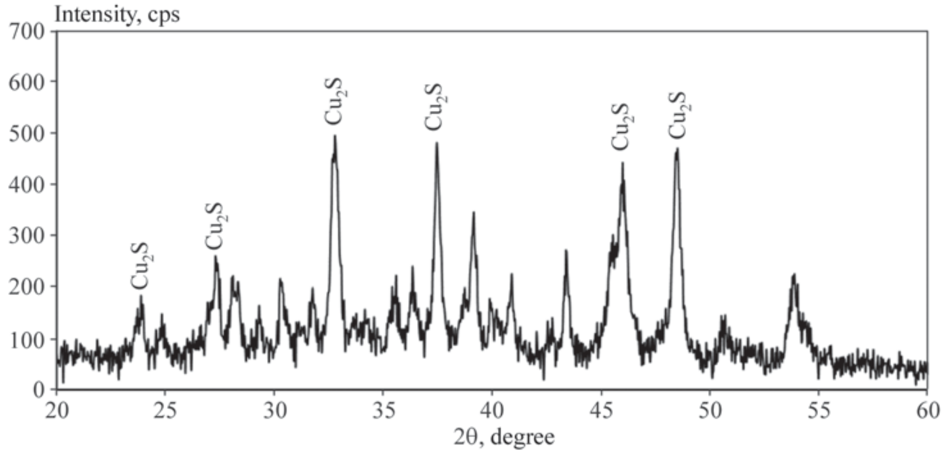

Fig. 3. *X*-ray diffraction pattern of the sulfide portion of the intermediate layer

Рис. 3. Рентгенограмма сульфидной части (промежуточного слоя)

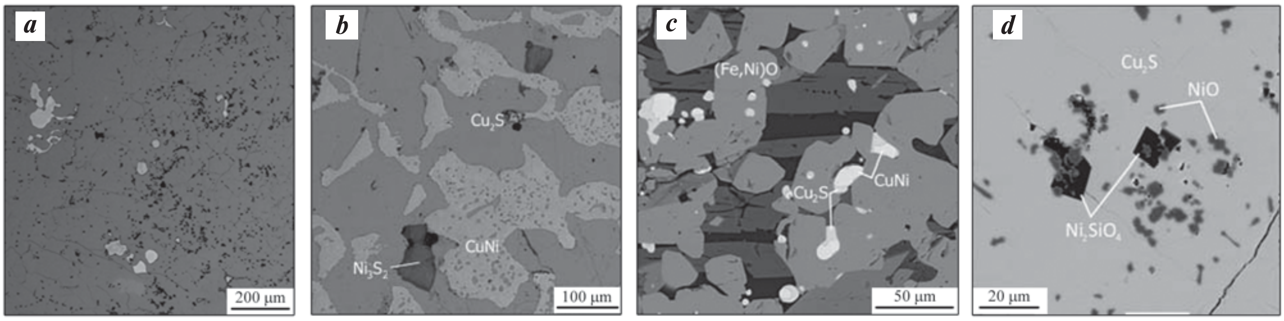

Fig. 4. General view of the sulfide sample (***a***) and phase distribution (***b***–***d***) in the analyzed material

Рис. 4. Общий вид проб сульфидной части (***a***) и распределение фаз (***b***–***d***) в исследуемой пробе

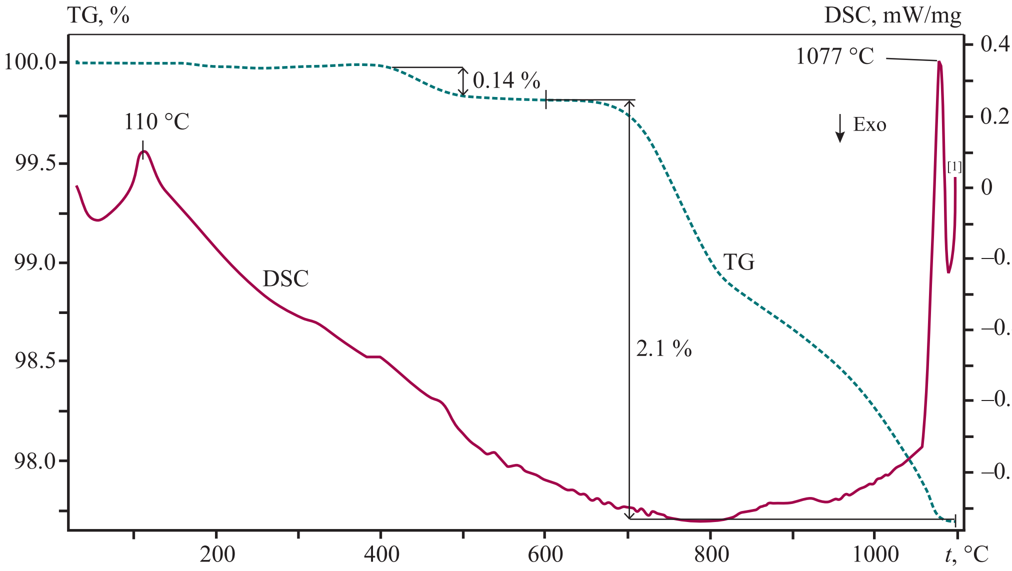

Fig. 5. Thermogravimetric and differential scanning calorimetry (DSC) results for the sulfide portion of the intermediate layer

Рис. 5. Общий вид результатов ТГА и ДСК для сульфидной части промежуточного слоя

be associated with the release of sulfur from Cu_2S, either due to the β-to-δ phase transition of Cu_2S or through δ-Cu_2S dissociation accompanied by sulfur volatilization. The apparent endothermic effect observed at 110 °C may be attributed to the relatively large sample mass (101 mg), which caused significant baseline drift in the DSC signal. Endothermic events recorded at 1077 °C and 1100 °C correspond to phase transition and subsequent melting of Cu_2S (which, according to phase diagrams, occurs at 1067 °C and 1105 °C, respectively) [33].

Results of oxide phase analysis

The main elements in the oxide portion of the intermediate layer are Fe (31.77 wt. %) and O (37.35 wt. %). Nickel and silicon are present in subordinate amounts (~8 wt. %), while copper, aluminum, titanium, and magnesium are found in the range of 2—3 wt. %. The contents of other elements do not exceed 1 wt. %.

X-ray diffraction analysis (XRD, Fig. 6) of the oxide phase showed that the sample contains spinel-type phases (magnetite), delafossite, cuprite, the tetragonal modification of SiO_2, and forsterite. SEM and EDS analyses further revealed that the oxide phase is compositionally and structurally homogeneous. The bulk of the sample is represented by oxide phases of variable composition, with a total volume fraction of approximately 80—95 %. In addition to the above phases, the sample also contains: a complex silicate component in the amount of 10—15 vol. % (pyroxene, clinopyroxene); dispersed metallic copper particles with minor iron content, up to 160 μm in size, with a total volume fraction not exceeding 0.1 %; and metallic copper with inclusions of cuprous oxide (Cu_2O).

Microstructural images of the oxide phase are presented in Fig. 7.

Additional analysis of the oxide portion was carried out using TGA and DTA, as was done for the sulfide part. The sample was tested under both inert (Ar) and oxidizing (O_2) atmospheres. The heating rate in both cases was 15 °C/min to a maximum of 1450 °C, and the cooling rate was 30 °C/min. The thermogram of the oxide portion of the intermediate layer is shown in Fig. 8. The analysis showed that in an inert atmosphere, the sample mass remained unchanged. However, two endothermic effects were observed, starting at approximately 1057 °C (with a peak at 1110 °C) and 1355 °C. The exact peak of the second effect could not be determined due to the temperature limit of the equipment (1450 °C). The first effect is attributed to the melting of metallic copper present in the intermediate layer. The second effect is tentatively associated with the onset of magnetite melting; however, complete melting of this primary phase was not observed at these temperatures. This is consistent with literature data [34, 35], according to which the melting point of magnetite exceeds 1590 °C.

In an oxidizing atmosphere (Fig. 8, *c*, *d*), two exothermic effects accompanied by mass gain were observed. These may be associated with partial oxidation of metallic or monovalent copper (Cu_2O, $CuFeO_2$) followed by decomposition at temperatures above 1000 °C to divalent copper oxide.

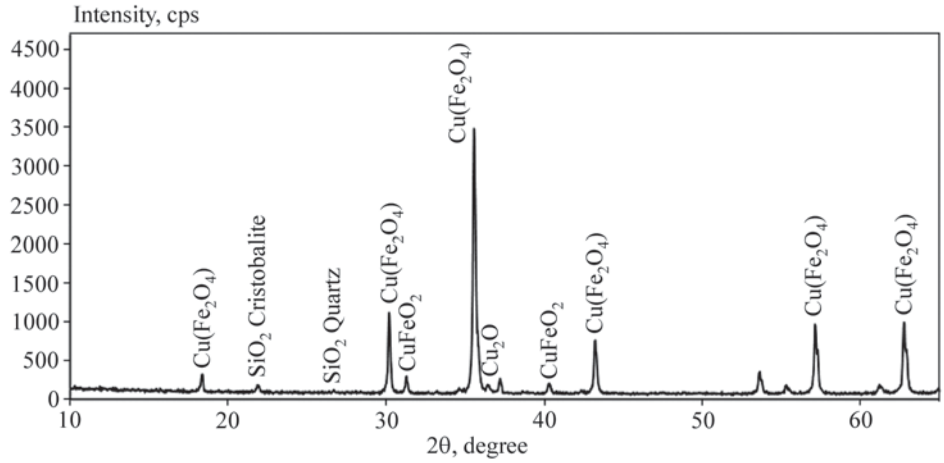

Fig. 6. *X*-ray diffraction pattern of the oxide portion of the intermediate layer

Рис. 6. Рентгенограмма оксидной части промежуточного слоя

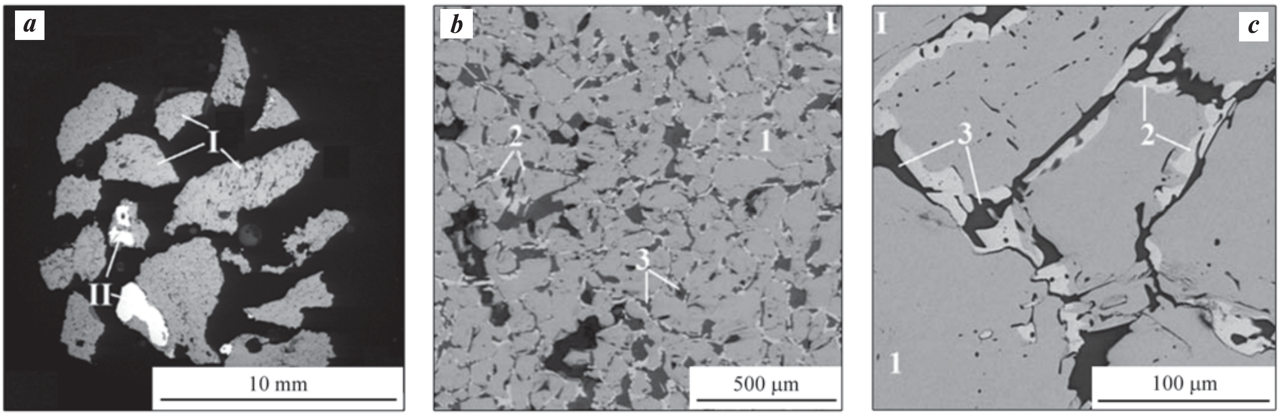

Fig. 7. General view of the oxide sample (***a***) and phase distribution (***b***, ***c***) in the analyzed material

a: I – slag particles, II – bottom phase
b, ***c***: *1* – iron oxide, *2* – copper-iron oxide, *3* – silicate phase

Рис. 7. Общий вид проб оксидной части (***a***) и распределение фаз (***b***, ***c***) в исследуемой пробе

a: I – шлаковые частицы, II – донная фаза
b, ***c***: *1* – оксид железа, *2* – оксид железа-меди, *3* – силикатная составляющая

As the data show, the magnetite-based phase formed at high temperatures cannot be removed without process adjustments or additional measures due to its high melting point. On the other hand, the high oxidation potential of the environment in which copper sulfide ores or concentrates are processed in Vanyukov furnaces does not allow the reduction of previously formed overoxidized refractory iron oxides. The primary cause of intermediate layer formation is a disruption in the operating mode of the furnace, particularly when the oxygen consumption ratio does not correspond to the composition of the processed feedstock.

To address this, thermodynamic calculations were performed to evaluate the conditions under which solid phase formation occurs in compositions close to the operational parameters of the Vanyukov furnace at the Copper Plant.

Thermodynamic modeling of copper sulfide feed oxidation

Table 2 presents the baseline compositions of the materials used in the thermodynamic calculations. These compositions are representative of the actual materials processed at the Copper Plant of PD NN. The modeling was performed using the FactSage software package [36].

The calculations were carried out in four stages. At the first stage, the process parameters were determined at $t = 1300$ °C obtain matte of the specified composition

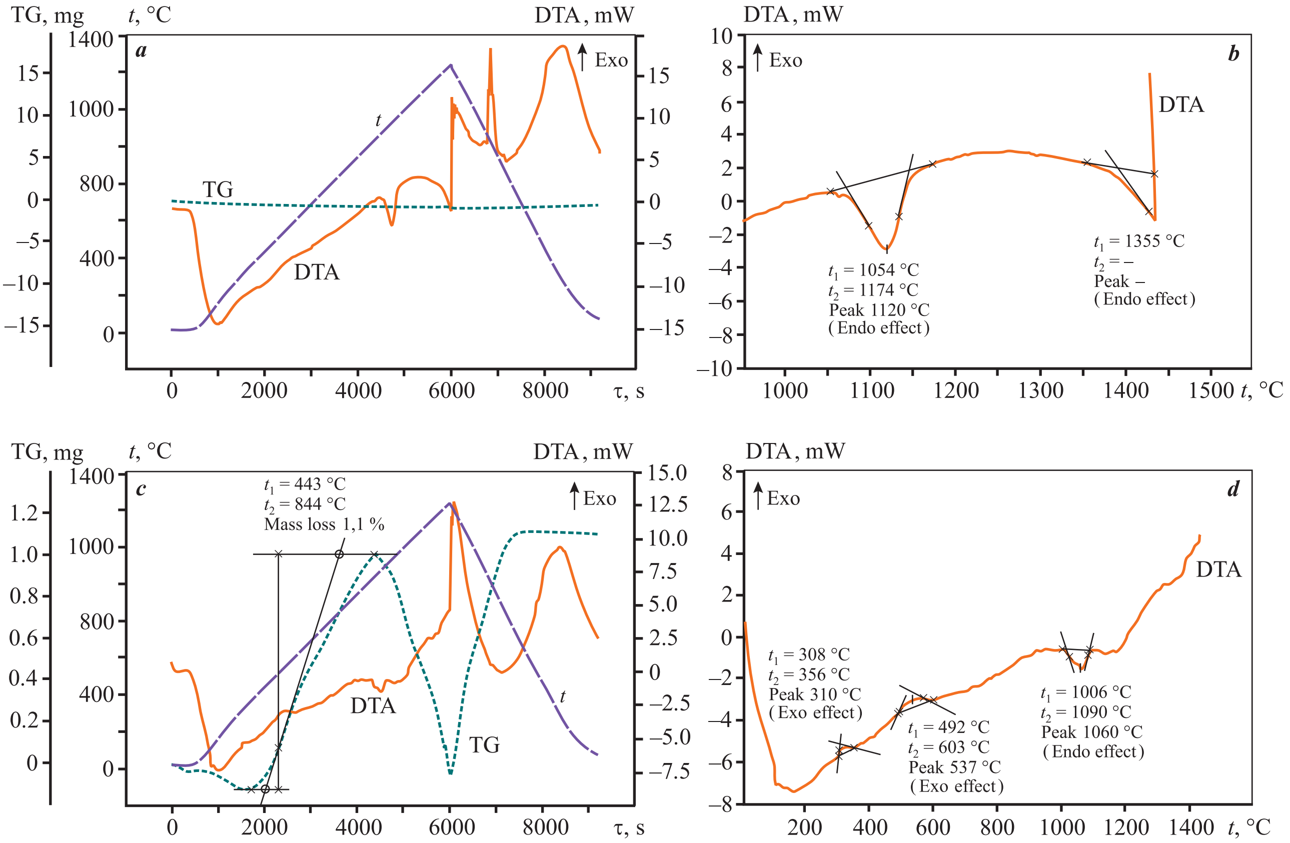

Fig. 8. TGA and DTA results for the oxide portion of the intermediate layer in argon (***a***, ***b***) and oxygen (***c***, ***d***) atmospheres

Рис. 8. Общий вид результатов ТГА и ДТА для оксидной части промежуточного слоя в атмосфере аргона (***a***, ***b***) и кислорода (***c***, ***d***)

(Fe ~15 %) and a silica content in the slag of about 30 %, which corresponds to the products obtained at the Copper Plant of the PD NN. A key requirement at this stage was the absence of solid phase formation in the system under consideration. At the second stage, the parameters established in Stage 1 were fixed, and the temperature was varied to identify the threshold conditions under which refractory compounds begin to form. At the third stage, the influence of copper concentrate—obtained from the flotation separation of nickel slag generated during copper production — on solid phase formation in the system was assessed at t = 1250 °C. The calculations were performed for a baseline case (without concentrate addition), assuming matte containing approximately 15 % Fe and slag with about 30 % SiO_2. At the fourth stage, for the slag composition from Stage 1 (where no solid phase had formed), a calculation was performed to evaluate the effect of increasing the system's oxidation potential (via oxygen addition) on solid phase formation at a fixed temperature of 1250 °C.

Thus, in Stage 1, thermodynamic modeling was performed to define conditions for the formation of a bottom phase containing ~15 wt. % Fe, with silica concentration in the slag at ~30 wt. %. The results were obtained under the following conditions: oxygen and quartzite additions of 14.8 and 17 rel. % relative to the metal-bearing feed, and a process temperature of 1300 °C.

Stages 2 to 4 were based on the parameters established at Stage 1. Solid solution phases from the software database were used in the calculations, including: Spinel-type phases of the AB_2O_4 or A_3O_4 type (with cation oxidation states 2+ and 3+); monoxides (A_xO); clinopyroxenes ($(A,B)_2SiO$); orthopyroxenes ($(Mg,Fe)_2Si_2O_6$); wollastonite ($CaSiO_3$); calcium silicate (Ca_2SiO_4); olivine ($(Mg,Fe)_2[SiO_4]$); cordierite ($Al_4Fe_2Si_5O_{18}$); mullite ($Al_6Si_2O_{13}$). Figs. 9 and 10 show the results of thermodynamic calculations, including the most stable phases within the modeled temperature range. As seen from the data, under the current calculation parameters and compositions (see Table 2), solid phase formation begins at temperatures below 1225 °C. The solid phase consists of a spinel-type magnetite phase (~25 rel. % Fe_3O_4) and clinopyroxene-group phases composed of silicates containing Fe, Mg, and Ca, with a gene-

Table 2. **Content of major components in the input feedstock materials**

Таблица 2. Содержание основных компонентов в исходных веществах

Material	Content, wt. %									
	Ni	Cu	Co	Fe	S	SiO_2	CaO	Al_2O_3	MgO	O_2
Metal-bearing feedstock	2.04	24.46	0.11	34.16	21.77	4.65	1.02	1.08	1.45	3.84
Flux	–	–	–	2.51	0.16	78	2.46	5.41	1.46	0.96
Copper concentrate (from flotation of nickel slag)	10.44	53.25	0.167	12.95	10.5	4.35	1.10	0.59	1.26	4.4
Oxidant (O_2)	–	–	–	–	–	–	–	–	–	100

ral composition of xFeSi$_2$O$_6$ (where x = Mg, Ca, Fe, Fe^{3+}). These phases account for approximately 75 rel. % of the total solid phase.

Fig. 9, *b* shows the modeling results for the effect of copper concentrate obtained from the flotation separation of copper production nickel slag on the formation of refractory phases. According to Table 2, this product is characterized by a reduced sulfur content and the presence of slag-forming components along with oxides of non-ferrous metals and iron. According to the data, at 1250 °C, the addition of more than 13 rel. % of this copper concentrate (derived from the flotation separation of nickel slag during the second stage of copper converting) to the metal-bearing charge results in the formation of refractory phases, which negatively affect the processing of the feedstock.

The study also examined slag behavior under increased oxidation potential. According to the results in Fig. 10, adding more than 1 rel. % oxygen (relative to the slag mass) disrupts equilibrium and leads to the formation of iron spinel phases similar to those identified in the experimental section. As the oxidation potential increases, the spinel fraction continues to grow, complicating the smelting process and promoting the formation of an intermediate layer rich in sulfide inclusions.

The conducted calculations indicate that deviations from standard operating conditions of the pyrometallurgical unit — whether due to changes in feed composition under a constant oxidation potential or due to increased oxidation potential with a stable feed composition — lead to the formation of high-melting compounds. These compounds cannot be decomposed under current processing conditions and, as a result, disrupt furnace operation. The destruction of such refractory phases formed at elevated temperatures inside the furnace can be achieved through chemical interaction with low-copper matte or by introducing metallized

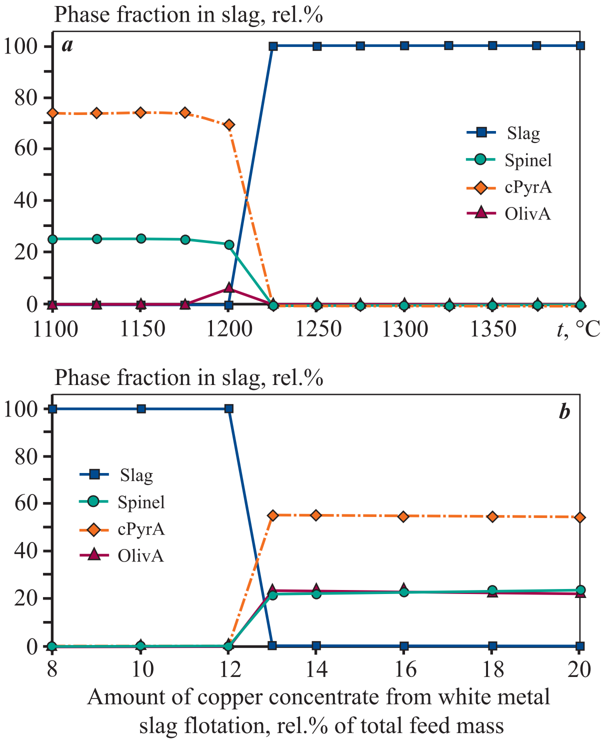

Fig. 9. Solid phase formation in slag as a function of (***a***) process temperature during oxidation of a copper-bearing sulfide charge and (***b***) the amount of copper concentrate (from white metal slag flotation) added to the charge

Spinel-type phase AB_2O_4 or A_3O_4 (oxidation states 2+ and 3+); cPyrA – clinopyroxene $(A,B)_2SiO_6$; OlivA – olivine $(Mg,Fe)_2[SiO_4]$; A and B = Fe, Fe^{3+}, Mg, Ca, Al, etc.

Рис. 9. Формирование твердой фазы в шлаке в зависимости от температуры процесса при окислении медной металлсодержащей сульфидной шихты (***а***) и от количества вводимого медного концентрата от разделения файнштейна (***b***)

Шпинель вида AB_2O_4 или A_3O_4 (степень окисления 2+ и 3+); cPyrA – клинопироксен вида $(A,B)_2SiO_6$; OlivA – оливин $(Mg,Fe)_2[SiO_4]$; A и B – Fe, Fe^{3+}, Mg, Ca, Al и др.

and carbon-containing materials. Approaches to the breakdown of high-melting compounds in flash smelting furnaces have been addressed in previous studies [37; 38].

Conclusion

The study identified the composition of the atypical product formed in Vanyukov furnaces and characterized the phase composition of the sulfide and oxide portions of the intermediate layer. The primary phase in the sulfide portion is chalcocite (Cu_2S), while the oxide portion consists of spinel, delafossite ($CuFeO_2$), cuprite (Cu_2O), and clinopyroxene with a general composition of $W_{1\text{-}p}(X,Y)_{1+p}[Z_2O_6]$, where W — Na, Ca; X — Mg, Fe^{2+}, Mn, Ni, Li; Y — Al, Fe^{3+}, Cr, Ti; Z — Si, Al.

Thermal analysis (TGA and DTA) of the sulfide phase showed a 2 rel. % mass loss in an inert atmosphere, which is attributed to the release of sulfur from non-stoichiometric Cu_2S_{1+x} as it transitions to stoichiometric Cu_2S. Endothermic effects were recorded at 1077 °C and 1100 °C, associated with the phase transformation and subsequent melting of Cu_2S (consistent with phase diagram values of 1067 °C and 1105 °C, see Fig. 5). These results indicate that the phase remains in a liquid state under Vanyukov furnace conditions and that its presence in the intermediate layer reflects mechanical entrapment within the higher-melting oxide matrix.

In an inert atmosphere, the oxide phase exhibited no change in mass. However, two endothermic effects were observed at 1057 °C (peak at 1110 °C) and 1355 °C, corresponding to the onset of melting in iron-rich oxides containing nickel and copper.

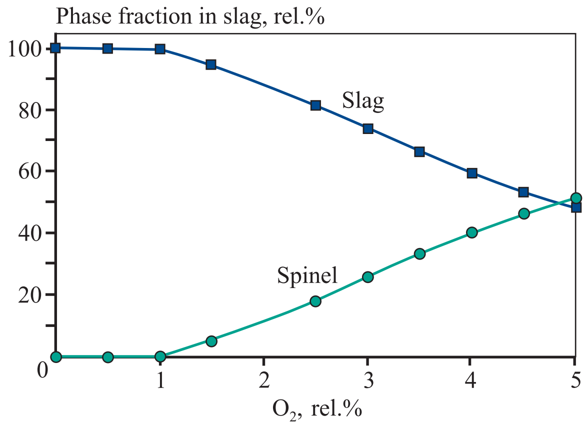

Fig. 10. Solid phase formation in slag as a function of oxidant addition to the system

Spinel-type phase AB_2O_4 or A_3O_4 (oxidation states 2+ and 3+)

Рис. 10. Формирование твердой фазы в шлаке в зависимости количества окислителя, поступающего в систему

Шпинель вида AB_2O_4 или A_3O_4 (степень окисления 2+ и 3+)

Stable operation of the Vanyukov furnace for processing the current feed composition — while avoiding the formation of refractory spinels — is constrained by the following factors:

— slag melt temperature must not fall below 1225 °c;
— the share of copper concentrate obtained from nickel slag flotation must not exceed 13 rel.% in the feed;
— excess oxidation potential in the slag system must be avoided (oxygen addition not exceeding 1 rel. %).

The results demonstrate that adjusting only the temperature of the smelting process is insufficient to eliminate the intermediate layer, since the furnace typically operates at lower temperatures (up to 1350 °C).

Thus, the most rational strategy for addressing such atypical products is to maintain strict control over the feed composition and the overall process parameters. In cases where the intermediate layer has already formed, the most effective approach to its breakdown involves chemical interaction with lean matte, the use of metallized or carbon-containing additives, and operating on lean matte to lower the oxidation potential of the system.

The findings of this study served as the basis for practical recommendations to ensure stable smelting operations in Vanyukov furnaces at the Copper Plant, particularly under conditions of fluctuating feedstock composition.

References

1. Vurdova N.G., Golubev O.V., Nedelin S.V., Petelin A.L., Polulyakh L.A., Chernousov P.I. Recycling: Textbook. Moscow: MISIS, 2020. 746 p. (In Russ.).
Вурдова Н.Г., Голубев О.В., Неделин С.В., Петелин А.Л., Полулях Л.А., Черноусов П.И. Рециклинг: Учебник. М.: МИСИС, 2020. 746 с.
2. Kandalam A, Reuter MA, Stelter M, Reinmöller M, Gräbner M, Richter A, et al. A review of top-submerged lance (TSL) processing. Part I: Plant and reactor engineering. *Metals*. 2023;13(10):1728.
http://dx.doi.org/10.3390/met13101728
3. Kandalam A, Reuter MA, Stelter M, Reinmöller M, Gräbner M, Richter A, et al. A Review of top submerged lance (TSL) processing. Part II: Thermodynamics, slag chemistry and plant flowsheets. *Metals*. 2023;13(10):1742.
http://dx.doi.org/10.3390/met13101742

4. Liu Z, Xia L. The practice of copper matte converting in China. *Mineral Processing and Extractive Metallurgy* . 2018;128(1-2):117—124.
http://dx.doi.org/10.1080/25726641.2018.1543147
5. Shibasaki T, Hayashi M. Top-blown injection smelting and converting: The Mitsubishi process. *JOM*. 1991;43(9):20—26.
http://dx.doi.org/10.1007/bf03222230
6. Swinbourne D.R., West R.C., Reed M.E., Sheeran A. Computational thermodynamic modelling of direct to blister copper smelting. *Mineral Processing and Extractive Metallurgy*. 2011;120(1):1—9.
http://dx.doi.org/10.1179/1743285510y.0000000003
7. Chen Ch., Zhang L., Jahanshahi Sh. Application of MPE model to direct-to-blister flash smelting and development of minor elements. In: *Copper International Conference: Proceeding of Copper 2013* (Santiago, Chile, 2013). P. 857—871.
https://doi.org/10.13140/2.1.4067.1360
8. Taskinen P., Kojo I. Fluxing options in the direct-to-blister copper smelting. In: *Proceedings of the VIII International Conference on Molten Slages, Fluxes and Salt — Molten 2009.* (Santiago, Chile, 2009). P. 1139—1151.
9. Sun Y.Q., Chen M., Cui Z.X., Contreras L., Zhao B.J. Phase equilibria of ferrous-calcium silicate slags in the liquid/spinel/white metal/gas system for the copper converting process. *Metallurgical and Materials Transactions: B.* 2020;5(51):2012—2020.
https://doi.org/10.1007/s11663-020-01887-9
10. Xie S., Zhao B.J. Phase equilibrium studies of nonferrous smelting slags: A review. *Metals*. 2024;14(278): 1—19.
https://doi.org/10.3390/met14030278
11. Krupnov L. V., Midyukov D. O., Malakhov P. V. Ways to cover the raw material demand in the copper-nickel sector. *Obogashchenie rud*. 2022;2:37—41. (In Russ.).
https://doi.org/10.17580/or.2022.02.06
Крупнов Л.В., Мидюков Д.О., Малахов П.В. Направления поддержания сырьевой базы медно-никелевой подотрасли. *Обогащение руд*. 2022;2:37—41.
https://doi.org/10.17580/or.2022.02.06
12. Krupnov L.V., Tsymbulov L.B., Malakhov P.V., Ozerov S.S. Operation of autogenous units in the Polar Division of Norilsk Nickel during processing of raw materials with reduced energy potential. *Tsvetnyye metally*. 2022;2:40—48. (In Russ.).
https://doi.org/10.17580/tsm.2022.02.05
Крупнов Л.В., Цымбулов Л.Б., Малахов П.В., Озеров С.С. Работа автогенных агрегатов в Заполярном филиале компании «Норникель» при переработке сырья с пониженным энергетическим потенциалом. *Цветные металлы*. 2022;2:40—48.
https://doi.org/10.17580/tsm.2022.02.05
13. Krupnov L.V., Rumyantsev D.V., Popov V.A., Malakhov P.V., Kaverzin A.V. Technical solutions to improve operating conditions of Vanyukov furnace while processing technogenic feed. *Metallurg*. 2024;4:106—111. (In Russ.). https://doi.org/10.52351/00260827_2024_4_106
Крупнов Л.В., Румянцев Д.В., Попов В.А., Малахов П.В., Каверзин А.В. Технические решения по улучшению условий эксплуатации печей Ванюкова при переработке техногенного сырья. *Металлург*. 2024;4:106—111.
https://doi.org/10.52351/00260827_2024_4_106
14. Taskinen P, Jokilaakso A. reaction sequences in flash smelting and converting furnaces: An in-depth view. *Metallurgical and Materials Transactions: B.* 2021; 52(5):3524—3542.
http://dx.doi.org/10.1007/s11663-021-02283-7
15. Krupnov L.V. Mechanism of refractory accretion formation in flash smelting furnaces and methods of accretion removal: Abstract of the dissertation of Cand. Sci. (Eng.). St. Petersburg: Federal State Budgetary Educational Institution of Higher Education “Saint Petersburg Mining University”, 2015. 19 p. (In Russ.).
Крупнов Л.В. Механизм образования тугоплавкой настыли в печах взвешенной плавки и способы ее устранения: Автореф. дис. ... канд. техн. наук. СПб, Национальный минерально-сырьевой ун-т «Горный», 2015. 19 с.
16. Kaur R., Nexhip C., Krippner D., George-Kennedy D., Routledge M. “Double Flash” technology after 16 years. In: *Papers to be presented at the thirteenth International Flash Smelting Congress* (2—8 October 2011, Zambia). Livingstone, Africa, 2011. 13 p.
17. Jiménez F., Ramos M., Pérez I. A review of recent improvements to control weak acid production at the Huelva smelter. In: *Papers to be presented at the thirteenth International Flash Smelting Congress* (2—8 October 2011, Zambia). Livingstone, Africa, 2011. 22 p.
18. Crundwell F.K., Moats M.S., Ramachandran V., Robinson T.G., Davenport W.G. Flash smelting of nickel sulfide concentrates. *Extractive Metallurgy of Nickel, Cobalt and Platinum Group Metals*. 2011;215—232.
http://dx.doi.org/10.1016/b978-0-08-096809-4.10018-8
19. Zhao B., Hayes P., Jak E. Effects of CaO, Al_2O_3 and MgO on liquidus temperatures of copper smelting and converting slags under controlled oxygen partial pressures. *Journal of Mining and Metallurgy, Section B: Metallurgy.* 2013;49(2):153—159.
http://dx.doi.org/10.2298/jmmb120812009z
20. Xie S., Yuan X., Liu F., Zhao B. Control of copper content in flash smelting slag and the recovery of valuable metals from slag. *A Thermodynamic Consideration Metals.* 2023;13(1):153. http://dx.doi.org/10.3390/met13010153

21. Kojo I., Storch H. Copper production with Outokumpu flash smelting: an update. In: *International Symposium on Sulfide smelting 2006. Vol. 8: Sohn International Symposium. Advanced Processing of Metals and Materials. The Minerals, Metals & Materials Society*. San Diego, California, USA, 2006. P.225—238.
22. Wang G., Cui Y., Li X., Shi R., Yang J., Yang S. et al. Structure and adaptability of $Fe_xO—SiO_2—MgO—$15 wt. % CaO—0.026 wt. % NiO slag with the Fe/SiO_2 mass ratio of 1.2 in flash matte smelting. *Ceramics International*. 2023;49(2):2531—2539.
http://dx.doi.org/10.1016/j.ceramint.2022.09.232
23. Yakimov I.S. System of *X*-ray phase identification of essentially multiphase materials. *Zavodskaya laboratoriya. Diagnostika materialov*. 2007;11(73):32—37. (In Russ.).
Якимов И.С. Система рентгенофазовой идентификации существенно многофазных материалов. *Заводская лаборатория. Диагностика материалов*. 2007;11(73):32—37.
24. Yakimov I.S., Dubinin P.S., Piksina O.E. Regularized multireflex method of reference intensities for quantitative *X*-ray phase analysis of polycrystalline materials. *Zavodskaya laboratoriya. Diagnostika materialov*. 2009;12(76):71—80. (In Russ.).
Якимов И.С., Дубинин П.С., Пиксина О.Е. Регуляризированный мультирефлексный метод ссылочных интенсивностей для количественного рентгенофазового анализа поликристаллических материалов. *Заводская лаборатория. Диагностика материалов*. 2009;12(76):71—80.
25. Piksina O.E., Ruzhnikov S.G., Dubinin P.S. *X*-ray spectral analysis: guidelines — Materials science and technology of new materials. Krasnoyarsk: SibFU, 2012. 43 p. (In Russ.).
Пиксина О.Е., Ружников С.Г., Дубинин П.С. Рентгеновский спектральный анализ: Методические указания. Материаловедение и технология новых материалов. Красноярск: СибФУ, 2012. 43 с.
26. Kolesnikov A.S. Kinetic investigations into the distillation of nonferrous metals during complex processing of waste of metallurgical industry. *Russian Journal of Non-Ferrous Metals*. 2015;56(1):1—5.
https://doi.org/10.3103/S1067821215010113
27. Kolesnikov A.S., Serikbaev B.E., Kenzhibaeva G.S., Botabaev N.E., Shapalov S.K., Kolesnikova O.G., Iztleuov G.M., Suigenbayeva A.A., Asylbekova D.D., Ashirbaev K.A., Kolesnikova V.A., Zolkin A.L., Isaev G.I., Alchinbaeva O.Z., Kutzhanova A.N. Processing of non-ferrous metallurgy waste slag for its complex recovery as a secondary mineral raw material. *Refractories and Industrial Ceramics*. 2021;62(4):375—380.
https://doi.org/10.1007/s11148-021-00611-7
28. Kolesnikov A.S., Kenzhibaeva G.S., Botabaev N.E., Kutzhanova A.N., Iztleuov G.M., Suigenbaeva A.Z., Ashirbaev K.A., Kolesnikova O.G. Thermodynamic modeling of chemical and phase transformations in a waelz process-slag — carbon system. *Refractories and Industrial Ceramics.* 2021;61(3):289—292.
https://doi.org/10.1007/s11148-020-00474-4
29. Kolesnikov A., Fediuk R., Amran M., Klyuev S., Klyuev A., Volokitina I., Naukenova A., Shapalov S., Utelbayeva A., Kolesnikova O., Bazarkhankyzy A. Modeling of non-ferrous metallurgy waste disposal with the production of iron silicides and zinc distillation. *Materials*. 2022;15(7):1—14.
https://doi.org/10.3390/ma15072542
30. Zhanikulov N., Kolesnikov A.S., Taimasov B.T., Zhakipbayev B.Y., Shal A.L. Influence of industrial waste on the structure of environmentally friendly cement clinker. *Complex Use of Mineral Resources*. 2022;4(323):84—91.
https://doi.org/10.31643/2022/6445.44
31. Kolesnikov A.S. Thermodynamic simulation of silicon and iron reduction and zinc and lead distillation in zincoligonite ore-carbon systems. *Russian Journal of Non-Ferrous Metals*. 2014;55(6):513—518.
https://doi.org/10.3103/S1067821214060121
32. Donayev A., Kolesnikov A., Shapalov Sh., Sapargaliyeva B., Ivakhniyuk G. Studies of waste from the mining and metallurgical industry, with the determination of its impact on the life of the population. *News of the National Academy of Sciences of the Republic of Kazakhstan. Series of Geology and Technical Sciences*. 2022;4(454):55—68.
https://doi.org/10.32014/2022.2518-170x.200
33. Sharma R.C., Chang Y.A. A thermodynamic analysis of the copper-sulfur system. *Metall Transactions: B*. 1980;11:575—583. https://doi.org/10.1007/BF02670137
34. Bannykh O.A., Budberg P.B., Alisova S.P., Drits M.E. State diagrams of binary and multicomponent systems based on iron: Handbook. Moscow: Metallurgiya, 1986. 440 p. (In Russ.).
Банных О.А., Будберг П.Б., Алисова С.П., Дриц М.Е. Диаграммы состояния двойных и многокомпонентных систем на основе железа: Справочник. М.: Металлургия, 1986. 440 с.
35. Levin M., Robbins C.R., McMurdie H.F. Phase diagrams for ceramists. The American Ceramic Society. Columbus, Ohio. 1964. 601 p.
36. Bale C. W., Bélisle E., Chartrand P., Decterov S. A., Eriksson G., Gheribi A.E., Hack K., Jung I.H., Kang Y.B., Melançon J., Pelton A.D., Petersen S., Robelin C.. Sangster J., Spencer P., Van Ende M-A. FactSage thermochemical software and databases 2010—2016. *Calphad*. 2016;54:35—53.
https://doi.org/10.1016/j.calphad.2016.05.002
37. Krupnov L.V., Starykh R.V., Petrov A.F. Mechanism of

formation of refractory crust in flash smelting furnaces of Nadezhda metallurgical plant. *Tsvetnye metally*. 2013;(2):46—49. (In Russ.).

Крупнов Л.В., Старых Р.В., Петров А.Ф. Механизм формирования тугоплавкой настыли в печах взвешенной плавки Надеждинского металлургического завода. *Цветные металлы*. 2013;(2):46—49.

38. Krupnov L.V., Pakhomov R.A., Kaverzin A.V., Kosov Ya.I., Malakhov P.V. Study of properties of intermediate layer formed in Vanyukov furnace while processing nickel-containing copper feed. In: Books of reports of the 12th International Congress of Non-Ferrous Metals and Minerals – 2024. Krasnoyarsk: 2024. P. 897—899. (In Russ.).

Крупнов Л.В., Пахомов Р.А., Каверзин А.В., Косов Я.И., Малахов П.М. Изучение свойств промежуточного слоя печей Ванюкова при переработке медного никельсодержащего сырья. В сб.: *Сборник докладов 12-го международного конгресса Цветные Металлы и Минералы — 2024.* (Красноярск, 09—13 сентября 2024 г.). Красноярск: Научно-инновационный центр, 2024. С. 883—888.

Information about the authors

Leonid V. Krupnov – Cand. Sci. (Eng), Chief Metallurgist, Head for Process Planning and Monitoring at the Science and Technology Department, Polar Division of PJSC «MMC «Norilsk Nickel»; Associate Professor at the Department of Non-Ferrous Metallurgy, N.M. Fedorovsky Polar State University.
https://orcid.org/0009-0008-7451-9610
E-mail: KrupnovLV@nornik.ru

Roman A. Pakhomov – Cand. Sci. (Eng), Senior Researcherof the Department of Research and Development of the Pyrometallurgy laboratory, LLC Gipronikel Institute.
https://orcid.org/0000-0002-9099-8059
E-mail: Pakhomovra@gmail.com

Anton V. Kaverzin – Senior Lecturer, Department of Non-Ferrous Metallurgy, N.M. Fedorovsky Polar State University.
https://orcid.org/0009-0001-4985-0044
E-mail: KaverzinAV@norvuz.ru

Yaroslav I. Kosov – Cand. Sci. (Eng), Researcher, Department of Research and Development of the Pyrometallurgy laboratory, LLC Gipronikel Institute.
https://orcid.org/0000-0001-7993-2799
E-mail: KosovYaI@nornik.ru

Pavel V. Malakhov – Main Engineer, Center for Engineering Support of Production, Polar Division of PJSC «MMC «Norilsk Nickel».
https://orcid.org/0009-0006-7189-5616
E-mail: MalakhovPV@nornik.ru

Информация об авторах

Леонид Владимирович Крупнов – к.т.н., гл. металлург, начальник управления технологического планирования и контроля научно-технического департамента, Заполярный филиал ПАО «ГМК «Норильский никель»; доцент кафедры металлургии цветных металлов, Заполярный государственный университет им. Н.М. Федоровского.
https://orcid.org/0009-0008-7451-9610
E-mail: KrupnovLV@nornik.ru

Роман Александрович Пахомов – к.т.н., ст. науч. сотрудник департамента по исследованиям и разработкам лаборатории пирометаллургии, ООО «Институт Гипроникель».
https://orcid.org/0000-0002-9099-8059
E-mail: Pakhomovra@gmail.com

Антон Викторович Каверзин – ст. преподаватель кафедры металлургии цветных металлов, Заполярный государственный университет им. Н.М. Федоровского.
https://orcid.org/0009-0001-4985-0044
E-mail: KaverzinAV@norvuz.ru

Ярослав Игоревич Косов – к.т.н., науч. сотрудник департамента по исследованиям и разработкам лаборатории пирометаллургии, ООО «Институт Гипроникель.
https://orcid.org/0000-0001-7993-2799
E-mail: KosovYaI@nornik.ru

Павел Вячеславович Малахов – гл. инженер Центра инженерного сопровождения производства, Заполярный филиал ПАО «ГМК «Норильский никель».
https://orcid.org/0009-0006-7189-5616
E-mail: MalakhovPV@nornik.ru

Contribution of the authors

L.V. Krupnov – development of the main concept, scientific supervision, formulation of the research goals and objectives, preparation of the manuscript, formulation of conclusions.

R.A. Pakhomov – thermodynamic modeling, supervision of experimental studies (TGA, DTA, SEM, EPMA, etc.), contribution to manuscript preparation.

A.V. Kaverzin – experiment setup and execution, thermodynamic calculations, analysis of experimental results.

Ya.I. Kosov – text editing and formatting, analysis of research results, refinement of conclusions.

P.V. Malakhov – resource support, planning and execution of experiments, contribution to the conceptual framework, formulation of research goals and objectives, manuscript writing, and conclusion development.

Вклад авторов

Л.В. Крупнов – формирование основной концепции, научное руководство, постановка цели и задачи исследования, подготовка текста, формулировка выводов.

Р.А. Пахомов – осуществление расчетов, курирование проведения экспериментальных исследований (ТГА и ДТА, РЭМ и РСМА и др.), подготовка текста статьи.

А.В. Каверзин – подготовка и проведение экспериментов, выполнение расчетов, анализ результатов исследований.

Я.И. Косов – корректировка и оформление текста, анализ результатов исследований, корректировка выводов.

П.В. Малахов – обеспечение ресурсами, подготовка и проведение экспериментов, формирование основной концепции, постановка цели и задачи исследования, подготовка текста, формулировка выводов.

The article was submitted 23.08.2024, revised 20.11.2024, accepted for publication 25.11.2024

Статья поступила в редакцию 23.08.2024, доработана 20.11.2024, подписана в печать 25.11.2024

UDC 66.087.97
https://doi.org/10.17073/0021-3438-2025-2-19-29

Research article
Научная статья

Spectroscopic study of MA-41P and MK-40 membranes in electromembrane purification of process solutions containing cobalt, copper, and cadmium ions

O.V. Dolgova, S.I. Lazarev, M.I. Mihaylin

Tambov State Technical University
106 Sovetskaya Str., Tambov 392000, Russia

✉ Olga V. Dolgova (o.v.dolgova@mail.ru)

Abstract: Infrared (IR) spectra were obtained for the surface layer of heterogeneous membranes — cation-exchange MK-40 and anion-exchange MA-41P — widely used in electromembrane processes. Spectra were recorded for air-dry, statically water-saturated, and operational (dynamically water-saturated) membrane samples. Dynamic water saturation was achieved during the electrodeionization purification of a solution containing cobalt, copper, and cadmium ions. Water saturation was found to increase the intensity and bandwidth of the absorption band at $\nu = 3000 \div 3700$ cm^{-1}, corresponding to the OH stretching vibration region. The appearance of an additional peak at $\nu \approx 3287$ cm^{-1} was attributed to the formation of stronger hydrogen bonds in the membrane pore space. The absence of shifts in the absorption bands corresponding to the membrane matrix components under air-dry, statically, and dynamically saturated conditions indicates their chemical stability. In the MA-41P membrane, after use in electrodeionization, changes were observed in both the intensity and position of absorption peaks in the $\nu \approx 1220 \div 1000$ cm^{-1} region, associated with the functional groups of the anion exchanger. The observed spectral changes were evaluated by calculating the normalized peak intensities of the absorption bands. It was shown that in the dynamically water-saturated state, both MK-40 and MA-41P membranes exhibit a reduction in the amount of weakly bound ("free") water and the formation of stronger hydrogen bonds. The results of optical density calculations for characteristic polyethylene absorption bands — the main component of the membrane matrix — are presented. Changes in optical density upon water saturation indicate conformational rearrangements of polyethylene macromolecules. The amounts of chemically unbound solute components retained within the membrane volume were quantified; these species do not affect the membranes' chemical stabiliy or operational performance.

Keywords: MK-40 membrane, MA-41P membrane, IR spectrum, water saturation, metal ions.

Acknowledgments: This study was carried out within the framework of the state assignment of the Ministry of Science and Higher Education of the Russian Federation, project No. FEMU-2024-0011.

For citation: Dolgova O.V., Lazarev S.I., Mihaylin M.I. Spectroscopic study of MA-41P and MK-40 membranes in electromembrane purification of process solutions containing cobalt, copper, and cadmium ions. *Izvestiya. Non-Ferrous Metallurgy*. 2025;31(2):19–29. https://doi.org/10.17073/0021-3438-2025-2-19-29

Спектроскопические исследования мембран МА-41П и МК-40 в процессе электромембранной очистки технологических растворов от ионов кобальта, меди и кадмия

О.В. Долгова, С.И. Лазарев, М.И. Михайлин

Тамбовский государственный технический университет
Россия, 392000, г. Тамбов, ул. Советская, 106

✉ Ольга Валерьевна Долгова (o.v.dolgova@mail.ru)

Аннотация: Получены ИК-спектры поверхностного слоя гетерогенных мембран: катионообменной МК-40 и анионообменной МА-41П, широко применяемых в электромембранных процессах. Спектры представлены для воздушно-сухого, статически и динамически водонасыщенного образцов мембран. Динамическое водонасыщение проводилось в процессе электродиионизационной очистки раствора, содержащего ионы кобальта, меди и кадмия. Выявлено, что изменения в спектрах мембран, происходящие в результате водонасыщения, приводят к увеличению интенсивности и ширины полосы поглощения $\nu = 3000 \div 3700$ см$^{-1}$ в диапазоне валентных колебаний OH$^-$-групп. Появление дополнительного максимума при $\nu \sim 3287$ см$^{-1}$ обусловлено образованием более прочных водородных связей в поровом пространстве мембран. Отсутствие смещения полос поглощения, определяющих соединения, составляющие матрицу мембран в воздушно-сухом, статически и динамически водонасыщенных состояниях, указывает на их химическую стабильность. Установлены изменения интенсивности и частоты поглощения пиков в диапазоне $\nu \sim 1220 \div 1000$ см$^{-1}$, отвечающем за идентификацию функциональной группы анионита, для образца МА-41П после его использования в процессе электромембранной очистки. Наблюдаемые изменения в ИК-спектрах мембран оценивались на основании расчета приведенных пиковых интенсивностей полос поглощения. Установлено, что в мембранах МК-40 и МА-41П в динамически водонасыщенном состоянии уменьшается количество слабосвязанной «жидкой воды» и образуются более прочные водородные связи. Представлены результаты расчета оптической плотности характеристических полос поглощения полиэтилена, входящего в состав матрицы мембран. Показано изменение оптической плотности при водонасыщении, указывающее на конформационную перестройку в волокнах полиэтилена. Установлено количество химически не связанных компонентов разделяемого раствора, задерживающихся в объеме мембран и не оказывающих влияние на их эксплуатационные характеристики.

Ключевые слова: мембрана МК-40, МА-41П, ИК-спектр, водонасыщение, ионы металлов.

Благодарности: Работа выполнена в рамках государственного задания Министерства науки и высшего образования Российской Федерации, проект № FEMU-2024-0011.

Для цитирования: Долгова О.В., Лазарев С.И., Михайлин М.И. Спектроскопические исследования мембран МА-41П и МК-40 в процессе электромембранной очистки технологических растворов от ионов кобальта, меди и кадмия. *Известия вузов. Цветная металлургия.* 2025;31(2):19–29. https://doi.org/10.17073/0021-3438-2025-2-19-29

Introduction

Electromembrane systems are used for the desalination of solutions and for the removal of electrically conductive contaminants from wastewater. Cation- and anion-exchange membranes act as selective barriers that allow the passage of cations and anions, respectively. Based on microstructural differences, ion-exchange membranes are classified into two types: heterogeneous and homogeneous [1]. Heterogeneous membranes are produced by combining ion-exchange and polymer resin powders (mainly inert polymers), followed by hot pressing to form a film [2; 3]. Compared to homogeneous membranes, they exhibit superior mechanical strength, chemical stability, and lower production cost [4], although homogeneous membranes provide better electrochemical performance [5].

Studying the structure and properties of membranes is essential for determining the optimal operating conditions of electrodialysis units, improving membrane permeability, and enhancing ion selectivity. Research into membrane performance, including that of the domestically manufactured MK-40 and MA-41P grades — especially relevant following the cessation of foreign supplies and the absence of viable alternatives — is aimed at optimizing the technological parameters of electromembrane systems.

In [6], the authors presented the chronopotentiogram and *X*-ray diffraction pattern of the MA-41P membrane, both unused and after operation. These techniques were employed to investigate scale formation on the membrane surface. In [7], the surface of the MA-41P membrane was modified using polyelectrolytes, and the samples were analyzed before and after modification using scanning electron microscopy and *X*-ray fluorescence spectroscopy. Current-voltage characteristics of the membranes were also obtained. It was shown that chemical surface modification led to an increase in the concentration of quaternary ammonium groups and a decrease in secondary and tertiary amine groups in the conductive surface layer, thereby enhancing electroconvection and significantly increasing the transport rate of salt counter-ions across the membrane.

The study in [8] examined the effect of ammonium nitrate solutions on the structural and kinetic parameters of MK-40 and MA-41 membranes. Membrane resistance was measured using a contact potential difference method. In [9], during the separation of phenylalanine and sodium chloride using MK-40, MA-40, and MA-41 membranes, it was shown that simultaneous use of strongly acidic and strongly basic membranes was more effective for demineralization compared to membranes with moderate basicity. Separation efficiency was assessed via spectrophotometric methods.

The study of membranes using infrared (IR) spectroscopy provides detailed information on the structure and properties of their surface layers, as well as on conformational rearrangements of the bonds within the polymer chains that make up the membrane. This method is widely used to identify organic contaminants on membrane surfaces after electrodeionization [10; 11], as well as to evaluate the effectiveness of membrane cleaning procedures [12; 13]. In the development of new cation- and anion-exchange membranes, IR spectroscopy is applied to confirm cross-linking reactions between reagents [14—16] or to assess surface modifications of widely used commercial membranes [17; 18]. This method is also used to determine the structure and surface properties of membrane surface layers [19; 20].

The aim of the present study was to investigate the structure of heterogeneous MK-40 and MA-41P membranes using IR spectroscopy and to determine the amount of not chemically bound metal ions in the cation-exchange membrane and sulfate ions in the anion-exchange membrane. The samples examined included air-dry, water-saturated, and operational (dynamically saturated during electrodeionization-based purification of aqueous copper, cobalt, and cadmium sulfate solutions) membranes.

Experimental procedure

The materials studied were industrially manufactured heterogeneous ion-exchange membranes produced in Russia by Shchekinoazot JSC, according to Technical Specifications TU 2255-001-95746392-2012: the strongly acidic cation-exchange membrane MK-40 and the strongly basic anion-exchange membrane MA-41P. Their properties are summarized in Table 1. These monopolar, weakly cross-linked heterogeneous membranes are intended for water treatment applications. The composite membrane layers are composed of polyethylene and nylon. The ion-exchange component of MK-40 is the strongly acidic cation-exchange resin KU-2, synthesized by sulfonation of a styrene copolymer containing 8 % divinylbenzene. In the MA-41P membrane, the ion-exchange component is the strongly basic anion-exchange resin AV-17-2, obtained via chloromethylation of a styrene copolymer with 2 % divinylbenzene, followed by amination with trimethylamine. The two membranes are similar in composition and structure, differing only in the type of functional group and, consequently, in their counter-ions.

Samples were prepared in three states: air-dry, statically water-saturated, and operational (i.e., dynamically saturated during electrodeionization). The MK-40 and MA-41P membranes in the operational state were used as part of an electrodeionization module in a laboratory setup designed for the separation of a multicomponent solution containing copper sulfate (15 mg/dm^3), cobalt sulfate (20 mg/dm^3), and cadmium sulfate (20 mg/dm^3). These concentrations simulate industrial electroplating wastewater. The solution had a pH of 3.2.

Membrane samples were cut from regions with the most uniform thickness. Water-saturated samples were equilibrated in deionized water for 2 h, followed by gentle blotting of surface moisture with filter paper. Operational membrane samples were rinsed with deionized water and blotted dry in the same manner. All samples were stored in a desiccator at 20 °C. Infrared (IR) spectra were collected using a Jasco FT/IR 6700 Fourier-transform infrared spectrometer (JASCO International Co., Ltd., Japan) over the range of $\nu = 500 \div 4000$ cm^{-1}, with a resolution of 4 cm^{-1} and 32 scans.

Ion desorption from the membranes was carried out as follows. Operational membrane samples without any visible damage, stains, or deposits were used in the experiment. For the desorption procedure, operational ion-exchange membrane samples with the most uniform thickness were selected. Each used membrane sample, previously employed in electrodeionization-based separation of copper, cobalt, and cadmium sulfate solutions, was placed in a 500 cm^3 vessel filled with distilled wa-

Table. 1. **Properties of the studied membranes**

Таблица 1. Характеристики исследуемых мембран

Parameter	MK-40	MA-41P
Ion-exchange group	$-SO_3H$ (sulfo group)	$-N+(CH_3)_3$ (quaternary ammonium base)
Counter-ion	Na^+	Cl^-
Moisture content, max, %	40 ± 5	31.2 ± 1
Ion-exchange capacity, mmol/cm^3	1.58 ± 0.06	0.92 ± 0.02
Thickness, μm	535 ± 10	535 ± 10

ter. Every 24 h, the sample was transferred to a fresh vessel with distilled water. Desorption was conducted over a period of four days, which was sufficient for the complete release of retained substances from the membranes. The concentration of substances transferred into the distilled water was determined daily in the used solution by photometric methods (for metal cations) and titrimetric analysis (for sulfates). Based on the obtained data, the concentrations of substances distributed within the membrane volume were calculated.

Results and discussion

The results obtained, presented in Figs. 1 and 2, provide information on the functional groups present in the studied membranes and their structural features, which is essential for understanding the processes involved in electromembrane treatment of solutions containing non-ferrous metal ions.

Fig. 1 shows the infrared (IR) spectra of MA-41P anion-exchange membrane samples in three states: air-dry, statically water-saturated, and operational (dynamically water-saturated). All spectra contain distinct characteristic absorption bands corresponding to functional groups of the membrane components, including C—H, O—H, aromatic (C_6H_6), and N—C groups [21—23].

Polyethylene, a component of the membrane matrix, is identified by asymmetric (ν ~ 2914 cm^{-1}) and symmetric (ν ~ 2846 cm^{-1}) C—H stretching vibrations. The doublet at $\nu \approx$ 1472 and 1470 cm^{-1} corresponds to asymmetric and symmetric C—H scissoring vibrations. Asymmetric and symmetric rocking vibrations of crystalline polyethylene are observed at $\nu \approx$ 717 and 714 cm^{-1}.

Minor stretching vibrations in the range of ν = = 3900÷3600 cm^{-1} observed in all spectra are attributed to trace amounts of water. A broad absorption band at ν = 3600÷3100 cm^{-1} corresponds to water associates exhibiting various hydrogen bond energies. The minimum at $\nu \approx$ 1646 cm^{-1} is associated with the bending vibrations of —OH groups in hydration water.

The absorption band at $\nu \approx$ 1541 cm^{-1} corresponds to stretching vibrations of conjugated C=C bonds in the benzene ring. In-plane deformation vibrations of C—H and C—C groups of a disubstituted benzene ring are observed at $\nu \approx$ 900, 830, and 770 cm^{-1}. The increased intensity of these bands in the water-saturated sample is explained by the higher water content.

Weak absorption bands in the range of ν = 1250÷ ÷950 cm^{-1} (at approximately 1218, 1114, 1040, and 975 cm^{-1}) correspond to quaternary trimethylammonium groups, which are the principal functional groups of the anion-exchange resins used in the membrane. Additional weak peaks at $\nu \approx$ 890 and 825 cm^{-1} are associated with C—N vibrations adjacent to the benzene ring.

The weak vibrations detected in the $\nu \approx$ 2350÷ ÷2255 cm^{-1} range for all membrane samples are due to the absorption of atmospheric CO during sample preparation.

The IR spectrum of the cation-exchange membrane (Fig. 2) shows substantial overlap with that of the MA-41P anion-exchange membrane over a broad spectral range. Differences are observed in the regions of $\nu \approx$ 1300÷800 cm^{-1} and 700÷600 cm^{-1}, where the peaks correspond to vibrations associated with the presence of sulfonic acid groups in the membrane structure.

The bands at $\nu \approx$ 1171, 1122, 1036, and 1006 cm^{-1}

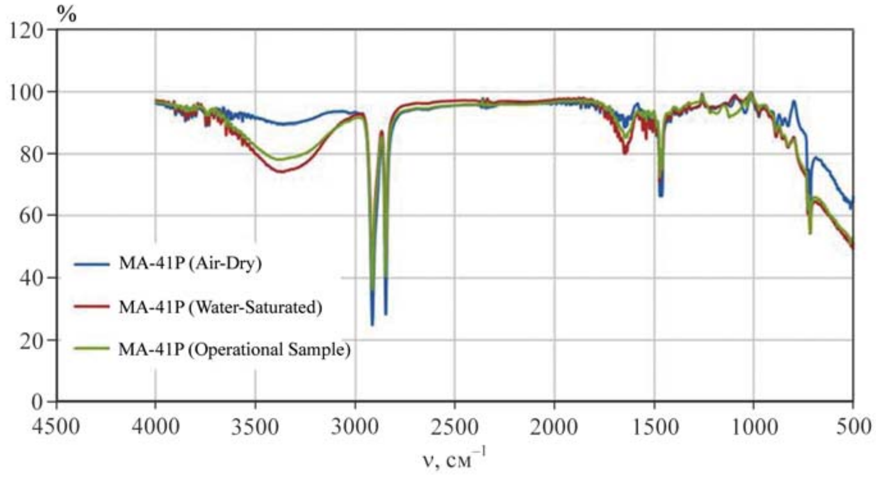

Fig. 1. IR spectra of MA-41P membrane samples

Рис. 1. ИК-спектрограмма образцов мембран МА-41П

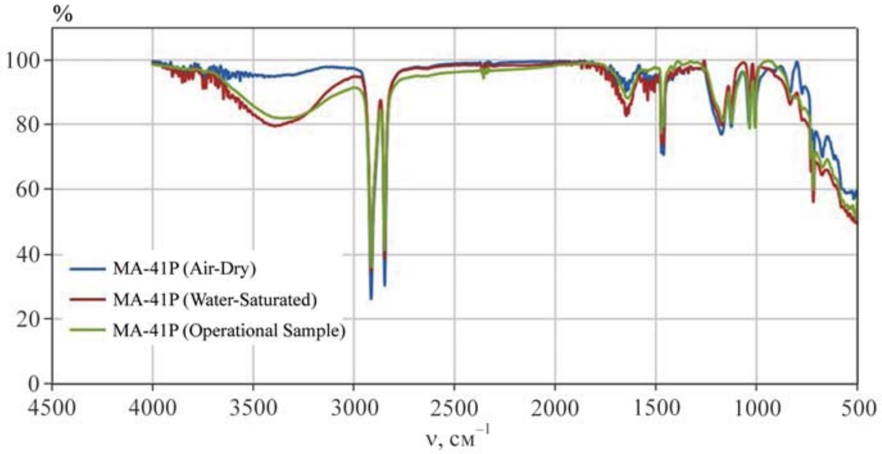

Fig. 2. IR spectra of MK-40 membrane samples

Рис. 2. ИК-спектрограмма образцов мембран МК-40

correspond to the asymmetric and symmetric stretching vibrations of sulfonic acid group atoms. The bands at $\nu \approx 671$ and 618 cm^{-1} are attributed to bending vibrations of C—S bonds attached to benzene rings.

A comparison of the IR spectra in the $\nu = 1500 \div 600$ cm^{-1} region of the studied samples provides insight into the chemical stability of the macromolecular structure in the active layer of the membranes. For MK-40, the spectra show complete agreement in the frequencies of the absorption bands corresponding to the structural elements of the functional groups, without any detectable shifts. In contrast, for MA-41P, a shift in peaks is observed in the range of $\nu \approx 1220 \div 1000$ cm^{-1} in the operational membrane compared to the air-dry and statically water-saturated samples. Both the intensity and frequency of the absorption bands are altered. This spectral region is characteristic of the quaternary ammonium groups that serve as the membrane's ion-exchange sites.

Changes in the spectrum are characterized by a shift in peaks, but they do not disappear completely. It is known [23] that trimethylamine forms water complexes with a symmetric top configuration, where the water molecule is able to rotate freely about the symmetry axis defined by the trimethylamine moiety. The observed shifts and changes in band intensity in this range are likely related to displacement of the trimethylamine symmetry axis caused by bond rearrangements under dynamic exposure.

A comparison of the IR spectra (Figs. 1 and 2) in the OH stretching vibration region ($\nu \approx 3000 \div 3700$ cm^{-1}) for water-saturated and air-dry membranes indicates a substantial increase in the full width at half maximum (FWHM) of the absorption band at $\nu \approx 3392$ cm^{-1} (see Table 2), along with asymmetry in the band shape and the clear appearance of an additional peak at $\nu \approx 3287$ cm^{-1} in the water-saturated membranes. Additionally, the intensity and FWHM of the absorption band at $\nu \approx 1646$ cm^{-1}, corresponding to H—O—H bending vibrations of water molecules, increase as well. A comparative analysis of OH vibration frequencies and calculated hydrogen bond energies for MK-40 and MA-41P membranes is provided in Table 2.

The hydrogen bond energy was calculated using the equation [24]

$$E_{OH} = \frac{1}{K}\frac{\nu_0 - \nu}{\nu_0},$$

where $\nu_0 = 3650$ cm^{-1} is the absorption frequency of a free hydroxyl group, ν is the observed absorption frequency of the hydrogen-bonded OH group, and $1/K = 2.625 \cdot 10^2$ kJ/mol is the equilibrium constant.

The maximum absorption band for both membranes is observed at $\nu = 3392$ cm^{-1}, with a full width at half maximum (FWHM) of 403 for MK-40 and 424 for MA-41P. This frequency is significantly lower than that of a free OH group ($\nu_0 = 3650$ cm^{-1}), indicating hydrogen bonding. The similar peak intensities across all membrane types reflect the stability of the membrane matrix under both static and dynamic water saturation. The appearance of an additional low-frequency peak in the water-saturated membranes suggests the formation of stronger hydrogen bonds

Undoubtedly, these spectral features indicate that pore-confined water OH groups interact with all components of the membranes' polymer system, forming energetically diverse hydrogen bonds.

To assess the observed changes in the IR spectra, normalized peak intensities at $\nu = 1646$, 2846, and 3550 cm^{-1} were monitored relative to the C—H bending

Table. 2. **Observed frequencies of OH stretching vibrations in MK-40 and MA-41P membranes at 20 °C**

Таблица 2. Наблюдаемые частоты валентных колебаний OH-групп мембран МК-40 и МА-41П при температуре 20 °С

Parameter	MK-40			MA-41P		
	Air-dry	Water-saturated	Operational	Air-dry	Water-saturated	Operational
ν_1, cm^{-1} (FWHM)	3392 (160)	3392 (403)	3392 (356)	3392 (170)	3392 (424)	3392 (360)
E_{OH}, kJ/mol	19.97	19.97	19.97	19.97	19.97	19.97
$\nu_{д}$, cm^{-1}	–	3285	3289	–	3288	3284
E_{OH}, kJ/mol	–	29.41	28.81	–	28.9	29.26
ν_2, cm^{-1} (FWHM)	1646 (48)	1646 (64)	1635 (58)	1646 (56)	1646 (73)	1646 (71)

Table. 3. **Relative absorption band intensities of MK-40 and MA-41P membranes at 20 °C**

Таблица 3. Относительная интенсивность полос поглощения мембран МК-40 и МА-41П при температуре 20 °С

Parameter	MK-40			MA-41P		
	Air-dry	Water-saturated	Operational	Air-dry	Water-saturated	Operational
$I(1646)/I(1472)$	0.33	0.67	0.44	0.32	0.77	0.42
$I(2846)/I(1472)$	2.53	2.57	2.26	2.48	2.6	2.6
$I(3550)/I(1472)$	0.07	0.45	0.23	0.03	0.59	0.42

vibration at $\nu = 1472$ cm^{-1} (expressed as $I(X)/I(1472)$). The frequency at 3550 cm^{-1} corresponds to weakly bound or "free" water [25]. The results are presented in Table 3. These data show that the relative intensity of all analyzed absorption bands increases in statically water-saturated membranes compared to air-dry samples, while in dynamically saturated membranes it decreases relative to the statically saturated ones. Based on these results, it can be concluded that in the pore space of the active layer, static water saturation leads to an increased amount of weakly bound (liquid-like) water, whereas in dynamically saturated membranes, this fraction decreases and is replaced by more strongly bound water. This indicates minor structural changes within the membrane matrix.

Polyethylene serves as the base material of the MK-40 and MA-41P membrane matrices. Upon water saturation, conformational changes occur in its macromolecular structure, as indicated by variations in the optical density of characteristic absorption bands. The bands at 1472 cm^{-1} (CH_2 scissoring vibrations) and 717 cm^{-1} (CH_2 rocking vibrations) are considered characteristic for polyethylene [26].

Optical density was calculated using the formula:

$$D = \lg (I_0/I),$$

where I_0 and I are the intensities of the incident and transmitted radiation, respectively, determined using the baseline method. Table 4 presents the calculated values for these characteristic bands.

Upon water saturation, the optical density of the membranes decreased and remained unchanged under dynamic conditions. These results indicate conformational rearrangements of polyethylene macromolecules due to water uptake, caused by the redistribution of bonds involving CH_2 groups within the polymer structure in the presence of adsorbed water. The similar optical density values observed for water-saturated and operational samples suggest that conformational changes in the polyethylene macromolecules result primarily from water saturation and are not caused by the potential difference applied across the membrane.

The electrodeionization process is accompanied by the sorption of solutes from the solution onto the membrane surfaces [27; 28]. The obtained results show that fouling of the membranes by extractable

Table. 4. **Optical density variation in MK-40 and MA-41P membranes at 20 °C**

Таблица 4. Изменение оптической плотности мембран МК-40 и МА-41П при температуре 20 °C

Показатель	MK-40			MA-41P		
	Air-dry	Water-saturated	Operational	Air-dry	Water-saturated	Operational
ν_1, cm^{-1}	1472	1472	1471	1472	1472	1472
D	0.12	0.11	0.1	0.13	0.09	0.09
ν_2, cm^{-1}	717	717	717	717	717	717
D	0.091	0.087	0.077	0.11	0.08	0.08

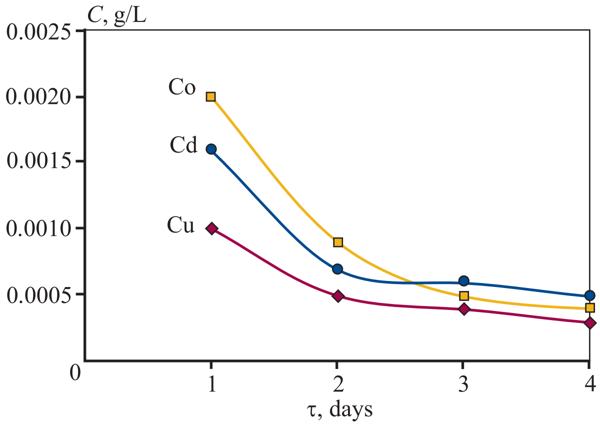

Fig. 3. Desorption of metal ions from the MK-40 cation-exchange membrane into distilled water at 20 °C

Рис. 3. Десорбция металлов из катионообменной мембраны МК-40 в дистиллированную воду при температуре 20 °C

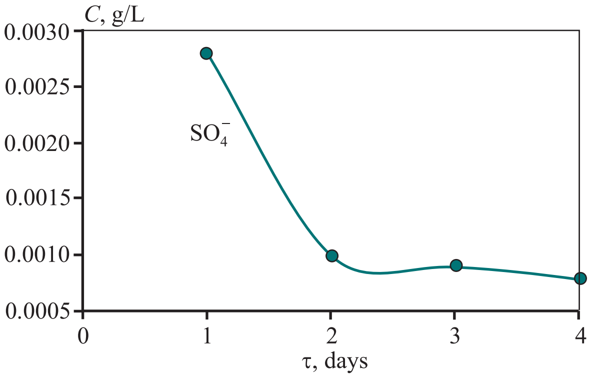

Fig. 4. Desorption of sulfate ions from the MA-41P anion-exchange membrane into distilled water at 20 °C

Рис. 4. Десорбция сульфат-ионов из анионообменной мембраны МА-41П в дистиллированную воду при температуре 20 °C

components does not affect their structure or chemical stability.

To assess desorption, the amounts of copper, cobalt, and cadmium ions, as well as sulfate ions, that were not chemically bound to the membrane components but were retained during electrodeionization and had no effect on the membranes' operational characteristics were determined (Figs. 3 and 4).

The desorption profiles of metal and sulfate ions from the MK-40 cation-exchange and MA-41P anion-exchange membranes consistently show a rapid release during the first 24 h, followed by a gradual decrease over the next three days. The difference in concentrations of desorbed Cu^{2+}, Cd^{2+}, and Co^{2+} is attributed to the selectivity of the KU-2 cation-exchange resin used in the MK-40 membrane. The amounts of unbound metals retained in MK-40 were 0.11 mg/g of copper, 0.17 mg/g of cadmium, and 0.19 mg/g of cobalt. The amount of sulfate retained in the MA-41P membrane was 0.26 mg/g of membrane mass.

Conclusion

1. Infrared spectral analysis demonstrated that the matrices of the MK-40 and MA-41P membranes retain their chemical stability after the electromembrane purification of process solutions from cobalt, copper, and cadmium ions, and do not undergo degradation under the influence of the applied potential difference or components of the treated solution.

2. The macromolecules in the active layer of the MK-40 membrane remain stable, whereas in the active layer of the MA-41P sample, dynamic water saturation leads to a rearrangement of bonds within the ion-exchange group (quaternary ammonium bases). These changes indicate that anion-exchange membranes should be replaced more frequently than cation-exchange membranes in order to maintain the performance characteristics of the electromembrane separation process for copper, cadmium, and cobalt solutions.

3. Static water saturation of the membranes results in an increased amount of weakly bound water in the pore space of the active layer, whereas dynamic saturation is characterized by a decrease in weakly bound water and the formation of stronger hydrogen bonds, indicating minor structural changes in the membrane matrices.

4. In the polyethylene that forms the basis of the MK-40 and MA-41P membrane matrices, water saturation causes a redistribution of bonds involving CH_2 functional groups and, accordingly, a conformational rearrangement of the macromolecules. The similar calculated optical density values for water-saturated and operational membrane samples suggest that this rearrangement is due to water saturation and is not related to the effect of the applied potential difference or the presence of metal sulfates from the treated solution.

5. The amount of chemically unbound metals sorbed within the volume of the MK-40 cation-exchange membrane was 0.11 mg/g for copper, 0.17 mg/g for cadmium, and 0.19 mg/g for cobalt. The amount of sulfate retained in the MA-41P membrane was 0.26 mg/g relative to the membrane's mass. Thus, the transfer of contaminant components from the treated solution into the volume of the membranes does not affect their chemical stability.

References

1. Shaoxiang Leeabc, Wenqiao Mengabc, Yupeng Wangd, Dong Wang, Meng Zhang, Guohui Wang, Jiaji Cheng, Yue Zhou, Wenjuan Qu. Comparison of the property of homogeneous and heterogeneous ion exchange membranes during electrodialysis process. *Ain Shams Engineering Journal*. 2021;12(1):159—166. https://doi.org/10.1016/j.asej.2020.07.018
2. Jaime-Ferrer J.S., Mosqueda-Quintero M., Suárez-Toriello V.A., Anderson S.M., González Vargas O.A., Villafaña-López L. Heterogeneous PVC cation-exchange membrane synthesis by electrospinning for reverse electrodialysis. *International Journal of Chemical Reactor Engineering*. 2020;18(7):20200020. https://doi.org/10.1515/ijcre-2020-0020
3. Zhao X., Liu L., Zhang X., Cheng X., Sun J., Pan J. Preparation of high-performance semihomogeneous cation exchange membranes for electrodialysis via solvent-free polyethylene particle-confined monomer polymerization. *Industrial & Engineering Chemistry Research*. 2023;62(14):5945—5953. https://doi.org/10.1021/acs.iecr.2c04475
4. Kikhavani T., Ashrafizadeh S.N., Van der Bruggen B. Identification of optimum synthesis conditions for a novel anion exchange membrane by response surface methodology. *Journal Applied Polymer Science*. 2014;133(3):39888. https://doi.org/10.1002/app.39888
5. Xu T. Ion exchange membranes: state of their development and perspective *Journal of Membrane Science*. 2005; 263(1-2):1—29. https://doi.org/10.1016/j.memsci.2005.05.002
6. Butyl'skiy D.Yu., Troickiy V.A., Skudarnova A.S., Sharafan M.V. Sedimentation on the surface of the anion exchange membrane MA-41P in the concentration chamber of the electrodialyzer during the processing of dilute imitates of reservoir waters. *Membrany i membrannye tekhnologii*. 2022;12(5):384—395. (In Russ.). https://doi.org/10.31857/S2218117222050030
   Бутыльский Д.Ю., Троицкий В.А., Скударнова А.С., Шарафан М.В. Осадкообразование на поверхности анионообменной мембраны МА-41П в камере концентрирования электродиализатора при переработке разбавленных имитатов пластовых вод. *Мембраны и мембранные технологии*. 2022;12(5):384—395. https://doi.org/10.31857/S2218117222050030
7. Pis'menskaya N.D., Mareeva S.A., Pohidnya E.V., Larshe K., Dammak L., Nikonenko V.V. The effect of surface modification of a heterogeneous anion exchange membrane on the intensity of electroconvection at its surface. *Elektrohimiya*. 2019;55(12):1471—1489. (In Russ.). https://doi.org/10.1134/S0424857019120132
   Письменская Н.Д., Мареева С.А., Похидня Е.В., Ларше К., Даммак Л., Никоненко В.В. Влияние модификации поверхности гетерогенной анионообменной мембраны на интенсивность электроконвекции у ее поверхности. *Электрохимия*. 2019;55(12):1471—1489. https://doi.org/10.1134/S0424857019120132
8. Niftaliev S.I., Kozaderova O.A., Vlasov YU.N., Kim K.B., Matchina K.S. Structural and kinetic parameters of MK-40 and MA-41 ion exchange membranes in ammonium nitrate solutions. *Sorbcionnye i hromatograficheskie processy*. 2015;15(5):708—713. (In Russ.). https://doi.org/10.17308/sorpchrom.2015.15/324
   Нифталиев С.И., Козадерова О.А., Власов Ю.Н., Ким К.Б., Матчина К.С. Структурно-кинетические параметры ионообменных мембран МК-40 и МА-41 в растворах нитрата аммония. *Сорбционные и хроматографические процессы*. 2015;15(5):708—713. https://doi.org/10.17308/sorpchrom.2015.15/324

9. Saud A.M., Vasil'eva V.I., Goleva E.A., Akberova E.M., Kozlov A.T. The choice of an anion exchange membrane during the separation of phenylalanine and sodium chloride by neutralization dialysis. *Sorbcionnye i khromatograficheskie processy*. 2020;20(6):749—759. (In Russ.).
https://doi.org/10.17308/sorpchrom.2020.20/3143
Сауд А.М., Васильева В.И., Голева Е.А., Акберова Э.М., Козлов А.Т. Выбор анионообменной мембраны при разделении фенилаланина и хлорида натрия нейтрализационным диализом. *Сорбционные и хроматографические процессы*. 2020;20(6):749—759.
https://doi.org/10.17308/sorpchrom.2020.20/3143
10. Dammak L., Fouilloux J., Bdiri M., Larchet C., Renard E., Baklouti L., Pismenskaya N. A review on ion-exchange membrane fouling during the electrodialysis process in the food industry. Part 1: Types, effects, characterization methods, fouling mechanisms and interactions. *Separation and Purification Technology*. 2021;199:114—123. https://doi.org/10.3390/membranes11100789
11. Bdiri M., Perreault V., Mikhaylin S., Larchet C., Hellal F., Bazinet L., Dammak L. Identification of phenolic compounds and their fouling mechanisms in ion-exchange membranes used at an industrial scale for wine tartaric stabilization by electrodialysis. *Separation and Purification Technology*. 2020;233:115995.
https://doi.org/10.1016/j.seppur.2019.115995
12. Bdiri M., Dammak L., Larchet C., Hellal F., Porozhnyy M., Nevakshenova E., Nikonenko V. Characterization and cleaning of anion-exchange membranes used in electrodialysis of polyphenol-containing food industry solutions; comparison with cation-exchange membranes. *Separation and Purification Technology*. 2019;210:636—650.
https://doi.org/10.1016/j.seppur.2018.08.044
13. Barros K.S., Martí-Calatayud M.C., Pérez-Herranz V., Espinosa D.C.R. A three-stage chemical cleaning of ion-exchange membranes used in the treatment by electrodialysis of wastewaters generated in brass electroplating industries. *Desalination*. 2020;492:114628.
https://doi.org/10.1016/j.desal.2020.114628
14. Villafaña-López L., Reyes-Valadez D.M., González-Vargas O.A., Suárez-Toriello V.A., Jaime-Ferrer J.S. Custom-made ion exchange membranes at laboratory scale for reverse electrodialysis. *Membranes*. 2019;9(11):145.
https://doi.org/10.3390/membranes9110145
15. Cseri L., Baugh J., Alabi A., AlHajaj A., Zou L., Dryfe R.A., Szekely G. Graphene oxide-polybenzimidazolium nanocomposite anion exchange membranes for electrodialysis. *Journal of Materials Chemistry A*. 2018;6(48)^24728—24739.
https://doi.org/10.1039/C8TA09160A
16. Hosseini S.M., Sohrabnejad S., Nabiyouni G., Jashni E., Van der Bruggen B., Ahmadi A. Magnetic cation exchange membrane incorporated with cobalt ferrite nanoparticles for chromium ions removal via electrodialysis. *Journal of Membrane Science*. 2019;583:292—300.
https://doi.org/10.1016/j.memsci.2019.04.069
17. Bonizzoni S., Stucchi D., Caielli T., Sediva E., Mauri M., Mustarelli P. Morpholinium-modified, polyketone-based anion exchange membranes for water electrolysis. *ChemElectroChem*. 2023;10(6):202201077.
https://doi.org/10.1002/celc.202201077
18. Xu X., Lin L., Ma G., Wang H., Jiang W., He Q., Xu P. Study of polyethyleneimine coating on membrane permselectivity and desalination performance during pilot-scale electrodialysis of reverse osmosis concentrate. *Separation and Purification Technology*. 2018;207:396—405. https://doi.org/10.1016/j.seppur.2018.06.070
19. Konovalov D.N., Horohorina I.V., Lazarev S.I., Nagornov S.A., Kornev A.Yu., Kotenev S.I. Spectroscopic and kinetic studies of the permeability of the surface layers of membranes in the process of microfiltration separation of aqueous organic solutions. *Poverhnost'. Rentgenovskie, sinhrotronnye i nejtronnye issledovaniya*. 2023;3:98—104. (In Russ.).
https://doi.org/10.31857/S1028096023030056
Коновалов Д.Н., Хорохорина И.В., Лазарев С.И., Нагорнов С.А., Корнев А.Ю., Котенев С.И. Спектроскопические и кинетические исследования проницаемости поверхностных слоев мембран в процессе микрофильтрационного разделения водно-органических растворов. *Поверхность. Рентгеновские, синхротронные и нейтронные исследования*. 2023;3:98—104.
https://doi.org/10.31857/S1028096023030056
20. Lazarev S.I., Golovin Yu.M., Konovalov D.N., Yanovskaya E.Yu., Rodionov D.A. IR spectroscopic studies of adsorbed water and structural changes in hydrophobic and hydrophilic microfiltration membranes. *Fizikohimiya poverhnosti i zashchita materialov*. 2023;59(2):155—160. (In Russ.).
https://doi.org/10.31857/S0044185623700183
Лазарев С.И., Головин Ю.М., Коновалов Д.Н., Яновская Э.Ю., Родионов Д.А. ИК-спектроскопические

исследования адсорбированной воды и изменения структуры в гидрофобных и гидрофильных микрофильтрационных мембранах. *Физикохимия поверхности и защита материалов.* 2023;59(2):155—160.
https://doi.org/10.31857/S0044185623700183

21. Smith B. The infrared spectra of polymers II: Polyethylene. *Spectroscopy.* 2021;36(9):24—29.
https://doi.org/10.56530/spectroscopy.xp7081p7
22. Wen Y., Liang M., Wang Y., Ren W., Lü X. Perfectly green organocatalysis: quaternary ammonium base triggered cyanosilylation of aldehydes. *Chinese Journal of Chemistry.* 2012;30(9):2109—2114.
https://doi.org/10.1002/cjoc.201200598
23. Tubergen M.J., Kuczkowski R.L. Microwave spectroscopic characterization of a strong hydrogen bond: trimethylamine-water. *Journal of the American Chemical Society.* 1993;115(20):9263—9266.
https://doi.org/10.1021/ja00073a048
24. Lazarev S.I., Golovin Yu.M., Horohorina I.V., Hohlov P.A. Investigation of the structural organization of the surface layer and the state of water in ultrafiltration composite membranes. *Fizikohimiya poverhnosti i zashchita materialov.* 2020;56(2):132—137. (In Russ.).
https://doi.org/10.31857/S0044185620020151
Лазарев С.И., Головин Ю.М., Хорохорина И.В., Хохлов П.А. Исследование структурной организации поверхностного слоя и состояния воды в ультрафильтрационных композиционных мембранах. *Физикохимия поверхности и защита материалов.* 2020;56(2):132—137.
https://doi.org/10.31857/S0044185620020151
25. Sinitsa L.N., Emel'yanov N.M., Lugovskoy A.A., Shcherbakov A.P., Annenkov V.V. Determination of the pore size of silicon materials from the IR spectra of adsorbed water. *Optika atmosfery i okeana.* 2021;34(07):483—487. (In Russ.).
https://doi.org/10.15372/AOO20210701
Синица Л.Н., Емельянов Н.М., Луговской А.А., Щербаков А.П., Анненков В.В. Определение размера пор кремниевых материалов по ИК-спектрам адсорбированной воды. *Оптика атмосферы и океана.* 2021;34(07):483—487.
https://doi.org/10.15372/AOO20210701
26. Dekhant I., Danc R., Kimmer V. Infrared spectroscopy of polymers. Moscow: Khimiya, 1976. 473 p. (In Russ.).
Дехант И., Данц Р., Киммер В. Инфракрасная спектроскопия полимеров. М.: Химия, 1976. 473с.
27. Konovalov D.N., Lazarev S.I., Lua P., Polyansky K.K. Studies of kinetic and sorption characteristics of OPAM-K and OPMN-P membranes in the process of electronanofiltration separation of an aqueous solution of potassium sulfate. *Vestnik VGUIT.* 2023;1(85):24—32. (In Russ.).
https://doi.org/10.20914/2310-1202-2023-1-24-32
Коновалов Д.Н., Лазарев С.И., Луа П., Полянский К.К. Исследования кинетических и сорбционных характеристик мембран ОФАМ-К и ОПМН-П в процессе электронанофильтрационного разделения водного раствора сульфата калия. *Вестник ВГУИТ.* 2023;1(85):24—32.
https://doi.org/10.20914/2310-1202-2023-1-24-32
28. Sarapulova V.V., Klevtsova A.V., Pishevskaya N.D. Electrostatic interactions of ion-exchange materials with anthocyanins in the processes of their sorption and electrodialysis extraction from liquid media. *Membrany i membrannye tekhnologii.* 2020;4(10):281—292. (In Russ.).
https://doi.org/10.1134/S2218117220040100
Сарапулова В.В., Клевцова А.В., Письменская Н.Д. Электростатические взаимодействия ионообменных материалов с антоцианами в процессах их сорбционного и электродиализного извлечения из жидких сред. *Мембраны и мембранные технологии.* 2020;4(10):281—292.
https://doi.org/10.1134/S2218117220040100

Information about the authors

Olga V. Dolgova – Cand. Sci. (Eng.), Senior Lecturer of the Department «Nature Management and Environmental Protection», Tambov State Technical University (TSTU).
https://orcid.org/0009-0000-9588-4897
E-mail: o.v.dolgova@mail.ru

Sergey I. Lazarev – Dr. Sci. (Eng.), Professor, Head of the Department «Mechanics and Engineering Graphics», TSTU.
https://orcid.org/0000-0002-3429-1139
E-mail: sergey.lazarev.1962@mail.ru

Maxim I. Mikhaylin – Postgraduate of the Department «Mechanics and Engineering Graphics», TSTU.
https://orcid.org/0000-0001-7540-5924
E-mail: ckiburs@yandex.ru

Информация об авторах

Ольга Валерьевна Долгова – к.т.н., ст. преподаватель кафедры «Природопользование и защита окружающей среды», Тамбовский государственный технический университет (ТГТУ).
https://orcid.org/0009-0000-9588-4897
E-mail: o.v.dolgova@mail.ru

Сергей Иванович Лазарев – д.т.н., профессор, зав. кафедрой «Механика и инженерная графика», ТГТУ.
https://orcid.org/0000-0002-3429-1139
E-mail: sergey.lazarev.1962@mail.ru

Максим Игоревич Михайлин – аспирант кафедры «Механика и инженерная графика», ТГТУ.
https://orcid.org/0000-0001-7540-5924
E-mail: ckiburs@yandex.ru

Contribution of the authors

O.V. Dolgova – conducted the experiments, participated in the discussion of results, wrote the manuscript.

S.I. Lazarev – defined the research objective and participated in the discussion of results.

M.I. Mihaylin – prepared the initial membrane samples, performed IR analysis, and contributed to the discussion of results.

Вклад авторов

О.В. Долгова – проведение экспериментов, участие в обсуждении результатов, написание текста статьи.

С.И. Лазарев – определение цели работы, участие в обсуждении результатов.

М.И. Михайлин – подготовка исходных образцов, проведение ИК-анализа, участие в обсуждении результатов.

The article was submitted 11.09.2024, revised 05.12.2024, accepted for publication 10.12.2024

Статья поступила в редакцию 11.09.2024, доработана 05.12.2024, подписана в печать 10.12.2024

METALLURGY OF RARE AND PRECIOUS METALS / МЕТАЛЛУРГИЯ РЕДКИХ И БЛАГОРОДНЫХ МЕТАЛЛОВ

UDC 66.021.2.081.3
https://doi.org/10.17073/0021-3438-2025-2-30-40

Research article
Научная статья

Theoretical and experimental justification of kinetic and isotherm equations for gold adsorption from solutions onto activated carbon considering intraparticle mass transfer

V.V. Elshin, A.P. Mironov, A.A. Lisitsyna

Irkutsk National Research Technical University
83 Lermontov Str., Irkutsk 664074, Russia

✉ Anastasia A. Lisitsyna (Gerasimovan19@rambler.ru)

Abstract: This study continues the research presented in our previous article [1], which examined the process of gold adsorption from gold cyanide solutions onto activated carbon (AC) over a relatively short time interval – up to 40 h – during which adsorption occurred predominantly within the near-surface layer of the sorbent. The aim of the present work was to improve the previously developed mathematical model of gold adsorption onto activated carbon from gold cyanide solutions [1] by incorporating the intraparticle mass transfer stage into the model. This goal was achieved by adding an additional term to the adsorption kinetics equation that accounts for gold sorption driven by intraparticle mass transfer. This modification preserved the entire theoretical framework of adsorption described by the earlier kinetics equation, incorporating it as a special case within a more general sorption model based on the improved kinetics equation. An analytical solution to the modified equation was derived, from which a new-type adsorption isotherm was obtained in analytical form. The paper presents the derivation and analysis of this new-type isotherm equation and its identification based on experimental data.

Keywords: gold, kinetics, adsorption, activated carbon (AC), adsorption isotherm, cyanide solution, intraparticle mass transfer rate constant, mathematical modeling.

Acknowledgments: The express their gratitude to the staff of Laboratory No. 15 at Irgiredmet OJSC (Irkutsk) for providing the experimental data on gold adsorption kinetics onto activated carbon and for their assistance in conducting the analyses.

For citation: Elshin V.V., Mironov A.P., Lisitsyna A.A. Theoretical and experimental justification of kinetic and isotherm equations for gold adsorption from solutions onto activated carbon considering intraparticle mass transfer. *Izvestiya. Non-Ferrous Metallurgy.* 2025;31(2):30–40.
https://doi.org/10.17073/0021-3438-2025-2-30-40

Теоретическое и экспериментальное обоснование уравнений кинетики и изотермы сорбции золота из растворов на активированный уголь с учетом внутридиффузионного массопереноса

В.В. Ёлшин, А.П. Миронов, А.А. Лисицына

Иркутский национальный исследовательский технический университет
Россия, 664074, г. Иркутск, ул. Лермонтова, 83

✉ Анастасия Андреевна Лисицына (Gerasimovan19@rambler.ru)

Аннотация: Настоящая работа является продолжением предыдущей статьи [1], в которой рассматривался процесс адсорбции золота из золотоцианистых растворов на активированный уголь (АУ) в течение относительно короткого отрезка времени –

до 40 ч. При этом процесс адсорбции протекал в тонком приповерхностном слое сорбента. Целью данного исследования являлось усовершенствование разработанной нами ранее математической модели адсорбции золота на активированный уголь из золотоцианистых растворов [1] в направлении учета в ней внутридиффузионной стадии массопереноса золота. Поставленная задача была достигнута путем включения в уравнение кинетики адсорбции еще одного члена, описывающего сорбцию золота за счет внутридиффузионного массопереноса. Такая модернизация уравнения кинетики позволила полностью сохранить всю теорию адсорбции, описываемую предыдущим уравнением кинетики, и включить ее как частный случай в более общую теорию сорбции с учетом усовершенствованного уравнения кинетики. Получено аналитическое решение предложенного уравнения, из которого аналитически выводится изотерма нового типа. Приведены вывод и анализ уравнения изотермы нового типа, а также выполнена идентификация по экспериментальным данным.

Ключевые слова: золото, кинетика, сорбция, активированный уголь (АУ), изотерма сорбции, цианистый раствор, константа скорости внутридиффузионного массопереноса, математическое моделирование.

Благодарности: Авторы благодарны сотрудникам лаборатории №15 АО «Иргиредмет» (г. Иркутск) за предоставленные экспериментальные данные по кинетике адсорбции золота на активированный уголь и за содействие в проведении анализов.

Для цитирования: Ёлшин В.В., Миронов А.П., Лисицына А.А. Теоретическое и экспериментальное обоснование уравнений кинетики и изотермы сорбции золота из растворов на активированный уголь с учетом внутридиффузионного массопереноса. *Известия вузов. Цветная металлургия*. 2025;31(2):30–40. https://doi.org/10.17073/0021-3438-2025-2-30-40

Introduction

A significant increase in the duration of gold adsorption from two days or more — as well as the loading of activated carbon (AC) beyond 40—60 % of its total maximum gold capacity, causes the process kinetics to shift toward a stage limited by intraparticle mass transfer[1] [1]. Accordingly, it becomes necessary to derive a new kinetic equation for the adsorption of gold from gold cyanide solutions onto activated carbon, taking into account this limiting factor. The resulting solution must adequately describe the process kinetics both at the near-surface adsorption stage and as it transitions into the stage governed by intraparticle mass transfer. Additionally, the analytical solution should allow for the derivation of the adsorption isotherm equation. oth the kinetic and isotherm equations must be identified using experimental adsorption kinetic curves and isotherm data, based on four physical constants introduced during the development of the kinetic model. These constants, whose numerical values are determined during the identification procedure, must be linked to the specific ionic composition of the solution and to a particular grade of activated carbon. Once identified, they will serve as physical constants under the given conditions and may be used for predictive calculations of both equilibrium adsorption values and kinetic parameters under conditions matching those of the experimental data. The identification of the kinetic equation solution using experimental curves should reveal how the fourth model parameter depends not only on the initial gold concentration in the solution and the AC loading in the adsorption column volume, but also on the time-varying conditions of intraparticle mass transfer during the adsorption process.

The main objective of this study was to develop a mathematical model of gold adsorption from gold cyanide solutions onto activated carbon that would reliably describe the process under various initial gold concentrations and AC loadings in the closed volume of an adsorption column. A key indicator of the model's validity is that the adsorption isotherm equation was derived analytically from the solution of the adsorption kinetics equation. As the results presented here show good agreement with experimental data, they can be applied in practical calculations for countercurrent industrial adsorption process flowsheets using activated carbon, provided the specific operating conditions are taken into account.

The developed mathematical model was identified based on experimental data obtained at the Irgiredmet Research Institute (Russia), using standard methodologies for investigating the kinetics of gold adsorption from synthetically prepared gold cyanide solutions onto regenerated activated carbon of the NORIT-3515 grade.

Research methodology

The adsorption isotherm of gold onto activated carbon of the NORIT-3515 grade was determined using the static method with constant AC mass of 1.5 g and varying gold concentrations ranging from 3.2 to 39.8 mg/dm^3 in gold cyanide solutions containing 176.0 mg/dm^3 NaCN (pH = 10.8). The temperature of

---

[1] Termed *intradiffusion* in the authors' earlier work [1]; here, *intraparticle mass transfer* is used to reflect a broader mechanism.

the solutions during the experiments was maintained within the range of 20—22 °C. The adsorber was a cylindrical vessel made of organic glass with a flat bottom, equipped with a stirrer and rotation speed controller, which ensured uniform suspension of the adsorbent throughout the entire volume of the solution [1]. The height-to-diameter ratio of the adsorber was 2.5:1.0. The solution volume for each experiment was 3 dm^3, and the total time required to achieve one equilibrium isotherm value was 216 h. At predetermined time intervals from the start of the experiment, samples were collected to construct the kinetic curves.

The gold concentration in the solutions was measured using an ICE 3300 atomic absorption spectrophotometer (Thermo Fisher Scientific, USA) at the certified analytical center of Irgiredmet OJSC [1]

Theoretical basis for selecting the form of the adsorption kinetics equation considering intraparticle mass transfer (intradiffusion), its solution, and derivation of the isotherm equation

The theoretical concepts of gold adsorption kinetics onto activated carbon presented earlier [1] remain valid at low degrees of AC particle saturation, when $Au(CN)_2^-$ is primarily concentrated within a thin near-surface shell of the adsorbent granule, with a thickness not exceeding 20 % of the particle's effective radius. Under these conditions, the adsorption kinetics are adequately described by Equation (1), while the adsorption isotherm is described by a modified Langmuir equation (2):

$$\frac{dC_y}{dt} = K_1(C_0 - C_y)\left(\frac{m}{V}C_p\right) - K_2C_y, \qquad (1)$$

$$C_{y2} = \frac{C_0\, m/VC_p}{K_2/K_1 + C_p\, m/V}, \qquad (2)$$

where C_y is the gold content in loaded carbon, mg/g; C_p is the gold concentration in the solution, mg/dm^3; C_0 is the maximum adsorption capacity of the adsorbent, mg/g; K_1 is the adsorption rate constant, dm^3/(mg·h); K_2 is the desorption rate constant, h^{-1}; m is the carbon mass, g; V is the solution volume, dm^3; t is time, h; C_{y2} is the equilibrium gold content in the carbon for a given equilibrium gold concentration (C_p), mg/dm^3.

However, under practical conditions, as demonstrated by experiments conducted by researchers at the Irgiredmet Research Institute using standard methodologies for synthetically prepared gold cyanide solutions with regenerated NORIT-3515 activated carbon as the adsorbent (Figs. 1—3), an increase in the duration of the adsorption process from 40—50 h to 200 h or more results in two notable effects. First, the gold content in the carbon continues to increase while gold remains in the cyanide solution at a concentration exceeding the equilibrium value C_p, as defined by isotherm (2). Second, the shape of the experimental kinetic curve changes in such a way that it can no longer be adequately described by Equation (1). A theoretical explanation for this phenomenon becomes possible if we adopt the hypothesis that the rate-limiting stage of gold adsorption shifts to intraparticle mass transfer from the near-surface layer into the interior of the adsorbent particle. This stage is characterized by the inward movement of a spherical adsorption front within the particle — that is, from the outer surface toward the center of the granule [2; 3]. In this interpretation, the value C_0 acquires the meaning of the total ultimate gold content per unit mass of activated carbon. Practically, this means that in a fully saturated adsorbent granule, where the adsorption front has reached the center, the local gold content throughout the particle volume equals C_0. Assuming that within the region already traversed by the adsorption front in the adsorbent granule, the gold content is equal to C_0, the current gold content in the carbon (C_y) can, with sufficient accuracy, be determined by the following expression:

$$C_y = \frac{C_0 V_{\text{дз}}}{V_з} = \frac{C_0\left(\frac{4}{3}\pi R^3 - \frac{4}{3}\pi r^3\right)}{\frac{4}{3}\pi R^3} = C_0\left(1 - \frac{r^3}{R^3}\right), \qquad (3)$$

where $V_{\text{дз}}$ is the volume of the adsorbent particle saturated with gold; $V_з$ is the total volume of the adsorbent particle; R is the adsorbent average particle radius; r is the radius of the central core not yet saturated with gold.

To account for intraparticle mass transfer, it is necessary to introduce an additional term into the kinetics equation (1), which should adequately reflect the kinetics of internal gold transport within the adsorbent. According to the law of mass action, this term must be proportional to the product of the current gold content in the carbon (C_y) and the concentration of active sites in the adsorbent that are still free of gold, expressed as ($C_0 - C_y$). This assumption holds true if we accept the premise that the adsorption front is diffuse under real conditions — that is, its boundary extends over a finite thickness, within which a concentration gradient of adsorbed $Au(CN)_2^-$ ions is formed along the radius of the adsorbent particle. If the adsorption front had a sharply defined spherical boundary, the factor C_y would appear with an exponent of 2/3, reflecting its proportionality to the surface area of a sphere. In such a case, only those adsorbed $Au(CN)_2^-$ ions located at the boundary of the spherical adsorption front would interact with the remaining active sites. The number of these ions would be proportional to the surface area of the spherical front. Numerical simulations confirmed the validity of the assumption regarding the diffuseness of the adsorption front.

Taking this into account, the kinetics equation takes the following form:

$$\frac{dC_\text{y}}{dt} = K_1(C_0 - C_\text{y})\frac{m}{V}C_\text{p} - K_2C_\text{y} + K_3(C_0 - C_\text{y})C_\text{y}, \quad (4)$$

where K_3 is the rate constant of intraparticle mass transfer, s^{-1}.

Using the material balance equation for a closed system:

$$C_\text{p} = C_\text{p0} - \frac{m}{V}(C_y - C_\text{y0}), \quad (5)$$

after simple transformations, the kinetics equation (4) can be reduced to a mass-action-type equation with a known solution [4]:

$$C_\text{y} = \frac{C_\text{y2}\left(\dfrac{C_\text{y0} - C_\text{y1}}{C_\text{y0} - C_\text{y2}}\right)\exp\left\{K_3\left[K_{13}\left(\dfrac{m}{V}\right)^2 - 1\right](C_\text{y1} - C_\text{y2})t\right\} - C_\text{y1}}{\left(\dfrac{C_\text{y0} - C_\text{y1}}{C_\text{y0} - C_\text{y2}}\right)\exp\left\{K_3\left[K_{13}\left(\dfrac{m}{V}\right)^2 - 1\right](C_\text{y1} - C_\text{y2})t\right\} - 1}, \quad (6)$$

$$C_\text{y1} = \frac{-b + \sqrt{b^2 - 4ac}}{2a}, \quad (7)$$

$$C_\text{y2} = \frac{-b - \sqrt{b^2 - 4ac}}{2a}, \quad (8)$$

$$a = K_{13}\left(\frac{m}{V}\right)^2 - 1, \quad (9)$$

$$b = -\left[K_{13}\frac{m}{V}\left(\frac{m}{V}C_0 + C_\text{p0} + \frac{m}{V}C_\text{y0}\right) + K_{23} - C_0\right], \quad (10)$$

$$c = K_{13}\frac{m}{V}C_0\left(C_\text{p0} + \frac{m}{V}C_\text{y0}\right). \quad (11)$$

Here, $K_{13} = K_1/K_3$ and $K_{23} = K_2/K_3$ — are the equilibrium constants of adsorption and desorption, respectively, with reference to the rate-limiting stage of the process — intraparticle mass transfer.

The coefficients K_{13}, K_{23}, and C_0 are true identification constants whose values are determined by fitting the isotherm equation (8) to experimental data obtained over a wide range of C_p0 and m/V. This isotherm is of a new type, as it does not correspond to any of the known isotherm models. It establishes a relationship between the equilibrium values of C_y2 and the initial process parameters — C_p0, C_y0, m, and V — in a closed system. The identification coefficients K_{13}, K_{23}, and C_0 can be regarded as physical constants that are specific to the adsorption conditions and the type of adsorbent used. The constant C_0 represents the total ultimate adsorption capacity of the activated carbon. The identification parameter K_3 defines the rate constant of intraparticle mass transfer. This parameter varies over time, and its change reflects the dependence of the mass transfer rate on the degree of gold saturation within the adsorbent particles. Furthermore, K_3 is also influenced by the initial gold concentration in the solution (C_p0) and the activated carbon loading (m/V) n the solution volume of the adsorption column. Therefore, K_3 is an identification parameter whose functional dependence on C_p0, m/V, and time t must be determined through numerical simulations and theoretical analysis, supported by experimental data.

The solution presented in Equation (6) has a notable property: as the adsorption time tends toward infinity, it approaches a limiting equilibrium value C_y2. This means that C_y2 represents the equilibrium gold loading on the activated carbon (C_y) that is inherently contained in the solution to the kinetic Equation (6). Alternatively, C_y2 может быть найдено исходя из заданных начальных условий по выражению (8), which defines an adsorption isotherm of a new type. This equation enables the calculation of equilibrium values of C_y based on the known identification constants K_{13}, K_{23}, and C_0, as well as the specified initial values C_y0, C_p0, m, and V, under batch adsorption conditions in a closed system. y combining Equation (8) with the material balance equation (5), an isotherm equation is readily derived that describes the relationship between the equilibrium gold loading on the carbon ($C_\text{y} = C_\text{y2}$) and the corresponding equilibrium gold concentration in the solution (C_p):

$$C_\text{y2} = \frac{-(K_{13}\,m/VC_\text{p} + K_{23} - C_0) - \sqrt{(K_{13}\,m/VC_\text{p} + K_{23} - C_0)^2 + 4K_{13}C_0C_\text{p}\,m/V}}{2}. \quad (12)$$

From this, the inverse isotherm can be obtained:

$$C_\text{p} = \frac{C_\text{y2}^2 + C_\text{y2}(K_{23} - C_0)}{K_{13}\,m/V\,(C_0 - C_\text{y2})}. \quad (13)$$

Here, C_{y2} is calculated using Equation (8), in combination with Equations (9)—(11). Thus, both equilibrium gold loading C_y and equilibrium solution concentration C_p an be predicted in advance for any given combination of initial process parameters C_{p0}, C_{y0}, m, and V, provided that the identification constants K_{13}, K_{23}, and C_0 are known.

Identification of the mathematical model for gold adsorption dynamics onto activated carbon based on experimental kinetic curves and the adsorption isotherm

The isotherm derived in Equation (8) was identified using the initial parameters C_{p0}, C_{y0}, m, and V, and along with Equation (12), based on experimental data for the equilibrium concentration C_p . This yielded the following constants [5]: $K_{13} = 8.004$, $K_{23} = 83.519$, and $C_0 = 82.632$. These values may be considered reference characteristics for the investigated activated carbon grade (NORIT-3515) and the specified experimental conditions.

Subsequent identification of the solution to the kinetic Equation (6), with respect to the identification parameter K_3 and experimental kinetic curves, was performed using theoretical concepts of the gold adsorption process on activated carbon [6—12] and analysis of the experimental data. As a first approximation, a functional expression was obtained for K_3, allowing its dependence to be considered as a function of the degree of gold saturation in the activated carbon particles and, consequently, on the process time (t), the initial gold concentration in the solution (C_{p0}), and the carbon loading per unit solution volume (m/V). For adequately determine the time dependence of K_3, an important requirement is that the adsorption process must proceed continuously during the kinetic experiments on gold adsorption onto activated carbon:

$$K_3 = \frac{K_{03}}{\sqrt[3]{C_{p0}}\,\frac{m}{V}\,t^{\frac{1}{3}}}, \qquad (14)$$

where $K_{03} = 0.00073$ is true identification constant for the intraparticle mass transfer rate. This constant is independent of both process parameters and time.

Expression (8) and the resulting isotherm (12) represent a new type of adsorption isotherm that relates the equilibrium values of C_y to the initial values of the process parameters C_{p0} and m/V in closed systems. This differs from classical isotherms, which relate the equilibrium values of C_p and C_y, equiring one of the parameters to be determined experimentally. Together, isotherms (8) and (12), in combination with the kinetic Equation (6), provide an adequate description of both the equilibrium gold loading on activated carbon under any initial concentration in solution and the kinetics of the gold adsorption process at extended contact times and a broad range of carbon loadings (m/V).

For brevity, the newly introduced isotherm model — represented by Equation (8) together with the intermediate Equations (9)—(11), and its derivative form Equation (12) — will hereafter be referred to as the “MEGA isotherm” [13]. Notably, the MEGA isotherm expression excludes all kinetic parameters that were previously required to describe the process dynamics, including the coefficient K_3, which depends on the degree of gold saturation in activated carbon particles and, therefore, on the adsorption time t. Moreover, K_3 is also a function of the initial gold concentration in the solution and the carbon loading (m/V) per unit volume of the adsorption apparatus or process stage.

The identified constants K_{13}, K_{23}, and C_0, as well as the functional dependence of K_{13} on C_{p0}, m/V , and t, allow for an accurate description of both the adsorption kinetics (Figs. 1 and 2) and the adsorption isotherm (Fig. 3) of gold from gold cyanide solutions onto activated carbon (see table). The kinetic and isotherm plots include confidence intervals for the experimen-

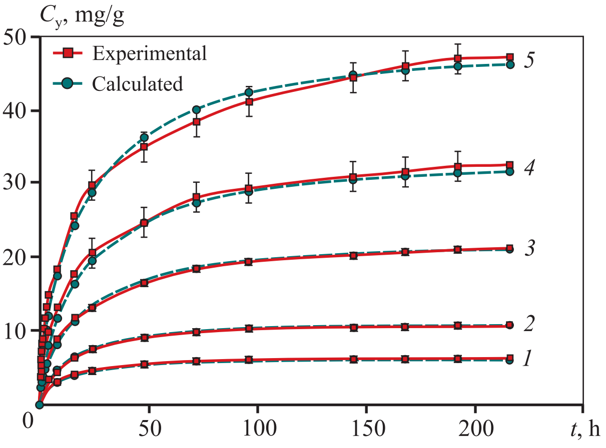

Fig. 1. Kinetic curves of $Au(CN)_2^-$ adsorption onto activated carbon at different initial gold concentrations in the solution and different AC loadings $m/V = 0.5$ g/dm^3 ($m = 1.5$ g, $V = 3$ dm^3)

1 – $C_{p0} = 3.2$, ***2*** – 5.9, ***3*** – 12.7, ***4*** – 21.6, ***5*** – 39.8 mg/dm^3

Рис. 1. Кинетические кривые адсорбции $Au(CN)_2^-$ на активированном угле при различной начальной концентрации золота в растворе и загрузке АУ $m/V = 0,5$ г/дм^3 ($m = 1,5$ г, $V = 3$ дм^3)

1 – $C_{p0} = 3,2$, ***2*** – 5,9, ***3*** – 12,7, ***4*** – 21,6, ***5*** – 39,8 мг/дм^3

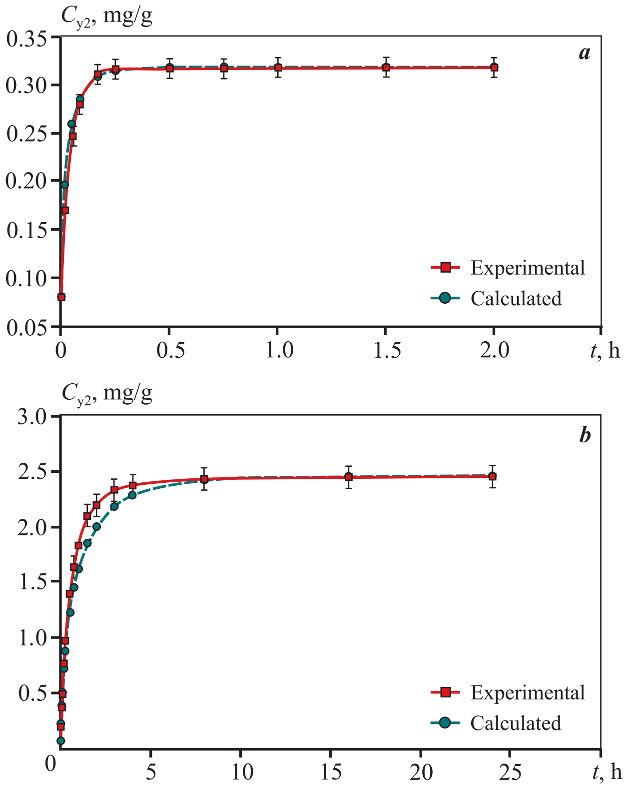

Fig. 2. Kinetic curves of $Au(CN)_2^-$ adsorption onto activated carbon at an initial gold concentration in the solution $C_{p0} = 11.9$ mg/dm^3 and carbon loading $m/V = 50$ g/dm^3 ($m = 75$ g, $V = 1.5$ dm^3) (***a***) and 5 g/dm^3 ($m = 7{,}5$ g, $V = 1{,}5$ dm^3) (***b***)

Рис. 2. Кинетические кривые адсорбции $Au(CN)_2^-$ на АУ при начальной концентрации золота в растворе $C_{p0} = 11{,}9$ мг/дм^3 и загрузке АУ $m/V = 50$ г/дм^3 ($m = 75$ г, $V = 1{,}5$ дм^3) (***a***) и 5 г/дм^3 ($m = 7{,}5$ г, $V = 1{,}5$ дм^3) (***b***)

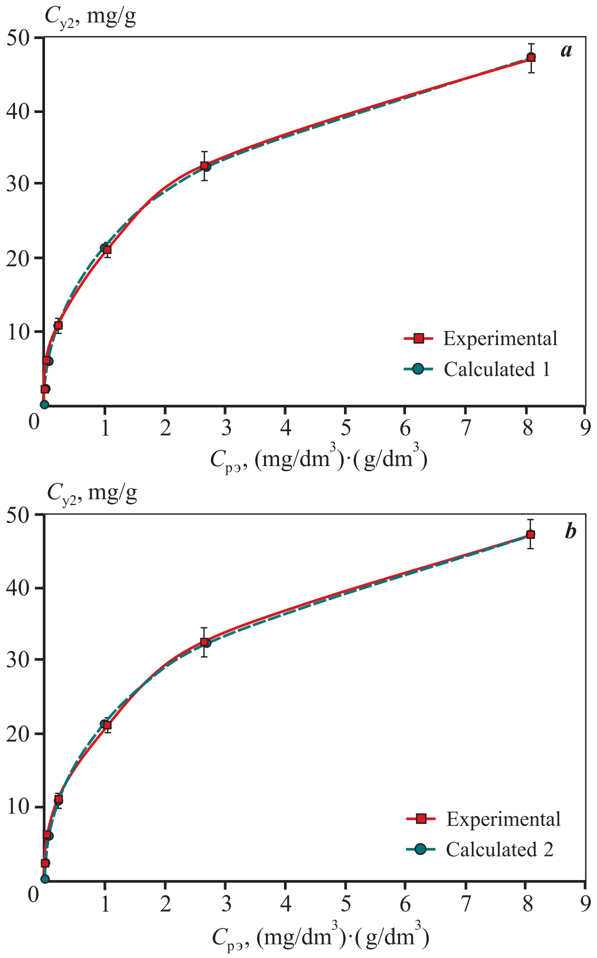

Fig. 3. MEGA isotherms: experimental and calculated curves

a – calculation using Equation (8),
b – calculated using Equation (12)

Рис. 3. Экспериментальные и расчетная изотермы МЕГА

a – расчет по формуле (8), ***b*** – по (12)

tal data points, calculated at a confidence level of $P = 0.95$ [1].

The degree of agreement between the calculated results and the experimental data confirms that the applied physicochemical concepts of gold adsorption onto activated carbon from gold cyanide solutions, as well as the derived adsorption kinetics equation with its analytical solution, provide an adequate mathematical framework for describing the process. This model can be used both for predictive purposes and for the development of optimal discrete and continuous, co-current and counter-current technological process flowsheets.

Comparative evaluation of the developed mathematical model and existing Fleming models

The most commonly used and practically applied models for describing the kinetics of gold adsorption onto activated carbon are Fleming's "*Kn*" and "*Kk*" models [14—16].

The *Kn* model is expressed as:

$$C_y - C_{y0} = KC_p t^n. \tag{15}$$

For batch adsorption processes in a closed system, the material balance equation must be added:

$$C_p = C_{p0} - \frac{m}{V}(C_y - C_{y0}). \tag{16}$$

The resulting solution takes the following form:

$$C_y = C_{y0} + \frac{KC_{p0}t^n}{1 + K\frac{m}{V}t^n}. \tag{17}$$

From this, it follows that as $t \to \infty$

$$C_y = C_{y0} + \frac{m}{V}C_{p0}, \tag{18}$$

Experimental and calculated data of the MEGA isotherm

Экспериментальные и расчетные данные изотермы МЕГА

Parameter	Experiment No.						
	1	*2*	*3*	*4*	*5*	*6*	*7*
Experimental isothermal values значения ($C_{y2\,exp}$)	0.318	2.45	6.34	10.98	21.3	32.68	47.28
Isothermal values C_{y2}, calculated using initial values C_{p0}, C_{y0}, m, V and Equation (8)	0.318	2.46	6.19	10.97	21.53	32.48	47.34
Isothermal values C_{y2}, calculated using Equation (12) and equilibrium concentrations of gold using Equation (13)	0.326	2.462	6.186	10.975	21.531	32.481	47.343
Experimental equilibrium gold concentrations in solution (C_p)	0	0	0.07	0.45	2.09	5.3	16.2
Experimental equilibrium gold concentrations in solution. $C_{pэ} = C_p m/V$ – generalized parameter	0	0	0.035	0.225	1.045	2.65	8.1
Equilibrium gold concentration in solution (C_p), calculated using Equation (13)	0.000012	0.00257	0.143	0.454	1.974	5.4	16.168
Equilibrium gold concentrations in solution calculated using Equation (13). $C_{pэ} = C_p m/V$ – generalized parameter	0.0006	0.01285	0.0715	0.227	0.987	2.7	8.084

In other words, the model implies that adsorption will proceed until all gold is removed from the solution and fully absorbed by the activated carbon — an outcome that contradicts the physicochemical understanding of the process and the behavior described by the adsorption isotherm.

Under practical conditions, where free cyanide is present in solution (as is typically the case), the adsorption process is accompanied by desorption. As a result, equilibrium is established at certain concentrations, and the collection of these equilibrium states forms the adsorption isotherm. Under such conditions, the adsorption process can never proceed to completion, meaning that some residual concentration of the adsorbate must always remain in the solution. These residual concentrations — particularly at high sorbent loadings — can become so low that they fall below the detection limits of standard analytical methods. This may lead to the mistaken conclusion that the adsorption process has gone to completion.

This phenomenon can be readily explained by the hypothesis that gold desorption proceeds through the formation of intermediate species derived from $Au(CN)_2^-$ within the carbon sorbent, in which one CN^--ion is replaced by a hydroxyl ion OH^-. The resulting intermediate partially decomposes to form , which — due to its weak interaction with the carbon lattice and relatively small molecular size — tends to desorb. However, for this desorption to proceed, free cyanide must be present in the solution to convert Au(CN) back into the soluble $Au(CN)_2^-$ complex. In the absence of free cyanide, water-insoluble AuCN remains within the structure of the carbon sorbent, and desorption does not occur [17—20].

For practical purposes, when modeling gold adsorption kinetics over limited time intervals and within a restricted range of C_{p0} and m/V values, the use of the *Kn* model may be acceptable as a first approximation for fitting kinetic curves — especially given that many such curves can be adequately approximated by a power-law function. If an experimental kinetic curve is available, it is often permissible — within specific time intervals — to fit it using the *Kn* model by identifying suitable values of K and n that minimize the root-mean-square relative deviation between the experimental and model-predicted curves. To that end, the original *Kn* kinetic equation for a closed system (Equation 17) can be rewritten as:

$$\frac{C_{yi}-C_{y0}}{C_{p0}-\frac{m}{V}(C_{yi}-C_{y0})}=Kt_i^n, \qquad (19)$$

where C_{yi} and ti are the values of the experimental data points along the kinetic curve, and K and n are the identification constants to be determined. Taking the logarithm of this expression yields a linearized form of the kinetic equation, from allows the identification constants K and n to be estimated in a first approximation using the least squares method:

$$\ln\left(\frac{C_{yi}-C_{y0}}{C_{p0}-\frac{m}{V}(C_{yi}-C_{y0})}\right)=\ln K+n\ln t_i. \qquad (20)$$

The resulting values of K and n are then refined directly using Equation (17) by minimizing the sum of squared relative deviations between the experimental C_{yi} values and those calculated from the model. It is important to note that the values of K and n obtained using this procedure are valid only under the specific experimental conditions used to obtain the kinetic curve employed in the identification process. If the conditions are altered and a new kinetic curve is obtained, new values of K and n must be determined accordingly.

Since the identification constants K and n in Fleming's *Kn* model lack clear physical meaning, their functional dependence on external conditions also lacks a well-defined interpretation. As an empirical model, it provides limited scientific or predictive value beyond that of conventional regression approaches. When applying this model in practice, it is essential to take into account the specific assumptions and conditions under which it was developed and, most importantly, the purposes it was originally intended to serve. All semi-empirical models share a fundamental limitation: they are based on physically undefined parameters and tend to yield physically inconsistent results when extrapolated to limiting cases, which diminishes their theoretical rigor and predictive reliability.

Fleming's *Kk* model (1984) offers only marginal improvements over the *Kn* model. While the parameters it employs have a somewhat clearer physical interpretation — particularly K, which functions as an equilibrium constant — the model inherently incorporates a Henry-type isotherm. This imposes significant constraints on its applicability for designing real-world technological flowsheets.

In contrast, the theoretical model of gold adsorption onto activated carbon developed in this study offers a more consistent and scientifically grounded description when fitted to specific empirical kinetic data. Unlike Fleming's models, it is derived from fundamental principles and allows for the analytical derivation of a new type of isotherm — referred to as the MEGA isotherm — directly from the kinetic equation. This isotherm provides an accurate description of the experimentally obtained adsorption curve and enables the calculation of equilibrium values of C_y (Equation 12) and C_p (Equation 13) across a wide range of initial conditions, including carbon loading and the initial concentrations of gold in solution (C_{p0}) and in regenerated activated carbon (C_{y0}).

Conclusion

Unlike Fleming's *Kk*- and *Km* models, the kinetic model of gold adsorption from gold cyanide solutions onto activated carbon presented in this work is developed on the basis of well-established fundamental theoretical principles. All parameters introduced into the model have clear physical meaning, and both the adsorption kinetics equation and the resulting new-type adsorption isotherm adequately describe the complete set of experimental data obtained for both adsorption kinetics and isotherm. The experimental data were collected over a wide range of process parameters, including initial gold concentrations in solution from C_{p0} = 3.2 to 39.8 mg/dm^3 and activated carbon loadings ranging from m/V = 0.5 to 50 g/dm^3. These values cover nearly the entire practical range of initial gold concentrations and sorbent loadings typically encountered in real-world gold adsorption systems.

The mathematical model of adsorption dynamics and the MEGA isotherm proposed in this study enable an accurate description of gold adsorption onto activated carbon from gold cyanide solutions. This applies both to predictive modeling and to the design and optimization of technological process flowsheets [21—23]. The generality of the developed model is largely determined by the structure of the proposed kinetics equation and its analytical solution, from which the MEGA isotherm is derived.

References

1. Elshin V.V., Mironov A.P., Lisitsyna A.A. Development and solution of the kinetics equation and adsorption isotherm for gold adsorption from cyanide solutions onto activated carbon. *Izvestiya. Non-Ferrous Metallurgy.* 2024;(3):45—56.
https://doi.org/10.17073/0021-3438-2024-3-45-56
Елшин В.В., Миронов А.П., Лисицына А.А. Разработка и решение уравнения кинетики и изотермы адсорбции золота из цианистых растворов на активированный уголь. *Известия вузов. Цветная металлургия*. 2024; 30(3):45—56.
https://doi.org/10.17073/0021-3438-2024-3-45-56
2. Fomkin A.A., Tsivadze A.Yu., Shkolin A.V., Mukhin V.M., Dudarev V.I. Carbon adsorbents used for gold recovery

technology with cyanide. *Fizikokhimiya poverkhnosti i zashchita materialov*. 2014; 50(6):563—567. (In Russ.).
https://doi.org/10.7868/S0044185614060035
Фомкин А.А., Цивадзе А.Ю., Школин А.В., Мухин В.М., Дударев В.И. Углеродные адсорбенты в технологии цианистого извлечения золота. *Физикохимия поверхности и защита материалов*. 2014; 50(6):563—567.
https://doi.org/10.7868/S0044185614060035

3. Medveď I., Černý R., Surface diffusion in porous media: A critical review. *Microporous and Mesoporous Materials*. 2011;142(2-3):405—422.
https://doi.org/10.1016/j.micromeso.2011.01.015
4. Kamke E. Differentialgleichungen. Leipzig: Akademische Verlagsgesellschaft Geest & Portig K.-G., 1962. 336 s.
5. Mironov A.P., Elshin V.V. Lisitsyna A.A. An algorithm for identifying a mathematical model of the kinetics of gold sorption with activated carbon in a closed volume. In: *Prospects for the development of technology for processing hydrocarbon and mineral resources*: Materials of the XIII All-Russian Scientific and Practical Conference with international participation (Irkutsk, 19–20 April, 2023). Irkutsk National Research Technical University. P. 208–212. (In Russ.).
https://elibrary.ru/item.asp?id=53860882
Миронов А.П., Елшин В.В. Лисицына А.А. Алгоритм идентификации математической модели кинетики сорбции золота активированным углем в замкнутом объеме. В сб.: *Перспективы развития технологии переработки углеводородных и минеральных ресурсов*: Материалы XIII Всероссийской научно-практической конференции с международным участием (г. Иркутск, 19—20 апреля 2023 г.). Иркутский национальный исследовательский технический университет С. 208—212.
https://elibrary.ru/item.asp?id=53860882
6. Weber W.J., Morris J.C. Kinetics of adsorption on carbon from solution. *Journal of the Sanitary Engineering Division*. 1963;89(2):31—60.
https://doi.org/10.1061/JSEDAI.0000430
7. Xie F., Chen J., Zhang X., Xu B., Wang W. Adsorption mechanism of copper and gold thiosulfates onto activated carbon. *Transactions of Nonferrous Metals Society of China*. 2023;33(10):3210—3221.
https://doi.org/10.1016/S1003-6326(23)66328-9
8. Romero H., Suarez C., Salazar N., Zambrano C., Lapo B. Evaluation of gold adsorption on activated carbon from real cyanide and thiourea leachate solutions. *Heliyon*. 2024;10(11):e31606.
https://doi.org/10.1016/j.heliyon.2024.e31606
9. Galyaltdinov Sh., Brusko V., Khannanov A., Dimiev A.M. Oxidatively modified carbon as a promising material for gold extraction. *Diamond and Related Materials*. 2024;142:110826.
https://doi.org/10.1016/j.diamond.2024.110826
10. Xia J., Mahandra H., Ghahreman A. Efficient gold recovery from cyanide solution using magnetic activated carbon. *ACS Applied Materials & Interfaces*. 2021;13(40):47642—47649. https://pubs.acs.org/doi/10.1021/acsami.1c13920
11. Jia Y.F., Steele C.J., Hayward I.P., Thomas K.M. Mechanism of adsorption of gold and silver species on activated carbons. *Carbon*. 1998;36(9):1299—1308.
https://doi.org/10.1016/S0008-6223(98)00091-8
12. Jinsong X., Rajashekhar M., Twinney J., Ghahreman A. A review on adsorption mechanism of gold cyanide complex onto activation carbon. *Journal of Industrial and Engineering Chemistry*. 2022; 111:35—42.
https://doi.org/10.1016/j.jiec.2022.04.014
13. Mironov A.P., Elshin V.V., Gerasimova A.A. Modeling of the kinetics of the process of sorption of gold by activated carbons. In: Prospects for the development of technology for processing hydrocarbon and mineral resources: Materials of the XII All-Russian Scientific and Practical Conference with international participation (Irkutsk, 20–21 April, 2022). Irkutsk National Research Technical University. P. 252–255. (In Russ.).
https://elibrary.ru/item.asp?id=48404717
Миронов А.П., Елшин В.В., Герасимова А.А. Моделирование кинетики процесса сорбции золота активными углями. В сб.: *Перспективы развития технологии переработки углеводородных и минеральных ресурсов*: Материалы XII Всероссийской научно-практической конференции с международным участием (г. Иркутск, 20—21 апреля 2022 г.). Иркутский национальный исследовательский технический университет. С. 252—255.
https://elibrary.ru/item.asp?id=48404717
14. Nicol M. J., Fleming C. A., Cromberge G. The absorption of gold cyanide onto activated carbon. I. The kinetics of absorption from pulps. *Journal of the Southern African Institute of Mining and Metallurgy*. 1984;84 (2):50—54.
15. Nicol M. J., Fleming C. A., Cromberge G. The absorption of gold cyanide onto activated carbon. II. Application of the kinetic model to multistage absorption circuits. *Journal of the Southern African Institute of Mining and Metallurgy*. 1984; 84 (3):70—78.
16. Nicol M. J., Fleming C. A. The absorption of gold cyanide onto activated carbon. III. Factors influencing the rate of loading and the equilibrium. *Journal of the Southern African Institute of Mining and Metallurgy*. 1984;84(4):85—93.
17. Ibragimova R.I., Kubyshkin S.A., Fateev A.A., Krivov A.S., Fedyukevich V.A., Shcherbakov Yu.S., Mil'Man B.M., Vorob'Ev-Desyatovskii N.V. Transformations of $[Au(CN)_2]^-$ at the contact with activated carbon surface. *Zhurnal*

obshchei khimii. 2013;83(12):2254—2259. (In Russ.). https://doi.org/10.1134/S1070363213120050
Ибрагимова Р.И., Кубышкин С.А., Фатеев А.А., Кривов А.С., Щербаков Ю.С., Мильман Б.М., Воробьев-Десятовский Н.В. Процессы, происходящие с анионом $[Au(CN)_2]^-$ при контакте с поверхностью активированного угля. *Журнал общей химии.* 2013;83(12):2254—2259.
https://doi.org/10.1134/S1070363213120050

18. Meretukov M.A. Active carbons and cyanide process. Moscow: Ruda i metally, 2007. 285 p. (In Russ.).
Меретуков М.А. Активные угли и цианистый процесс. М.: Руда и металлы, 2007. 285 с.
19. Ibragimova R.I., Grebennikov S.F., Guryanov V.V., Pichugina D.A., Krivov A.S., Vorob'Ev-Desyatovskii N.V. The effect of the specific surface area of activated carbons on the sorption of ions $[Au(CN)_2]^-$ from aqueous solutions. *Zhurnal fizicheskoi khimii.* 2014;88(4):679—685. (In Russ.). https://doi.org/10.7868/S0044453714040116
Ибрагимова Р.И., Гребенников С.Ф., Гурьянов В.В, Пичугина Д.А., Кривов А.С., Воробьев-Десятовский Н.В. Влияние удельной поверхности активированных углей на сорбцию ионов $[Au(CN)_2]^-$ из водных растворов. *Журнал физической химии.* 2014;88(4):679—685.
https://doi.org/10.7868/S0044453714040116
20. Ibragimova R.I., Grebennikov S.F., Guryanov V.V., Vorob'ev-Desyatovskii N.V. Influence of porous structure of absorbent carbon on adsorption of the gold (I) tsianid complex. *Bulletin of the St. Petersburg State University of Technology and Design. Series 1: Natural and Technical Sciences.* 2012;2:3—9. (In Russ.).
https://www.elibrary.ru/item.asp?id=17905729
Ибрагимова Р.И., Гребенников С.Ф., Гурьянов В.В., Воробьев-Десятовский Н.В. Влияние пористой структуры активированного угля на адсорбцию цианидного комплекса золота (I). *Вестник Санкт-Петербургского государственного университета технологии и дизайна. Серия 1: Естественные и технические науки.* 2012;2:3—9.
https://www.elibrary.ru/item.asp?id=17905729
21. Xiao Y., Azaiez J., Hill J.M. Erroneous application of pseudo-second-order adsorption kinetics model: ignored assumptions and spurious correlations. *Industrial & Engineering Chemistry Research.* 2018;57(7):2705—2709.
https://doi.org/10.1021/acs.iecr.7b04724
22. Zhukov V.V., Sharikov Yu.V., Turunen I., Laari A. Modeling of the periodic process of gold leaching by cyanidation. *Zapiski gornogo instituta.* 2013;202:178—180. (In Russ.).
https://www.elibrary.ru/item.asp?id=20864110
Жуков В.В., Шариков Ю.В., Турунен И., Лаари А. Моделирование периодического процесса выщелачивания золота цианированием. *Записки горного института.* 2013;202:178—180.
https://www.elibrary.ru/item.asp?id=20864110
23. Van Deventer J.S.J. Kinetic model for the reversible adsorption of gold cyanide on activated carbon. *Chemical Engineering Communications.* 1986;44(1-6):257—274.
https://doi.org/10.1080/00986448608911359

Information about the authors

Viktor V. Elshin – Dr. Sci. (Eng.), Professor of the Department “Automation and Control”, Irkutsk National Research Technical University (INRTU).
https://orcid.org/0000-0002-0447-4831
E-mail: dean_zvf@istu.edu

Alexander P. Mironov – Cand. Sci. (Eng.), Associate Professor of the Department “Automation and Control”, INRTU.
https://orcid.org/0009-0002-0530-8015
E-mail: mironoff.alexander@yandex.ru

Anastasia A. Lisitsyna – Assistant Lecturer of the Department “Automation and Control”, INRTU.
https://orcid.org/0009-0008-9781-1593
E-mail: Gerasimovan19@rambler.ru

Информация об авторах

Виктор Владимирович Ёлшин – д.т.н., профессор кафедры автоматизации и управления, Иркутский национальный исследовательский технический университет (ИРНИТУ).
https://orcid.org/0000-0002-0447-4831
E-mail: dean_zvf@istu.edu

Александр Петрович Миронов – к.т.н., доцент, науч. сотрудник кафедры автоматизации и управления, ИРНИТУ.
https://orcid.org/0009-0002-0530-8015
E-mail: mironoff.alexander@yandex.ru

Анастасия Андреевна Лисицына – ассистент кафедры автоматизации и управления, ИРНИТУ.
https://orcid.org/0009-0008-9781-1593
E-mail: Gerasimovan19@rambler.ru

Contribution of the authors

V.V. Elshin – defined the research concept, formulated the study objective, revised the manuscript, and participated in the discussion of the results.

A.P. Mironov – processed the experimental data, wrote the manuscript, and participated in the discussion of the results.

A.A. Lisitsyna – performed the mathematical processing of the experimental data, prepared the manuscript, and participated in the discussion of the results.

Вклад авторов

В.В. Ёлшин – определение концепции исследования, формулирование цели работы, корректировка текста статьи, участие в обсуждении результатов.

А.П. Миронов – обработка экспериментальных данных, написание текста статьи, участие в обсуждении результатов.

А.А. Лисицына – проведение математической обработки экспериментальных данных, оформление статьи, участие в обсуждении результатов.

The article was submitted 18.08.2024, revised 31.10.2024, accepted for publication 02.11.2024

Статья поступила в редакцию 18.08.2024, доработана 31.10.2024, подписана в печать 02.11.2024

UDC 66.081 (546.98 + 546.55 + 546.62)
https://doi.org/10.17073/0021-3438-2025-2-41-54

Research article
Научная статья

Selective sorption-based separation of palladium from process solutions using chemically modified silica

T.M. Buslaeva[1], **E.V. Volchkova**[1], **P.G. Mingalev**[2], **I.V. Boryagina**[3]

[1] **MIREA – Russian Technological University,**
Institute of Fine Chemical Technologies named after M.V. Lomonosov
86 Vernadskogo Prosp., Moscow 119571, Russia

[2] **Moscow State University**
1 Bld, 3 Leninskie Gory, Moscow 119991, Russia

[3] **JSC R&PC Supermetal**
2 Bld, 22/24 Ozerkovskaya nab., Moscow 115184, Russia

✉ Tat'yana M. Buslaeva (buslaevatm@mail.ru)

Abstract: This study focuses on investigating the possibility of selective separation of palladium (II) from solutions containing non-ferrous metals and iron by sorption onto chemically modified silica. The study used both individual (single-metal) and model multicomponent solutions. The sorbents included silicas functionalized with iminodiacetic acid (IDA-D), phosphonic acid (PA-D), and aminomethylphosphonic acid (AMPA-D) groups, as well as a well-known chemically modified silica bearing grafted γ-aminopropyltriethoxysilane (APTES) groups at a grafting density of 1.63 mmol/g. Under static conditions at room temperature, the time required to reach equilibrium sorption values for Cu(II), Ni(II), and Fe(III) ions – typically present in process solutions – was determined for the IDA-D, PA-D, and AMPA-D sorbents. Sorption dependencies on hydrochloric acid concentration were established for these metal ions. For IDA-D, the effect of halide ion concentration on sorption was also studied. It was shown that these ions are sorbed in weakly acidic media but not in 1–2 M HCl, and that sorption capacity decreases in the order: IDA-D > AMPA-D > PA-D. However, the conclusion that quantitative separation of Pd(II) from base metal ions could be achieved using these complexing sorbents (exemplified by IDA-D) under dynamic conditions was not confirmed. The sorption behavior of Pd(II), Cu(II), and Al(III) ions was also examined under static and dynamic conditions using the APTES-functionalized silica and chloride and chloride-bromide solutions, including model solutions simulating leach liquors generated from the treatment of spent catalysts for low-temperature carbon monoxide oxidation. These solutions contained 0.004–0.015 mol/L Pd, 0.014–0.049 mol/L Cu, and 0.015–0.060 mol/L Al. The results demonstrated the feasibility of selectively separating Pd(II) from leach solutions of spent catalysts using this sorbent. A processing scheme was proposed, comprising sorption from 0.1 M HCl, water rinsing of the loaded sorbent, and elution of Pd(II) with a 5 % thiourea solution in 0.1 M HCl. It was shown that separation of palladium from non-ferrous metals occurs already at the sorption and washing stages.

Keywords: sorption, chemically modified silicas, palladium, non-ferrous metals, desorption, thiourea.

For citation: Buslaeva T.M., Volchkova E.V., Mingalev P.G., Boryagina I.V. Selective sorption-based separation of palladium from process solutions using chemically modified silica. *Izvestiya. Non-Ferrous Metallurgy*. 2025;31(2):41–54.
https://doi.org/10.17073/0021-3438-2025-2-41-54

Выделение палладия из технологических растворов сорбцией на химически модифицированном кремнеземе

Т.М. Буслаева[1], Е.В. Волчкова[1], П.Г. Мингалев[2], И.В. Борягина[3]

[1] **МИРЭА – Российский технологический университет,**
Институт тонких химических технологий имени М.В. Ломоносова
Россия, 119571, г. Москва, пр-т Вернадского, 86

[2] **Московский государственный университет**
Россия, 119991, г. Москва, Ленинские горы, 1, стр. 3

[3] **АО «НПК «Суперметалл»**
Россия, 115184, г. Москва, Озерковская наб., 22/24, корп. 2

✉ Татьяна Максимовна Буслаева (buslaevatm@mail.ru)

Аннотация: Настоящая работа посвящена выявлению возможности селективного выделения сорбцией палладия на химически модифицированных кремнеземах из растворов, содержащих цветные металлы и железо. Объектами исследования являлись индивидуальные (содержащие соединения одного металла) и модельные многокомпонентные растворы. Сорбентами служили кремнеземы, модифицированные группами иминодиуксусной (IDA-D), фосфоновой (PA-D) и аминометилфосфоновой (AMPA-D) кислот, а также хорошо известный химически модифицированный кремнезем, содержащий привитые группы γ-аминопропилтриэтоксисилана (APTES) с плотностью прививки функциональных групп 1,63 ммоль/г. В статических условиях при комнатной температуре для сорбентов IDA-D, PA-D и AMPA-D установлено время достижения постоянных значений сорбции ионов меди (II), никеля (II) и железа (III), обычно присутствующих в технологических растворах различного состава. Построены зависимости сорбции ионов этих металлов от концентрации соляной кислоты. Для сорбента IDA-D изучена зависимость сорбции от концентрации галогенид-иона. Показано, что сорбция указанных ионов протекает в слабокислых средах и практически отсутствует в 1–2 М HCl, причем сорбционная способность сорбентов уменьшается в ряду: IDA-D > AMPA-D > PA-D. Сделанный из полученных результатов вывод о возможности количественного разделения ионов палладия (II) и неблагородных металлов на данных комплексообразующих сорбентах (на примере IDA-D) в динамических условиях не подтвердился. Изучена сорбция ионов Pd(II), Cu(II) и Al(III) в статических и динамических условиях на химически модифицированном кремнеземе, содержащем привитые группы γ-аминопропилтриэтоксисилана (APTES), из хлоридных и хлоридно-бромидных растворов, в том числе модельных, близких по составу к технологическим растворам, образующимся при вскрытии отработанных катализаторов низкотемпературного окисления монооксида углерода до его диоксида, содержащих палладий (0,004÷0,015 моль/л), медь (0,014÷0,049 моль/л) и алюминий (0,015÷0,060 моль/л). Выявлена возможность селективного выделения Pd(II) из растворов выщелачивания отработанных катализаторов указанным сорбентом. Предложена схема переработки отработанных катализаторов, включающая сорбцию из 0,1 М HCl, промывку насыщенной фазы сорбента водой, элюирование Pd(II) 5 %-ным раствором Thio в 0,1 М HCl. Показано, что разделение палладия и цветных металлов происходит уже на стадиях сорбции и промывки сорбента.

Ключевые слова: сорбция, химически модифицированные кремнеземы, палладий, цветные металлы, десорбция, тиомочевина.

Для цитирования: Буслаева Т.М., Волчкова Е.В., Мингалев П.Г., Борягина И.В. Выделение палладия из технологических растворов сорбцией на химически модифицированном кремнеземе. *Известия вузов. Цветная металлургия*. 2025;31(2):41–54.
https://doi.org/10.17073/0021-3438-2025-2-41-54

Introduction

Palladium is a unique platinum-group metal for which demand continues to grow year after year. According to market data [1], this demand cannot be met solely through the processing of primary raw materials: approximately one-third of palladium production over the past 2—3 years has been provided by the recycling of secondary raw materials, among which electronic scrap, jewelry scrap, and, most importantly, spent catalysts, are of particular significance.

Among the variety of palladium-based catalysts used for hydrogenation, dehydrogenation, oxidation, cross-coupling, and other reactions, a distinct group consists of catalysts also containing copper. Notable examples include the Moiseev reaction (oxidation of ethylene to vinyl acetate), the Sonogashira reaction, and several others [2—8]. Typically, these are heterogeneous catalysts supported on alumina, with metals, alloys, or salts deposited on the surface. This group includes catalysts for the low-temperature oxidation of carbon monoxide based on γ-Al_2O_3, containing palladium (II) chloride and copper (II) bromide [9—11].

The recycling of specific types of secondary raw materials is carried out by pyrometallurgical and hydrometallurgical methods, with hydrometallurgical processes clearly prevailing [12]. The leaching of spent catalysts results in the formation of complex process solutions containing a variety of cations and anions. This necessitates the use of tailored approaches suited to the processing of specific catalyst types to achieve selective separation and purification of palladium. It appears that the sorption method holds significant promise for recovering valuable components from such process solutions. This method enables the production of highly selective concentrates, is characterized by low energy consumption, high environmental friendliness, and simple equipment requirements. Implementing this technology requires a well-founded approach to selecting sorbents from the vast range available, comprising tens of thousands of options differing in chemical nature, structural characteristics, sorption capacity, and particle size.

The volume of scientific research focused on the synthesis and investigation of sorbents for specific applications continues to grow [13; 14]. However, considering the need not only for selective recovery of valuable components but also for the repeated reuse of sorbents, porous silica-based materials bearing covalently bonded organic ligands appear particularly promising. These chemically modified silicas (CMSs) interact specifically with molecules of target substances. Notably, the rigid mineral framework of such materials prevents them from swelling (i.e., changing volume) in aqueous and organic media, which is especially important for column processes involving extraction and separation. Moreover, the use of mesoporous silicas with an average pore diameter slightly exceeding 10 nm for CMS synthesis provides superior mass transfer characteristics compared to organic polymer-based sorbents [14—19].

Nitrogen-containing CMSs are among the most versatile and, in principle, allow the separation of platinum-group metals from non-ferrous metals by varying the binding mechanism and the conditions of sorption and desorption. In earlier work, we studied the sorption of platinum (IV) and palladium (II) ions onto one of the best-known CMSs functionalized with monoamine groups, synthesized using the relatively inexpensive and industrially produced γ-aminopropyltriethoxysilane [20]. It was found that Pd(II), unlike Pt(IV), tends to form polynuclear complexes in the sorbent phase at high metal concentrations (tens of grams per liter), which leads to a substantial increase in sorption capacity but also causes difficulties in elution. Under these conditions, quantitative elution of Pd(II) could only be achieved using a 5 % thiourea (Thio) solution in 0.1 M HCl [21].

The aim of this study was to investigate the possibility of selective separation of palladium by sorption onto chemically modified silica from solutions containing base metal ions, including those formed during the processing of secondary raw materials such as spent catalysts used for the low-temperature oxidation of carbon monoxide to carbon dioxide.

Experimental procedure

The starting compounds for the sorption studies were palladium chloride ($PdCl_2$), synthesized according to the procedure described in [22], copper (II) chloride ($CuCl_2$), nickel (II) chloride ($NiCl_2$), iron (III) chloride ($FeCl_3$), copper (II) bromide ($CuBr_2$), γ-Al_2O_3, hydrochloric acid (HCl), sodium chloride (NaCl), sodium bromide (NaBr), and thiourea (Thio). All the listed reagents, produced by OOO TD KHIMMED (Russia), were of analytical grade. All organic reagents used for the synthesis of sorbents were supplied by Sigma-Aldrich. Sorption solutions were prepared by dissolving accurate weighed amounts of the respective compounds in HCl solutions of various concentrations.

The sorbents used in this study were chemically modified silica materials based on Davisil Grade 62 silica gel (W.R. Grace and Co., USA; particle size: 0.07—0.2 mm; specific surface area: 325 m^2/g; average pore diameter: 13.6 nm) containing grafted iminodiacetic acid 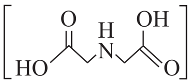 (IDA-D), phosphonic acid (PA-D), and aminomethylphosphonic acid 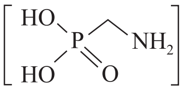 (AMPA-D) groups, as well as a well-known chemically modified silica based on Silochrom C-120, series VG-102/3A1 (specific surface area: 120 m^2/g; particle size: 0.1—0.2 mm; average pore diameter: 45 nm), containing grafted γ-aminopropyltriethoxysilane (APTES) groups with a grafting density of 1.63 mmol/g, having the following structure[1]:

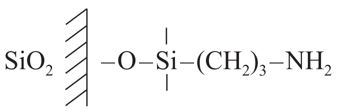

$$SiO_2 -O-Si-(CH_2)_3-NH_2$$

---

[1] Sorbent produced by JSC Biokhimmak ST. https://bcmst.ru/

The synthesis of the complexing sorbents was carried out according to the following procedures.

1. Silica Gel Functionalized with Iminodiacetic Acid (IDA-D). Twenty grams of iminodiacetic acid were dissolved in 180 mL of 4 M NaOH under stirring with a magnetic stirrer at room temperature for 10 min (the pH value of the solution should be in the range of 12.3—12.5). Then, 3 mL of 3-glycidyloxypropyltrimethoxysilane were added, and the two-phase mixture was stirred until a clear solution was obtained. This solution was then added to a suspension of 65 g of Davisil silica gel in 600 mL of 5 % acetic acid (the pH value of the resulting mixture should be in the range of 5.4—5.8). The mixture was stirred using a mechanical stirrer at 80 °C for 2 h. The sorbent was filtered, washed four times (300 mL each) with distilled water, dried on the filter, and then held in a drying oven at 100 °C for 2 h.

2. Silica gel functionalized with diethylphosphonate (DEP-D)[1]. A mixture of 17.6 mL of 3-glycidyloxypropyltrimethoxysilane and 10.2 mL of diethyl phosphite in 100 mL of acetonitrile was prepared. Then, 20 g of Davisil silica gel were added, and the mixture was stirred with a mechanical stirrer at 70 °C for 11 h. The sorbent was filtered, washed three times with acetonitrile, three times with water, three times with acetonitrile, and dried on the filter.

3. Silica gel functionalized with phosphonic acid (PA-D). A mixture of 10 g of DEP-D sorbent and 50 mL of 20 % hydrochloric acid was stirred for 8 hours at 100 °C. The sorbent was then washed with water until neutral washings were obtained, washed three times with acetonitrile (25 mL each), and dried on the filter.

4. Silica gel functionalized with aminomethylphosphonic acid (AMPA-D). A mixture of 35 mL of 3-aminopropyltriethoxysilane, 25 g of phosphorous acid, and 186 mL of a 10 % formaldehyde solution was placed into a flask and stirred. Then, 660 mL of concentrated hydrochloric acid and 30 g of Davisil silica gel were added. The mixture was stirred for 12 h at room temperature, followed by 8 hours at 80 °C, and then stirred again for 12 h at room temperature. The silica gel was separated from the solution, washed three times with distilled water, evaporated at 100 °C under vacuum generated by a water-jet pump, washed with 100 mL of ethanol, and dried at 100 °C under vacuum generated by a water-jet pump.

The elemental analysis results for the sorbents are presented in Table 1. The amounts of grafted groups were: 0.35 mmol/g for IDA-D, 0.42—0.55 mmol/g for PA-D, and 0.85 mmol/g for AMPA-D.

The sorption of palladium (II), non-ferrous metals, and iron (III) ions under static conditions was carried out from individual hydrochloric acid solutions (0.1—4 M) and mixed chloride-bromide solutions at room temperature (three parallel experiments for each test). The solution volumes ranged from 10 to 15 mL, and the mass of sorbent (m_{sorb}) was 0.030 ± 0.001 g.

After sorption under static conditions, the sorbent was separated by filtration through a glass funnel with a paper filter, washed with water, and then subjected to desorption (elution). The eluents used were 2 M and 3 M HCl solutions and a 5 % Thio solution in 0.1 M HCl; the volume of eluent in each individual experiment was 15 mL.

Experiments under dynamic conditions were carried out in glass columns with an internal diameter of 0.4 cm. The masses of the sorbents were 0.6 g for IDA-D and 0.15 g for APTES. The solutions passed through the column under gravity flow. After sorption, the sorbent saturated with the extracted ions was washed with water until the washings became colorless, and the eluent solution was subsequently introduced.

The amount of sorbed metal (m'_{sorb}) was determined as the difference between its content in the solution before sorption (m_{in}) and after sorption (m_{out}). The metal efficiency onto the sorbent was calculated as follows:

$$E_{\text{sorb}} = \frac{m'_{\text{sorb}}}{m_{\text{in}}} \cdot 100\ \%.$$

The fraction of metal removed during washing was calculated as the ratio of the amount of metal in the wash water to the amount sorbed:

$$E_{\text{wash}} = \frac{m_{\text{wash}}}{m'_{\text{sorb}}} \cdot 100\ \%.$$

The amount of metal remaining on the sorbent after washing (m'_{wash}) was determined as the difference between the amount of sorbed metal and the amount of metal found in the wash water.

The overall recovery of metal into the solution after sorption and washing ($E_{\text{overall (solution)}}$) was calculated as the ratio of the sum of the amounts of metal in the solution after sorption (m_{out}) and in the wash water (m_{wash}) to the initial amount of metal in the solution (m_{in}):

$$E_{\text{overall solution}} = \frac{m_{\text{out}} + m_{\text{wash}}}{m_{\text{in}}} \cdot 100\ \%.$$

The elution efficiency was determined as the ratio of

---

[1] DEP-D can also serve as a sorbent for the extraction of transition metal ions; however, in this study, it was used only as an intermediate product in the synthesis of PA-D.

Table 1. **Results of elemental analysis of the sorbents**[*]

Таблица 1. Результаты элементного анализа сорбентов[*]

Sorbent	Content, wt.%			
	C	H	N	P
IDA-D	5.61	1.31	0.58	–
DEP-D	5.22	1.29	–	1.27
PA-D	5.33	1.27	–	1.69
AMPA-D	4.04	1.55	1.30	2.59

[*] Elemental analysis of the sorbents was performed at the Shared Research Facility of the Institute of General and Inorganic Chemistry, Russian Academy of Sciences, Moscow, Russia.

the amount of metal in the eluent (m_{el}) to the amount of metal remaining on the sorbent after washing:

$$E_{\text{el}} = \frac{m_{\text{el}}}{m'_{\text{wash}}} \cdot 100~\%.$$

The initial metal concentrations used in the dynamic sorption experiments for model solutions simulating the composition of process solutions generated during the treatment of spent Pd—Cu catalysts for the low-temperature oxidation of carbon monoxide to carbon dioxide were varied based on their composition: 1.5 wt. % Pd and 3.5 wt. % Cu relative to the mass of the γ-Al_2O_3 carrier [9].

The analysis of aqueous solutions for palladium, copper, nickel, and iron was performed using a NOV AA 330 atomic absorption spectrometer with flame atomization (Analytik Jena, Germany), while the analysis of Al-containing solutions was carried out using a KVANT-Z atomic absorption spectrometer with electrothermal atomization (OOO "Kortek", Russia). If dilution of the samples was necessary prior to analysis, three aliquots of equal volume were taken from each solution, transferred into volumetric flasks, and brought to the mark with a 1:5 HCl solution. The analytical error did not exceed 5 % relative for flame atomization analysis and 7 % relative for electrothermal atomization analysis.

The investigation of complex model solutions was carried out by inductively coupled plasma mass spectrometry (ICP-MS) either without preliminary sample preparation or after additional dilution with deionized water by factors of 50—10 000. Measurements were performed using an Agilent 7900 mass spectrometer (Agilent Technologies, USA) equipped with a double-pass glass spray chamber, a MicroMist glass nebulizer, and a quartz torch. The obtained data were processed using Agilent MassHunter software (Agilent Technologies, USA). The measurement error did not exceed 5 % relative.

Electronic absorption spectra (EAS) of the solutions were recorded over the wavelength range $\lambda = 200\div\div1000$ nm using a Helios Alpha Local Control System spectrophotometer (Thermo Spectronic, USA) in quartz cuvettes with a 1 cm optical path length at room temperature. The wavelength setting accuracy was within 0.05—0.1 nm.

X-ray photoelectron spectra (XPS) were recorded using a LAS instrument (Riber) with calibration based on the C1s binding energy line (285.0 eV) as an external standard.

Results and discussion

In our previous study [23], we investigated the sorption of Pd(II) ions from chloride solutions containing non-ferrous metal ions onto silicas functionalized with N- and S-containing organic molecules. The conditions for their separation from non-ferrous metal ions present in process solutions formed during the processing of various platinum metal concentrates were identified. It was shown that impurity ions pass through the entire technological process and eventually end up in the discharge stream. At the stages of sorption and desorption, it is necessary to monitor the completeness of Pd(II) ion separation from non-ferrous metal ions and to introduce an additional sorbent washing operation, if required [23]. In our opinion, the removal of impurities prior to the stage of palladium and/or other platinum-group metal recovery should positively influence the reduction of the valuable component regeneration/recycling time and the volume of washing solutions.

According to the literature data [24—31], the most promising types of sorbents for impurity metal ion removal are sorbents bearing grafted aminocarboxylic acid groups, particularly iminodiacetic acid (such as Dowex A-1 type sorbents), aminomethylphosphonic acid, and phosphonic acid groups[1]. Therefore, for the preliminary removal of base metal ions (Cu(II), Ni(II), and Fe(III)), we tested silica gels functionalized with iminodiacetic acid (IDA-D), aminomethylphosphonic acid (AMPA-D), and phosphonic acid (PA-D, derived from H_3PO_3.

Traditionally, the synthesis of sorbents with grafted aminocarboxylic acid groups, particularly iminodiacetic

---

[1] At this stage of the study, the sorption of Al(III) ions was not investigated.

acid groups, involves the treatment of amino-containing sorbents with halogenoacetic acids (XCH_2COOH, where X = Cl or Br). We proposed an alternative synthesis scheme using 3-glycidyloxypropyltrimethoxysilane and iminodiacetic acid (IDA-D):

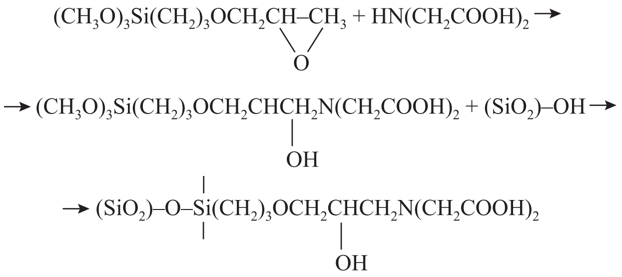

$$(CH_3O)_3Si(CH_2)_3OCH_2\underset{\diagdown O \diagup}{CH\text{–}CH_3} + HN(CH_2COOH)_2 \rightarrow$$
$$\rightarrow (CH_3O)_3Si(CH_2)_3OCH_2\underset{OH}{CH}CH_2N(CH_2COOH)_2 + (SiO_2)\text{–}OH \rightarrow$$
$$\rightarrow (SiO_2)\text{–}O\text{–}\overset{|}{\underset{|}{Si}}(CH_2)_3OCH_2\underset{OH}{CH}CH_2N(CH_2COOH)_2$$

IDA-D

The synthesis of the modifier was carried out in an alkaline medium at pH = 12.3—12.5, while the deposition of the modifier onto the silica gel surface was performed at pH = 5.6—5.8. It should be noted that all stages of the process were conducted in aqueous solutions without the use of organic solvents.

It is important to emphasize that an attempt to apply a similar procedure to obtain silica gel functionalized with phosphonic acid was unsuccessful: during the reaction in an alkaline medium, a side process involving the oxidation of phosphorous acid by atmospheric oxygen occurred, which reduced the yield of the target product.

Therefore, an alternative method was used to synthesize the sorbent bearing diethylphosphonate groups (DEP-D), which consisted of the grafting of a phosphonic acid ester followed by its hydrolysis:

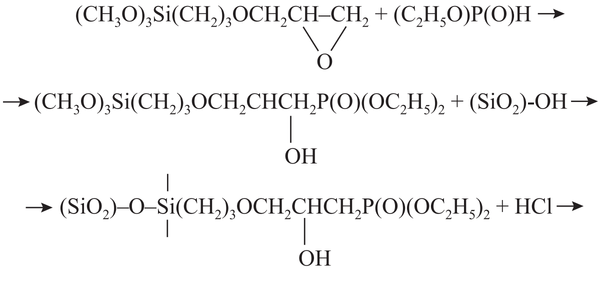

$$(CH_3O)_3Si(CH_2)_3OCH_2\underset{\diagdown O \diagup}{CH\text{–}CH_2} + (C_2H_5O)P(O)H \rightarrow$$
$$\rightarrow (CH_3O)_3Si(CH_2)_3OCH_2\underset{OH}{CH}CH_2P(O)(OC_2H_5)_2 + (SiO_2)\text{-}OH \rightarrow$$
$$\rightarrow (SiO_2)\text{–}O\text{–}\overset{|}{\underset{|}{Si}}(CH_2)_3OCH_2\underset{OH}{CH}CH_2P(O)(OC_2H_5)_2 + HCl \rightarrow$$

DEP-D

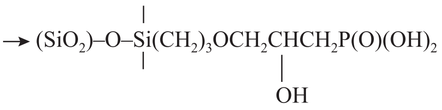

$$\rightarrow (SiO_2)\text{–}O\text{–}\overset{|}{\underset{|}{Si}}(CH_2)_3OCH_2\underset{OH}{CH}CH_2P(O)(OH)_2$$

PA-D

For the grafting of aminomethylphosphonic acid groups onto the silica gel surface (AMPA-D), the following scheme was used:

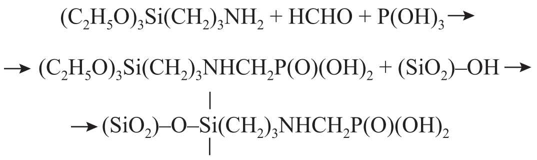

$$(C_2H_5O)_3Si(CH_2)_3NH_2 + HCHO + P(OH)_3 \rightarrow$$
$$\rightarrow (C_2H_5O)_3Si(CH_2)_3NHCH_2P(O)(OH)_2 + (SiO_2)\text{–}OH \rightarrow$$
$$\rightarrow (SiO_2)\text{–}O\text{–}\overset{|}{\underset{|}{Si}}(CH_2)_3NHCH_2P(O)(OH)_2$$

AMPA-D

The elemental analysis data of the obtained sorbent (Table 1) showed a C : N : P ratio of 4 : 1 : 1, corresponding to the AMPA-D sorbent with grafted aminomethylphosphonic acid groups.

Preliminary static sorption experiments demonstrated that a 10-minute contact time between the phases was sufficient to achieve constant sorption values for base metal ions using the selected sorbents.

The dependencies of Cu(II), Ni(II), and Fe(III) ion sorption on the solution acidity for the IDA-D, AMPA-D, and PA-D sorbents are shown in Figs. 1 and 2. It can be seen that sorption occurs in weakly acidic media and is practically absent in 1—2 M HCl. The sorption capacity of the sorbents decreases in the order: IDA-D > > AMPA-D > PA-D.

The data on the effect of chloride ion concentration on the sorption of Cu(II), Ni(II), and Fe(III) ions on the IDA-D sorbent are presented in Table 2. It can be seen that, within the concentration range of 10 to 90 g/L, the effect is practically negligible.

Thus, the overall results indicate that IDA-D is the most promising sorbent for the removal of base metal ions from complex process solutions.

Experiments on the separation of Pd(II), non-ferrous metal, and iron ions using the IDA-D sorbent under dynamic conditions, with the results summarized in Table 3, showed that Cu(II) and Fe(III) ions predominantly transfer into the sorbent phase. Although Pd(II) ions are also sorbed by this complexing sorbent, their degree of extraction into the sorbent phase does not exceed 39 %. During the washing stage, Pd(II) ions are almost completely (99.3 %) transferred into the wash water (with an overall recovery into solutions reaching 99.7 %). Ni(II) ions are likely displaced by Cu(II) and Fe(III) ions, which have a higher affinity for the sorbent. This leads to the conclusion that the separation of Pd(II) ions from base metal ions, primarily Ni(II) and Cu(II), by sorption onto complexing sorbents is theoretically feasible; however, quantitative sorption of the metal ions accompanying palladium is not achieved. Therefore, we returned to the traditional approach aimed at providing the selective separation of Pd(II) from process solutions. For this purpose, a well-established chemically modified silica, APTES, was used to test the sorption extraction of Pd(II) from solutions generated during the regeneration of low-temperature carbon monoxide oxidation catalysts based on γ-Al_2O_3, which initially contained palladium (II) chloride and copper (II) bromide.

Given that the composition and structure of complexes significantly affect the sorption process, and that the processing of such catalysts yields solutions containing both chloride and bromide ions, determining the composition of the complexes is a critical task. The speciation of Cu(II) and Pd(II) ions in this system can be conveniently analyzed using electronic absorption spectroscopy (EAS), as the absorption bands of Pd(II) halide complexes appear in the visible region at wavelengths between λ = 470÷505 nm, while the absorption of Cu(II) ions occurs at longer wavelengths. Fig. 3 shows the EAS of a model solution corresponding to the composition of process solutions generated during the leaching of spent catalysts for low-temperature carbon monoxide oxida-

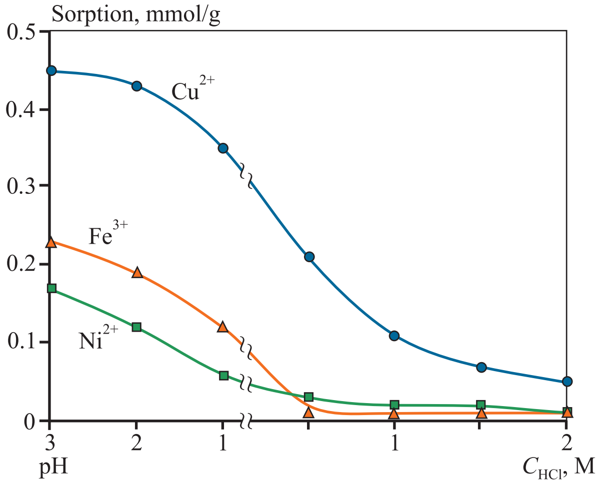

Fig. 1. Dependence of Cu(II), Ni(II), and Fe(III) sorption on HCl concentration on the IDA-D sorbent

$C_{met} = 5 \cdot 10^{-3}$ mol/L, $m_{sorb} = 0.03$ g, $V_{solution} = 10$ mL, contact time – 10 min

Рис. 1. Зависимость сорбции Cu(II), Ni(II) и Fe(III) от концентрации HCl на сорбенте IDA-D

$C_{мет} = 5 \cdot 10^{-3}$ моль/л, $m_{сорб} = 0{,}03$ г, $V_{р\text{-}р} = 10$ мл, время контакта фаз 10 мин

Table. 2. **Effect of chloride ion concentration on the sorption of Cu(II), Ni(II), and Fe(III) ions on the IDA-D sorbent**[*]

Таблица 2. Зависимость сорбции Cu(II), Ni(II), Fe(III) от концентрации хлорид-иона[*]

$[Cl^-]$, g/dm^3	Sorption, mmol/g		
	Cu^{2+}	Ni^{2+}	Fe^{3+}
10	0.36	0.07	0.13
30	0.33	0.07	0.16
50	0.33	0.07	0.11
70	0.38	0.05	0.11
90	0.38	0.05	0.12

[*] $C_{met} = 5 \cdot 10^{-3}$ mol/L, $m_{sorb} = 0.03$ g, $V_{solution} = 10$ mL, contact time = 10 min.

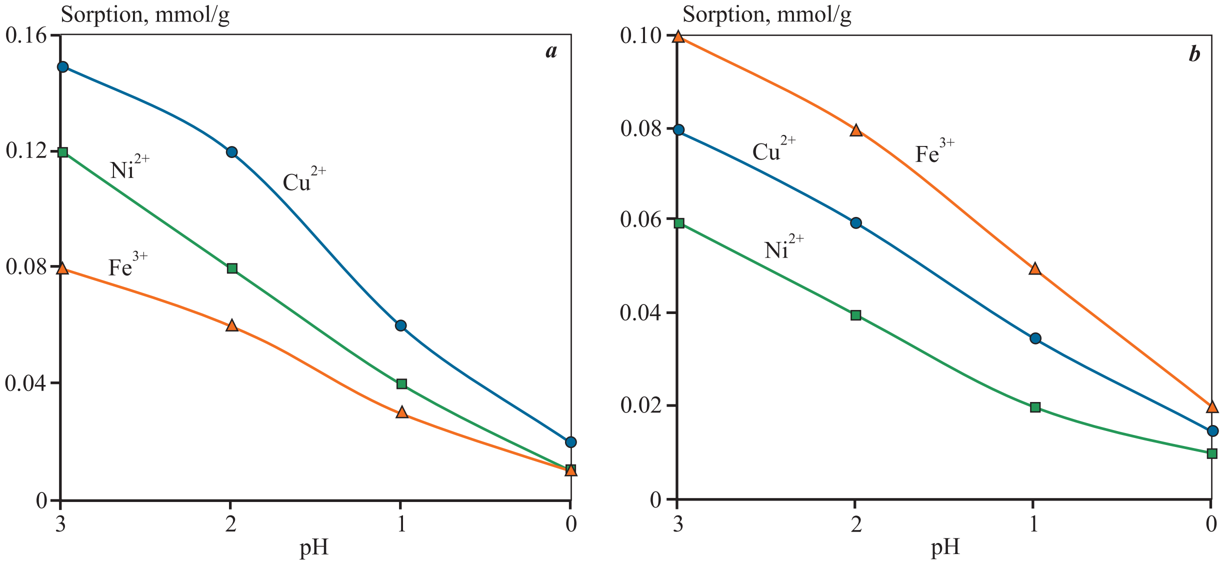

Fig. 2. Dependence of (II), Ni(II), and Fe(III) ion sorption on HCl concentration on the AMPA-D (***a***) and PA-D (***b***) sorbents

$C_{met} = 5 \cdot 10^{-3}$ mol/L, $m_{sorb} = 0.03$ g, $V_{solution} = 10$ mL, contact time – 10 min

Рис. 2. Зависимость сорбции ионов Cu(II), Ni(II) и Fe(III) от концентрации HCl на сорбентах AMPA-D (***a***) и PA-D (***b***)

$C_{мет} = 5 \cdot 10^{-3}$ моль/л, $m_{сорб} = 0{,}03$ г, $V_{р\text{-}р} = 10$ мл, время контакта фаз 10 мин

Table. 3. Results of separation of Pd(II), Cu(II), Ni(II), and Fe(III) ions during sorption on IDA-D sorbent under dynamic conditions (m_{sorb} = 0.6 g)

Таблица 3. Результаты разделения ионов Pd(II), Cu(II), Ni(II) и Fe(III) в процессе сорбции на сорбенте IDA-D в динамических условиях ($m_{\text{сорб}}$ = 0,6 г)

Paremeter	Pd(II)	Cu(II)	Ni(II)	Fe(III)
Sorption ($V_{\text{in}} = V_{\text{out}}$ = 7 mL)				
m_{in}, μg	3720	2220	2050	1960
m_{out}, μg	2280	77	1645	350
m'_{sorb}, μg	1440	2143	405	1610
E_{sorb}, %	38.7	96.5	19.8	82.1
Washing with water (V_{wash} = 5.4 mL)				
m_{wash}, μg	1430	130	405	162
m'_{wash}, μg	10	2013	0	1448
E_{wash}, %	99.3	6.1	>99.9	10.1
$E_{\text{overall (solution)}}$, %	99.7	9.3	>99.9	26.1
Elution with 2 M HCl (V_{el} = 7 mL)				
m_{el}, μg	0.7	1995	0	1295
E_{el}, %	7	99.1	0	89.4

tion [9]. The figure also presents the absorption spectra of $PdCl_2$ and $CuBr_2$ solutions in 1 M HCl.

As shown in Fig. 3, two absorption bands are observed in the visible region of the model solution spectrum, with maxima at λ = 480 nm and 830 nm. It is well established that in solutions containing both chloride and bromide ions, Pd(II) tends to form mixed halide complexes, $[PdCl_{4-n}Br_n]^{2-}$, with the complex composition determined by the halide ion ratio [32]. The EAS of solutions dominated by the $[PdCl_4]^{2-}$ complex is characterized by absorption bands at λ = = 473 nm (ε = 161 L·mol^{-1}·cm^{-1}) and λ = 606 nm (ε = = 10 L·mol^{-1}·cm^{-1}) [33]. In the visible region, the EAS of solutions containing $[PdBr_4]^{2-}$ anions exhibit a charge transfer band at λ = 417 nm (ε = 790 L·mol^{-1}·cm^{-1}) and a broad absorption band at λ = 495—505 nm (ε = = 360 L·mol^{-1}·cm^{-1}) corresponding to *d—d* transitions [32—34].

Preliminary experiments demonstrated that the addition of bromide ions to a hydrochloric Pd-containing solution causes the absorption band at λ = = 473 nm to shift toward longer wavelengths, reflecting the substitution of chloride ions in the inner coordination sphere by bromide ions. In 0.1 M HCl, complete substitution was observed at a $[PdCl_4]^{2-}$ to Br^- ratio of 1:100 (with the band shifting to λ = = 505 nm), whereas in 1 M HCl, even at a $[PdCl_4]^{2-}$ to Br^- ratio of 1:500, the formation of the $[PdBr_4]^{2-}$ complex did not occur.

Thus, the presence of an absorption band at λ = = 480 nm in the model solution spectrum indicates that, in the process solution obtained by leaching the catalyst in 1 M HCl, palladium remains predominantly in the form of $[PdCl_4]^{2-}$. However, as the solution acidity decreases, for example through dilution with water, the likelihood of forming mixed $[PdCl_{4-n}Br_n]^{2-}$ complexes increases significantly.

The state of Cu(II) ions in this solution is discussed below. The EAS of an individual solution obtained by dissolving a weighed sample of $CuBr_2$ in 1 M HBr is characterized by a broad absorption band in the range of λ = 810÷815 nm (Fig. 3). According to the literature [35], in chloride media, depending on the chloride ion concentration, Cu(II) may exist as a mixture of aquated complexes with the compositions $[Cu(H_2O)_4]^{2+}$, $[Cu(H_2O)_2Cl_2]$, $[Cu(H_2O)_3Cl]^+$ and $[Cu(H_2O)Cl_3]^-$. In the visible region, the $[Cu(H_2O)_3Cl]^+$ complex, which dominates at chloride ion concentrations of 0.1—1.0 mol/L, exhibits an absorption band at λ = 870 nm (ε = 80 L·mol^{-1}·cm^{-1}). A slight shift of its maximum to 830 nm in the leaching solution indicates the presence of mixed aquated and halide forms of Cu(II) in the solution.

Static sorption studies of Pd(II), Cu(II), and Al(III) ions on the APTES sorbent from individual hydrochloric solutions showed that equilibrium sorption values for Pd(II) were achieved after 5—10 min of phase

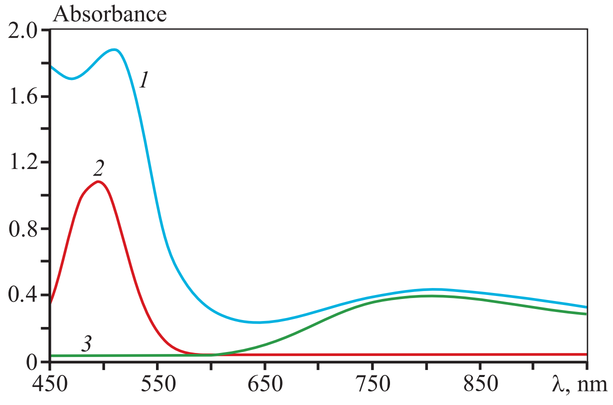

Fig. 3. Electronic absorption spectra (EAS) of the model solution in 1 M HCl (*1*), the $PdCl_2$ solution in 1 M HCl (*2*), and the $CuBr_2$ solution in 1 M HBr (*3*)
$C_{\text{Pd}} = 2\cdot10^{-3}$ mol/L, $C_{\text{Cu}} = 1\cdot10^{-2}$ mol/L

Рис. 3. ЭСП модельного раствора в 1 M HCl (*1*), раствора $PdCl_2$ в 1 M HCl (*2*) и раствора $CuBr_2$ в 1 M HBr (*3*)
$C_{\text{Pd}} = 2\cdot10^{-3}$ моль/л, $C_{\text{Cu}} = 1\cdot10^{-2}$ моль/л

mixing (0.156 mmol/g), for Cu(II) after 20—30 min (0.084 mmol/g for $CuCl_2$ and 0.060 mmol/g for $CuBr_2$ solution in 1 M HCl), whereas the equilibrium sorption time for Al(III) ions was 45 min (0.319 mmol/g). It should be noted that the sorption of Pd(II) by the selected sorbent, as well as complex formation during the sorption process, have been discussed in detail in our earlier work [20].

An increase in HCl concentration in the solution leads to a decrease in the sorption of Pd(II) and Cu(II) (Table 4). For example, in 0.1 M HCl, the sorption capacities for Pd(II) and Cu(II) are 1.43 and 0.97 mmol/g, respectively, whereas in 4 M HCl they decrease to 0.4 and 0.6 mmol/g, respectively.

A decrease in the sorption of palladium and copper ions on the APTES sorbent with increasing hydrochloric acid concentration is generally attributed to the competitive sorption of halide ions [20; 36; 37]. In contrast, Al(III) ions are sorbed only at HCl concentrations above 1 M, and their sorption capacity remains nearly constant at approximately 2.8 mmol/g of sorbent. This behavior is likely due to the involvement of silanol groups on the sorbent matrix in cation exchange, whereby protons are replaced by Al(III) cations [38]. It should also be noted that the formation of a certain proportion of anionic Al(III) chlorocomplexes at higher acid concentrations, as reported in several studies [39; 40], cannot be excluded.

Table 4. **Dependence of Pd(II), Cu(II), and Al(III) sorption under static conditions on HCl concentration**

Таблица 4. Зависимость сорбции Pd(II), Cu(II) и Al(III) в статических условиях от концентрации HCl

Metal*	Sorption, mmol/g, at C_{HCl}, M				
	0.1	0.5	1	2	4
Pd	1.43	1.07	0.77	0.43	0.4
Cu	0.97	**	0.67	0.65	0.6
Al	–	**	2.87	2.81	2.69

* C_{Pd}^{in} = 14 mmol/L, C_{Cu}^{in} = 55 mmol/L, C_{Al}^{in} = 56 mmol/L.
** No experiment was conducted.

Based on the static sorption data obtained, the possibility of separating Pd(II) ions from Cu(II) and Al(III) ions under dynamic conditions was evaluated. To achieve better separation of these elements, sorption was carried out from a solution with an HCl concentration of 0.1 M.

Solutions of 2 M and 3 M HCl (at room temperature and at 60—65 °C) were initially tested as eluents. However, the desorption results proved unsatisfactory under both static and dynamic conditions. Therefore, a 5 % thiourea (Thio) solution in 0.1 M HCl was subsequently used as the eluent [21].

The separation of non-ferrous metal ions from palladium was studied under dynamic conditions using a model solution simulating the leaching solution of the catalyst, diluted to 0.1 M HCl. Three sorption—washing—desorption cycles were carried out using the same portion of the sorbent. The initial volumes of solution used in the sorption stage were 2.4, 1.7, and 1.2 mL for the first, second, and third cycles, respectively. After sorption, the sorbent was washed with distilled water until the washings became colorless (the volume of wash water was approximately 50 mL), followed by elution of palladium ions using a 5 % Thio solution in 0.1 M HCl (8.5—11.4 mL). The data presented in Table 5 show that during sorption, more than 99.9 % of Pd(II) ions were transferred to the sorbent phase, while the sorption of Cu(II) ions ranged from 15.1 % to 18.3 %, and that of Al ions from 1.3 % to 17.2 %. Washing the sorbent with distilled water allowed for the almost complete removal of non-ferrous metal ions from the sorbent phase ($E_{Cu}^{\Sigma} = 95.4 \div 97.0$ %, $E_{Al}^{\Sigma} = 95.2 \div 99.0$ %).

Thus, nearly complete separation of Pd(II) from accompanying non-ferrous metals was achieved during the sorption and washing stages. The degree of Pd(II) recovery into the eluate was 85—90 %. It was demonstrated that the proposed sorbent remains stable over at least three sorption cycles.

Based on the results of the present study, we propose a process scheme for the recycling of spent low-temperature carbon monoxide oxidation catalysts containing $PdCl_2$ and $CuBr_2$, which includes the following stages:

1) leaching of the spent catalysts with 1 M HCl;
2) adjustment of the acidity of the resulting solution to pH 1;
3) sorption onto the APTES sorbent;
4) washing of the sorbent with water;
5) desorption of palladium using a hydrochloric acid solution of Thio;
6) recovery of palladium from the resulting eluate.

During the sorption stage, selective sorption of palladium onto the APTES sorbent occurs, while non-ferrous metals are concentrated in the solution combined with the wash water after sorption [21].

It should be noted that during the desorption stage, a tetrathiourea complex of the composition $[Pd(Thio)_4]^{2+}$ of orange color is formed in the eluate [20], from which an *X*-ray amorphous precipitate of metallic palladium can be obtained by treatment with a 5 M NaOH solu-

Table. 5. **Results of the experiment on the separation of Pd(II), Cu(II), and Al(III) using the APTES sorbent**

Таблица 5. Результаты эксперимента по разделению Pd(II), Cu(II) и Al(III) на сорбенте APTES

Experiment	Sorption stage E_{sorb}, %			Washing stage (combined solutions after sorption and washing), E_{wash}, %			Elution stage (solution after elution with 5 % Thio in 0.1 M HCl)		
	Pd	Cu	Al	Pd	Cu	Al	$V_{solution}$, mL	C_{Pd}, μg/mL	E_{el}^{Pd}, %
1st cycle	>99.9	15.1	1.3	**	95.2	99.0	8.5	406	90.1
2st cycle	>99.9	17.0	4.6	**	98.0	97.1	11.4	212	89.1
3st cycle	>99.9	18.3	17.2	**	97.0	95.2	9.9	164	84.8

* C_{Pd} = 15 mmol/L, C_{Cu} = 49 mmol/L, C_{Al} = 60 mmol/L, C_{HCl} = 0.1 M, m_{sorb} = 0.15 g.

** Pd(II) ions were not detected in the solutions.

tion. Indeed, according to *X*-ray photoelectron spectroscopy data, the binding energies of the Pd $3d_{3/2}$ and $3d_{5/2}$ electrons in the investigated sample are 341.1 and 335.8 eV, respectively, which correspond to metallic palladium (Pd^0) [41]. In this process, thiourea, which is oxidized to formamidinodisulfide (Fds), acts as a reducing agent for palladium ($E^0_{Pd^{2+}/Pd} = 0.92$ V); the standard redox potential of the Fds/2Thio system is 0.42—0.48 V [42].

The recovery of palladium into the solid product is practically quantitative.

Conclusions

1. Under static conditions, the sorption behaviors of Cu(II), Ni(II), and Fe(III) ions on IDA-D, AMPA-D, and PA-D sorbents as a function of solution acidity were investigated. For the IDA-D sorbent, the effect of chloride ion concentration was additionally studied. Based on the obtained results, IDA-D can be recommended for the removal of base metals.

2. Based on the sorption data for Pd(II), Cu(II), Ni(II), and Fe(III) ions onto the specified sorbent under dynamic conditions, it was established that the preliminary recovery of base metal ions from process solutions formed during the processing of various types of noble metal-bearing raw materials (in this study, palladium) by sorption onto complexing chemically modified silicas does not ensure the selective separation of Pd(II).

3. Using model solutions simulating those formed during the regeneration of low-temperature carbon monoxide oxidation catalysts and containing chloride and bromide anions, the possibility of separating palladium from non-ferrous metals by sorption onto chemically modified silica bearing grafted γ-aminopropyltriethoxysilane (APTES) groups was demonstrated.Considering the chemical states of the sorbed ions, the equilibrium times for Pd(II), Cu(II), and Al(III) sorption were determined under static conditions, and the dependencies of their sorption on solution acidity were established. It was shown that the sorption capacities for Pd(II) and Cu(II) decrease with increasing HCl concentration from 0.1 M to 4 M, while Al(III) begins to sorb at HCl concentrations above 1 M, with its sorption capacity remaining practically constant.

4. The optimal conditions for the separation of Pd(II), Cu(II), and Al(III) ions on the APTES sorbent under dynamic conditions were determined: sorption from 0.1 M HCl, washing the sorbent with water, and desorption of Pd(II) with a 5 % Thio solution in 0.1 M HCl. It was found that under these conditions, the separation of palladium from non-ferrous metals is achieved already during the sorption and washing stage.

5. Metallic palladium is obtained by reducing the thiourea eluate with 5 M NaOH solution.

References

1. PGM Market Report, May 2024. London: Johnson Matthey, 2024. P. 48. https://matthey.com/documents/161599/509428/PGM-Market-Report-24.pdf/4d557d3b-47d1-d975-c4af-5df1c81000f0?t=1715228936090
2. Chorkendorf I., Naimantsvedrait Kh. Modern catalysis and chemical kinetics. Dolgoprudny: Publishing House "Intellect", 2010. 599 p. (In Russ.).
   Чоркендорф И., Наймантсведрайт Х. Современный катализ и химическая кинетика. Долгопрудный: ИД «Интеллект», 2010. 599 с.
3. Valishina E.A., Guedes da Silva M.F.C., Kinzhalov M.A., Timofeeva S.A., Buslaeva T.M., Haukka M., Pombeiro A.J.L., Boyarskiy V.P, Kukushkin V.Yu., Luzyanin K.V. Palladium — ADC complexes as effective catalysts in copperfree and room temperature Sonogashi-

ra coupling. *Journal of Molecular Catalysis A: Chemical.* 2014;395:162—171.
https://doi.org/10.1016/j.molcata.2014.08.018

4. Goulas K.A., Sreekumar S., Song Y., Kharidehal P., Gunbas G., Dietrich P.J., Johnson G.R., Wang Y.C., Grippo A.M., Grabow L.C., Gokhale A.A., Toste F.D. Synergistic effects in bimetallic palladium—copper catalysts improve selectivity in oxygenate coupling reactions. *Journal of the American Chemical Society.* 2016;138(21): 6805—6812.
https://doi.org/10.1021/jacs.6b02247
5. Yang H., Qin S., Yue Y., Liu L., Wang H., Lu J. Entrapment of a pyridine derivative within a copper—palladium alloy: a bifunctional catalyst for electrochemical reduction of CO_2 to alcohols with excellent selectivity and reusability. *Catalysis Science and Technology.* 2016;6: 6490—6494.
https://doi.org/10.1039/ C6CY00971A
6. Kanwal I., Mujahid A., Rasool N., Rizwan K., Malik A., Ahmad G., Shah S.A.A., Rashid U., Nasir N.M. Palladium and copper catalyzed Sonogashira cross coupling an excellent methodology for C—C bond formation over 17 years: A review. *Catalysts.* 2020;10(4):443.
https://doi.org/10.3390/catal10040443
7. Obradović M.D., Lačnjevac U.Č., Radmilović V.V., Gavrilović-Wohlmuther A., Kovač J., Rogan J.R., Radmilović V.R., Gojković S.Lj. Palladium-copper bimetallic surfaces as electrocatalysts for the ethanol oxidation in an alkaline medium. Available at SSRN 4455250.2023.
https://dx.doi.org/10.2139/ssrn.4455250
8. Lesiak M., Binczarski M., Karski S., Maniukiewicz W., Rogowski J., Szubiakiewicz E., Berlowska J., Dziugan P., Witońska I. Hydrogenation of furfural over Pd—Cu/Al_2O_3 catalysts. The role interaction between palladium and copper on determining catalytic properties. *Journal of Molecular Catalysis A: Chemical.* 2014;395: 337—348.
https://doi.org/10.1016/j.molcata.2014.08.41
9. Bruk L., Titov D., Ustyugov A., Zubavichus Ya., Chernikova V., Tkachenko O., Kustov L., Murzin V., Oshanina I., Temkin O. The mechanism of low-temperature oxidation of carbon monoxide by oxygen over the $PdCl_2—CuCl_2/\gamma\text{-}Al_2O_3$ nanocatalyst. *Nanomaterials.* 2018;8(4):217.
https://doi.org/10.3390/nano8040217
10. Bruk L. G., Ustyugov A. V., Katsman E. A., Iskhakova L.D., Oshanina I.V., Tkachenko O.P., Kustov L.M., Temkin O.N. Kinetics and mechanism of the low-temperature oxidation of carbon monoxide with oxygen on a $PdCl_2—CuCl_2/\gamma\text{-}Al_2O_3$ catalyst. *Kinetics and Catalysis.* 2017;58 (2):179—190.
https://doi.org/10.1134/S0023158417020033
11. Feng Ya., Wang Li, Zhang Ya., Guo Yu. Deactivation mechanism of $PdCl_2—CuCl_2/Al_2O_3$ catalysts for CO oxidation at low temperatures. *Chinese Journal of Catalysis.* 2013;34(5):923—931.
https://doi.org/10.1016/S1872-2067(12)60556-7
12. Giovanna N., Goosey E., Yildiz D.S., Loving E., Nguyen V.T., Riaño S., Yakoumis I., Martinez A.M., Siriwardana A., Unzurrunzaga A., Spooren J., Atia T.A., Michielsen B., Dominguez-Benetton X., Lanaridi O. Platinum group metals recovery using secondary raw materials (PLATIRUS): Project overview with a focus on processing spent autocatalyst. *Johnson Matthey Technology Review.* 2021;65(1)127—147.
https://doi.org/10.1595/205651321X16057842276133
13. Ehrlich G.V., Buslaeva T.M., Maryutina T.A. Trends in sorption recovery of platinum metals: A critical survey. *Russian Journal of Inorganic Chemistry.* 2017;62(14): 1797—1818.
https://doi.org/10.1134/S0036023617140030
14. Lisichkin G.V., Olenin A.Y. Chemically modified silica in sorption-instrumental analytical methods. *Russian Journal of General Chemistry.* 2021;91(5):870—889.
https://doi.org/10.1134/S1070363221050182
15. Radi Smaail, El-Abiad Chahrazad, Moura Nuno M.M., Faustino Maria A.F., Neves M. Graça P.M.S. New hybrid adsorbent based on porphyrin functionalized silica for heavy metals removal: synthesis, characterization, isotherms, kinetics and thermodynamics studies. *Journal of Hazardous Materials.* 2019;370:80—90.
https://doi.org/10.1016/j.jhazmat.2017.10.058
16. Giannakoudakis D.A., Anastopoulos I., Barczak M., Antoniou E., Terpiłowski K., Mohammadi E., Shams M., Coy E., Bakandritsos A., Katsoyiannis I.A., Colmenares J.C., Pashalidis I. Enhanced uranium removal from acidic wastewater by phosphonate-functionalized ordered mesoporous silica: Surface chemistry matters the most. *Journal of Hazardous Materials.* 2021;413:125279.
https://doi.org/10.1016/j.jhazmat.2021.125279
17. Abdelrahman E.A., Khalil M.M.H., Khairy M., El-Reash Ya.G.A., Gad H.M., Katouah H.A., Saad F.A., Rayes S.M.E., Rehman Kh.U. Modification of hydroxysodalite nanoparticles by (3-aminopropyl)trimethoxysilane and isatoic anhydride as a novel composite for efficient sorption of Cu(II) ions from aqueous media. *Silicon.* 2024;16:1083—1096.
https://doi.org/10.1007/s12633-023-02743-6

18. Losev V.N., Volkova G.V., Maznyak N.V., Trofimchuk A.K., Yanovskaya E. Ya. Sorption of palladium by silica chemically modified with N-allyl-N'-propyltylthiourea, followed by spectrometric determination. *Zhurnal analiticheskoi khimii*. 1999;54(12):1254—1258. (In Russ.).
Лосев В.Н., Волкова Г.В., Мазняк Н.В., Трофимчук А.К., Яновская Э.Я. Сорбция палладия кремнеземом, химически модифицированном N-аллил-N'-пропилтилтиомочевиной с последующим спектрометрическим определением. *Журнал аналитической химии*. 1999; 54 (12): 1254—1258.
19. Losev V.N., Kudrina U.V., Trofimchuk A.K. Features of the interaction of chloride and tin chloride complexes of rhodium and iridium with N-(2,6-dimethyl-4-methylenetriphenylphosphonium chloride)—N'-propylthiourea groups covalently attached to the silica surface. *Zhurnal neorganicheskoi khimii*. 2005;50(6): 961—966. (In Russ.).
Лосев В.Н., Кудрина Ю.В., Трофимчук А.К. Особенности взаимодействия хлоридных и оловохлоридных комплексов родия и иридия с N-(2,6-диметил-4-метилентрифенилфосфоний-хлорид)—N'-пропилтиомочевинными группами, ковалентно закрепленными на поверхности кремнезема. *Журнал неорганической химии*. 2005;50(6):961—966.
20. Boryagina I.V., Volchkova E.V., Buslaeva T.M., Vasileva M.V., Erlich G.V. Sorption of chloride complexes of palladium and platinum by chemically modified silicas. *Tsvetnye metally*. 2012;(5):59—64. (In Russ.).
Борягина И.В., Волчкова Е.В., Буслаева Т.М., Васильева М.В., Эрлих Г.В. Сорбция хлоридных комплексов палладия и платины химически модифицированными кремнеземами. *Цветные металлы*. 2012;(5):59—64.
21. Volchkova E. V., Boryagina I. V., Mishikhina E. A., Buslaeva T. M., Erlich G.V., Lisichkin G. A. Method for extracting palladium (II) from spent catalysts: Patent 2442833 (RF). 2010. (In Russ.).
Волчкова Е.В., Борягина И.В., Мищихина Е.А., Буслаева Т.М., Эрлих Г.В., Лисичкин Г.А. Способ извлечения палладия (II) из отработанных катализаторов: Патент 2442833 (РФ). 2010.
22. Brauer G. Manual of inorganic synthesis. Vol. 5. Moscow: Mir, 1985. 360 p. (In Russ.).
Брауэр Г. Руководство по неорганическому синтезу. Т. 5. М.: Мир, 1985. 360 с.
23. Buslaeva T.M., Volchkova E.V., Boryagina I.V. Application of nitrogen- and sulfur-containing chemically modified silica for the selective sorption of Palladium. *Tsvetnye metally*. 2024;(1):24—32. (In Russ.).
https://doi.org/ 10.17580/tsm.2024.01.03
Буслаева Т.М., Волчкова Е.В., Борягина И.В. Применение азот- и серосодержащих химически модифицированных кремнеземов для селективной сорбции палладия. *Цветные металлы*. 2024;(1):24—32.
https://doi.org/ 10.17580/tsm.2024.01.03
24. Bruening R.L., Tarbet B.J., Krakowiak K.E., Bradshaw J.S., Izatt R.M. Support bonded polyalkylene-polyamine-poly(carboxylic acid) and extraction of metal ions therewith: Application WO9217403. (USA) 1992.
25. Bruening R.L., Tarbet B.J., Bradshaw J.S., Izatt R.M., Krakowiak K.E. Aminoalkylphosphonic acid containing ligands attached to solid supports for removal of metal ions: Patent 5182251 (USA). 1993.
26. Rosenberg E., Pang D.C. System for extracting soluble heavy metals from liquid solitions: Patent 5695882 (USA). 1997.
27. Fischer R.J., Pang D., Beatty S.T., Rosenberg E. Silica—polyamine composite materials for heavy metal ion removal, recovery, and recycling. II. Metal ion separations from mine wastewater and soft metal ion extraction efficiency. *Separation Science and Technology*. 1999;34(16):3125—3137.
https://doi.org/10.1081/ss-100100826
28. Hughes M.A., Wood J., Rosenberg E. Polymer structure and metal ion selectivity in silica polyamine composites modified with sodium chloroacetate and nitriloacetic acid (NTA) anhydride. *Industrial & Engineering Chemistry Research*. 2008;47(17):6765—6774.
https://doi.org/10.1021/ie800359k
29. Mingalev P.G., Lisichkin G.V. Chemical modification of oxide materials with organic acids of phosphorus (V) and their esters. *Uspekhi khimii*. 2006;75(6):604—624. (In Russ.).
https://doi.org/10.1070/RC2006v075n06ABEH002478
Мингалев П.Г., Лисичкин Г.В. Химическое модифицирование оксидных материалов органическими кислотами фосфора (V) и их эфирами. *Успехи химии*. 2006;75(6):604—624.
https://doi.org/10.1070/RC2006v075n06ABEH002478
30. Ehrlich G.V., Lisichkin G.V. Sorption in the chemistry of rare earth elements. *Russian Journal of General Chemistry*. 2017;87(6):1220—1245.
https://doi.org/10.1134/S1070363217060196
31. Tihomirova T.I., Nesterenko P.N. Features of complexation reactions on the surface of modified silica sorbents: sorption and complexation chromatography of metals. *Koordinatsionnaya khimiya*. 2022;48(10): 615—624. (In Russ.).
https://doi.org/10.31857/S0132344X22100085

Тихомирова Т.И. Нестеренко П.Н. Особенности реакций комплексообразования на поверхности модифицированных кремнеземных сорбентов: сорбция и комплексообразующая хроматография металлов. *Координационная химия*. 2022;48(10):615—624. https://doi.org/10.31857/S0132344X22100085

32. Biryukov A.A., Shelenskaya V.I., Alimarin I.I. Mixed halide and thiocyanate complex compounds of palladium (II) in aqueous solutions. *Izvestiya Akademii nauk SSSR. Ser. Khimicheskaya, neorganicheskaya i analiticheskaya khimiya*. 1966;(1):3—8. (In Russ.).
Бирюков А. А., Шленская В.И., Алимарин И.И. Смешанные галогенидные и роданидные комплексные соединения палладия (II) в водных растворах. *Известия Академии наук СССР. Сер. Химическая, неорганическая и аналитическая химия*. 1966;(1):3—8.
33. Buslaeva T. M., Simanova S.A. The state of platinum metals in hydrochloric acid and chloride aqueous solutions. Palladium, platinum, rhodium, iridium. *Koordinatsionnaya khimiya*. 1999;25(3):165—176. (In Russ.).
Буслаева Т.М., Симанова С.А. Состояние платиновых металлов в солянокислых и хлоридных водных растворах. Палладий, платина, родий, иридий. *Координационная химия*. 1999;25(3):165—176.
34. Gmelin L., Griffith W. P. Gmelin handbook of inorganic chemistry. Palladium. Berlin, Heidelberg, New York, London, Paris: Springer-Verlag, 1989. 354 p.
35. Kovalchukova O.V. Features of structure, geometrical, and spectral characteristics of the $(HL)_2[CuX_4]$ and $(HL)_2[Cu_2X_6]$ (X — Cl, Br) complexes. In book: Current trends in *X*-Ray Crystallography. 2011:450. https://doi.org/10.5772/27969
36. Ivanov V.M., Gorbunova G.N., Kudryavtsev G.V., Lisichkin G.V., Shurupova T.I. Sorption of palladium, iridium and platinum by chemically modified silicas. *Zhurnal analiticheskoi khimii*. 1984;39(11):504—509. (In Russ.).
Иванов В.М., Горбунова Г.Н., Кудрявцев Г.В., Лисичкин Г.В., Шурупова Т.И. Сорбция палладия, иридия и платины химически модифицированными кремнеземами. *Журнал аналитической химии*. 1984;39(11):504—509.
37. Tikhomirova T.I., Fadeeva V.I., Kudryavtsev G.V., Nesterenko P.N., Ivanov V.M., Savitchev A.T., Smirnovay N.S. Sorption of noble-metal ions on silica with chemically bonded nitrogen-containing ligands. *Talanta*. 1991;38(3):267—274.
https://doi.org/10.1016/0039-9140(91)80046-3
38. Onizhuk M., Ivanov V., Kholin Y., Panteleimonov A. Quantum chemical evaluation of dissociation constants. Test calculations. *National University Bulletin. Chemical Series*. 2016;26(49):65—72.
https://doi.org/10.26565/2220-637X-2016-26-07
39. Branzoi V., Golgovici F., Brânzoi F. Aluminium corrosion in hydrochloric acid solutions and the effect of some organic inhibitors. *Materials Chemistry and Physics*. 2003;78(1):122—131.
https://doi.org/10.1016/S0254-0584(02)00222-5
40. Abd El Aal Emad El Din, Wanees S., Farouk A., Abd El Haleem S. Factors affecting the corrosion behaviour of aluminium in acid solutions. II. Inorganic additives as corrosion inhibitors for Al in HCl solutions. *Corrosion Science*. 2013;68:14—24.
https://doi.org/10.1016/j.corsci.2012.09.038
41. Nefedov V.I. X-ray electron spectroscopy of inorganic compounds: Handbook. Moskow: Khimiya, 1984. 255 p. (In Russ.).
Нефедов В.И. Рентгеноэлектронная спектроскопия неорганических соединений: Справочник. М.: Химия, 1984. 255 с.
42. Buslaeva T.M., Buslaev A.V., Kopylova E.V. Sorption of iridium chlorocomplexes with chemically modified silica. *Izvestiya. Non-Ferrous Metallurgy*. 2000;(3):59—62. (In Russ.)
Буслаева Т.М., Буслаев А.В., Копылова Е.В. Сорбция хлорокомплексов иридия химически модифицированными кремнеземами. *Известия вузов. Цветная металлургия*. 2000;(3):59—62.

Information about the authors

Tat'yana M. Buslaeva – Dr. Sci. (Chem.), Professor of the Departments of Chemistry and Technology of Rare Elements, MIREA – Russian Technological University.
https://orcid.org/0000-0003-2043-8919
E-mail: buslaevatm@mail.ru

Elena V. Volchkova – Cand. Sci. (Chem.), Associate Professor of the Departments of Chemistry and Technology of Rare Elements, MIREA – Russian Technological University.
https://orcid.org/0000-0001-5737-6816
E-mail: volchkovaev@bk.ru

Pavel G. Mingalev – Cand. Sci. (Chem.), Leading Researcher of the Department of Chemistry of Petroleum and Organic Catalysis, Moscow State University named after M.V. Lomonosov.
https://orcid.org/0000-0002-8050-2216
E-mail: uuk2@mail.ru

Irina V. Boryagina – Deputy Head of the Testing laboratory, JSC R&PC Supermetal.
https://orcid.org/0009-0000-5320-8401
E-mail: irinaboryagina@mail.ru

Информация об авторах

Татьяна Максимовна Буслаева – д.х.н., профессор кафедры химии и технологии редких элементов, МИРЭА – Российский технологический университет.
https://orcid.org/0000-0003-2043-8919
E-mail: buslaevatm@mail.ru

Елена Владимировна Волчкова – к.х.н., доцент кафедры химии и технологии редких элементов, МИРЭА – Российский технологический университет.
https://orcid.org/0000-0001-5737-6816
E-mail: volchkovaev@bk.ru

Павел Германович Мингалев – к.х.н., вед. науч. сотрудник кафедры химии нефти и органического катализа, Московский государственный университет им. М.В. Ломоносова.
https://orcid.org/0000-0002-8050-2216
E-mail: uuk2@mail.ru

Ирина Валентиновна Борягина – зам. начальника испытательной лаборатории, АО «НПК «Суперметалл».
https://orcid.org/0009-0000-5320-8401
E-mail: irinaboryagina@mail.ru

Contribution of the authors

T.M. Buslaeva – defined the research objectives, investigated the speciation of sorbed metal ions in solutions, and wrote the manuscript.

E.V. Volchkova – conducted experiments on model solutions and participated in the discussion of the results.

P.G. Mingalev – synthesized the sorbents and participated in the discussion of the results.

I.V. Boryagina – conducted experiments on process solutions and participated in the discussion of the results.

Вклад авторов

Т.М. Буслаева – определение цели работы, изучение состояния ионов сорбируемых металлов в растворах, написание текста статьи.

Е.В. Волчкова – проведение экспериментов на модельных растворах, участие в обсуждении результатов.

П.Г. Мингалев – осуществление синтеза сорбентов, участие в обсуждении результатов.

И.В. Борягина – проведение экспериментов на технологических растворах, участие в обсуждении результатов.

The article was submitted 06.09.2024, revised 22.11.2024, accepted for publication 28.11.2024

Статья поступила в редакцию 06.09.2024, доработана 22.11.2024, подписана в печать 28.11.2024

UDC 669.245:621.74.045
https://doi.org/10.17073/0021-3438-2025-2-55-65

Research article
Научная статья

Grain structure simulation in a large-scale casting made of VZhL14N-VI nickel-base superalloy

A.V. Koltygin[1], **A.A. Nikitina**[1], **A.A. Belova**[1], **V.E. Bazhenov**[1], **V.D. Belov**[1], **E.Yu. Shchedrin**[2]

[1] **National University of Science and Technology "MISIS"**
1 Bld, 4 Leninskiy Prosp., Moscow 119049, Russia

[2] **UEC-Kuznetsov Public Joint Stock Company**
29 Zavodskoe Shosse, Samara 443009, Russia

✉ Andrey V. Koltygin (misistlp@mail.ru)

Abstract: The study addresses the problem of predicting the grain structure in large-scale castings made of the VZhL14N-VI nickel-base superalloy, which are bodies of revolution with very thin walls. To this end, the ProCast casting simulation software was used, including its CAFE module for grain structure prediction. Cooling rates in various areas of the casting were determined by computer simulation. Grain size measurements were then performed on real samples produced under industrial conditions at PJSC UEC Kuznetsov (Samara, Russia), and the correlation between grain size and cooling rate was established. It was found that grain size is affected not only by the cooling rate, but also by the geometric features of the casting, particularly its thermal modulus (according to Chvorinov's rule). The results show that ProCast can be effectively used to predict casting defects in large-scale castings made of nickel-base superalloys. A comparison of the temperature-dependent density, specific heat capacity, and thermal conductivity of the VZhL14N-VI alloy – obtained through both direct measurements and ProCast thermodynamic database calculations – showed that the computed data are sufficiently accurate for use in casting process simulations. The CAFE module was found to be applicable for predicting grain structure in castings; however, accurate simulation requires the specification of key parameters, primarily the degree of undercooling during solidification and the number of grain nuclei in the alloy. Since these parameters cannot be measured directly, further research is required to determine them.

Keywords: nickel-base superalloys, VZhL14N-VI, investment casting, grain size, casting simulation, ProCast, CAFE module, thermal modulus.

Acknowledgments: This study was supported by the Ministry of Science and Higher Education of the Russian Federation under Government Decree No. 218, in accordance with Subsidy Agreement No. 075-11-2022-023 dated April 6, 2022, titled: "Development of a manufacturing technology for unique large-scale castings made of heat-resistant alloys for gas turbine engines, aimed at the use of domestically produced equipment and the establishment of a modern, resource-efficient, computer-aided casting production".

For citation: Koltygin A.V., Nikitina A.A., Belova A.A., Bazhenov V.E., Belov V.D., Shchedrin E.Yu. Grain structure simulation in a large-scale casting made of VZhL14N-VI nickel-base superalloy. *Izvestiya. Non-Ferrous Metallurgy.* 2025;31(2):55–65.
https://doi.org/10.17073/0021-3438-2025-2-55-65

Моделирование макроструктуры крупногабаритной отливки из жаропрочного никелевого сплава ВЖЛ14Н-ВИ

А.В. Колтыгин[1], **А.А. Никитина**[1], **А.А. Белова**[1], **В.Е. Баженов**[1], **В.Д. Белов**[1], **Е.Ю. Щедрин**[2]

[1] **Национальный исследовательский технологический университет «МИСИС»**
Россия, 119049, г. Москва, Ленинский пр-т, 4, стр. 1

[2] **Публичное акционерное общество «ОДК-Кузнецов»**
Россия, 443009, г. Самара, Заводское шоссе, 29

✉ Андрей Вадимович Колтыгин (misistlp@mail.ru)

Аннотация: В работе рассмотрена проблема прогнозирования зеренной структуры в крупногабаритных отливках из никелевого жаропрочного сплава ВЖЛ14Н-ВИ, представляющих собой тела вращения с весьма тонкими литыми стенками. Для этого использовалась система компьютерного моделирования литейных процессов ProCast с модулем для расчета зеренной структуры CAFE. Путем компьютерного моделирования определена скорость охлаждения в различных частях отливки, после чего на реальных образцах, полученных в условиях промышленного производства в ПАО «ОДК-Кузнецов» (г. Самара, Россия), определены размеры зерен и построена их зависимость от скорости охлаждения отливки. Установлено влияние на размер зерна не только скорости охлаждения, но и геометрических особенностей отливки, в частности ее термический модуль (приведенная толщина). Показано, что система ProCast может быть эффективно использована для прогнозирования литейных дефектов в крупногабаритных отливках из жаропрочных никелевых сплавов. При этом путем сравнения температурных зависимостей плотности, теплоемкости и теплопроводности сплава ВЖЛ14Н-ВИ, полученных прямыми измерениями и расчетом с использованием термодинамической базы ProCast, выявлено, что расчетные данные достаточно точны для использования их в компьютерном моделировании литейных процессов. Установлено, что модуль CAFE может быть востребован для прогнозирования зеренной структуры в отливке, однако для его корректного применения необходимо установление параметров моделирования, прежде всего величины переохлаждения при затвердевании и количества зародышей зерен в сплаве. Поскольку эти параметры не поддаются прямому измерению, их определение потребует дополнительных исследований.

Ключевые слова: жаропрочные никелевые сплавы, ВЖЛ14Н-ВИ, литье по выплавляемым моделям, размер зерна, моделирование литейных процессов, ProCast, CAFE.

Благодарности: Работа выполнена при финансовой поддержке Министерства науки и высшего образования Российской Федерации в рамках Постановления Правительства № 218 по соглашению о предоставлении субсидии № 075-11-2022-023 от 06.04.2022 г. «Создание технологии изготовления уникальных крупногабаритных отливок из жаропрочных сплавов для газотурбинных двигателей, ориентированной на использование отечественного оборудования и организацию современного ресурсоэффективного, компьютероориентированного литейного производства».

Для цитирования: Колтыгин А.В., Никитина А.А., Белова А.А., Баженов В.Е., Белов В.Д., Щедрин Е.Ю. Моделирование макроструктуры крупногабаритной отливки из жаропрочного никелевого сплава ВЖЛ14Н-ВИ. *Известия вузов. Цветная металлургия.* 2025;31(2):55–65. https://doi.org/10.17073/0021-3438-2025-2-55-65

Introduction

Nickel-base superalloys are widely used as materials for manufacturing combustion chamber components of gas turbine engines (GTEs) [1; 2]. The composition of the VZhL14N-VI alloy (OST 1 90126-85) is given below (wt. %, max)[1]:

Ni....................................Balance
C.....................................0.08
Cr....................................20.0
Mo....................................5.0
Al.....................................1.5
Ti......................................2.9
Nb.....................................2.8
Fe.....................................10.0

This alloy is used for large-scale cast GTE components and is characterized by a high content of the strengthening γ′ phase ($Ni_3(Al,Ti)$) [1—3]. In addition, the alloy is further strengthened by the precipitation of fine particles of δ (Ni_3Nb), η (Ni_3Ti), and σ (CrFeMoNi, CrMoNi, $(Cr,Mo)_3Ni$) phases, as well as MC, M23C6, and M6C carbides (where M is mainly Cr, but also Ti, Nb, and Mo) [4—8]. The high performance properties of VZhL14N-VI castings depend on their as-cast structure and its evolution during heat treatment [1; 4; 9], which are determined by a combination of grain size and the amount, size, and distribution of carbide and strengthening phases.

The grain size in a casting is affected by the cooling rate achieved during the solidification interval of the alloy. An increase in cooling rate leads to a higher ther-

---

[1] Unless otherwise stated, all compositions are given in wt. %.

mal gradient in the melt ahead of the solidification front, which results in the formation of a larger number of crystals in the two-phase region of the solidifying casting. As a result, competitive grain growth leads to grain refinement [10—12].

To simulate the grain structure in castings, the ProCast (ESI Group) casting simulation system is commonly used, which includes a dedicated CAFE module for grain structure prediction [13]. This module enables the simulation of grain size, shape, and growth direction in castings with equiaxed, columnar, or single-crystal structures [14]. The CAFE module has shown good performance in predicting grain structures in small-scale nickel-base superalloy castings, including turbine blades [15, 16]. However, its application to large-scale castings is limited by the extremely large number of elements in the computational mesh.

In this study, the effect of casting conditions in a shell ceramic mold on the macrostructure of a VZhL14N-VI alloy casting was investigated using computer simulation methods. An attempt was also made to use the CAFE module to predict grain size in large-scale castings. The simulation results were compared with experimental measurements of grain size on samples cut from the casting, with the aim of assessing the effect of cooling rate on grain size in large-scale castings with significant wall thickness variations.

Materials and methods

The test casting was produced using refractory shell molds by investment casting technology. Fused quartz of various fractions, manufactured by JSC DINUR (Pervouralsk, Russia), was used as the filler for both slurry and stucco coatings. Ultracast One+ and Ultracast Prime binders (Technopark LLC, Moscow, Russia) were selected for preparing the refractory slurry. The charge material was a ready-made batch of VZhL14N-VI alloy produced by the All-Russian Scientific Research Institute of Aviation Materials (VIAM, Moscow, Russia). Melting and pouring were performed using the VIAM-24 vacuum induction melting and casting unit (Russia) according to the process specifications of PJSC UEC-Kuznetsov (Samara, Russia).

To reveal the macrostructure, a metallographic template was cut from the casting (Fig. 1) after heat treatment, in a plane passing through the axis of rotation. The sectioned surface of the template was ground and polished using abrasive materials to obtain a mirror-like metallographic surface. The surface was then etched using Marble's reagent (20 g Cu_2SO_4, 100 mL hydrochloric acid, 100 mL ethanol) [17]. Macrostructure images were acquired using a Canon EOS 6D digital camera equipped with a Volna-9 macro lens and extension tubes.

The casting process simulation was carried out using the ProCast software (ESI Group), which has proven effective for simulating investment casting processes involving ceramic shell molds [18—20]. The CAD model included representations of the casting, ceramic mold, insulation, flask, and internal furnace space. The simulation was performed taking into account a 20-minute pre-cooling period of the mold prior to pouring (pouring temperature: 1490 °C), as well as radiative heat transfer. A more detailed description of the simulation procedure is available in [13]. The thermophysical properties of the refractory materials used in the simulation were found to be in good agreement with data reported by other researchers [21; 22] The grain structure of the casting was simulated using the CAFE module of the ProCast software. The initial CAFE calculation parameters were adopted from [23].

To refine the thermophysical properties of the VZhL14N-VI alloy, measurements were conducted to determine the density (ρ), specific heat capacity (C_p), thermal conductivity (λ), and thermal diffusivity ($\lambda = a\rho C_p$), as well as their temperature dependence.

Density at 25 °C was measured using the hydrostatic weighing method. The $\rho(t)$ dependence was calculated based on the thermal expansion coefficient measured with a DIL 402C dilatometer (NETZSCH, Germany). Thermal diffusivity was evaluated by the laser flash method using an LFA 447 instrument (NETZSCH). Specific heat capacity was measured using a DSC 204 F1 Phoenix differential scanning calorimeter (NETZSCH).

Fig. 1. Schematic cross-section of the test casting
Maximum overall dimension: 690 mm

Рис. 1. Эскиз тестовой отливки в разрезе
Максимальный габаритный размер 690 мм

Results and discussion

The test component, produced at PJSC UEC-Kuznetsov, is a large shell-type casting in the form of a body of revolution, with a maximum diameter of about 685 mm and a predominant wall thickness of 6 mm. Figure 2 shows its macrostructure in a longitudinal section through the axis of rotation.

It can be seen that grain size varies significantly across different areas of the casting. During the solidification of massive regions near the mold surface, a fine-grained structure forms, which rapidly transitions into a coarse-grained one. In the thin-walled sections, such transitions are not observed, and the structure remains relatively homogeneous and fine-grained. It is well known that such a structure is most desirable in polycrystalline castings, including those made from nickel-base superalloys, as it ensures optimal mechanical properties of the cast part in accordance with the Hall—Petch relationship [10].

Thus, the highest cooling rates during solidification were observed in the regions with the smallest grain size, while the lowest cooling rates corresponded to coarser-grained areas. In practice, direct measurement of the cooling rate in a solidifying casting is difficult; therefore, the pouring and solidification processes of the VZhL14N-VI alloy were simulated to estimate the cooling rates in different regions of the casting.

Due to equipment limitations, direct measurements of the thermophysical properties of the VZhL14N-VI alloy were restricted to a relatively narrow temperature range (up to 300 °C). To extend the dataset, temperature-dependent properties were calculated using the ProCast thermodynamic database. These calculated values were validated by comparing them with experimental results. Fig. 3 shows both measured and simulated temperature dependencies of density, specific heat capacity, and thermal conductivity for the VZhL14N-VI alloy. The comparison confirms a good level of agreement. The calculated data were subsequently used in the simulation workflow.

The cooling rate in a ceramic shell mold is affected by numerous external factors, all of which were ac-

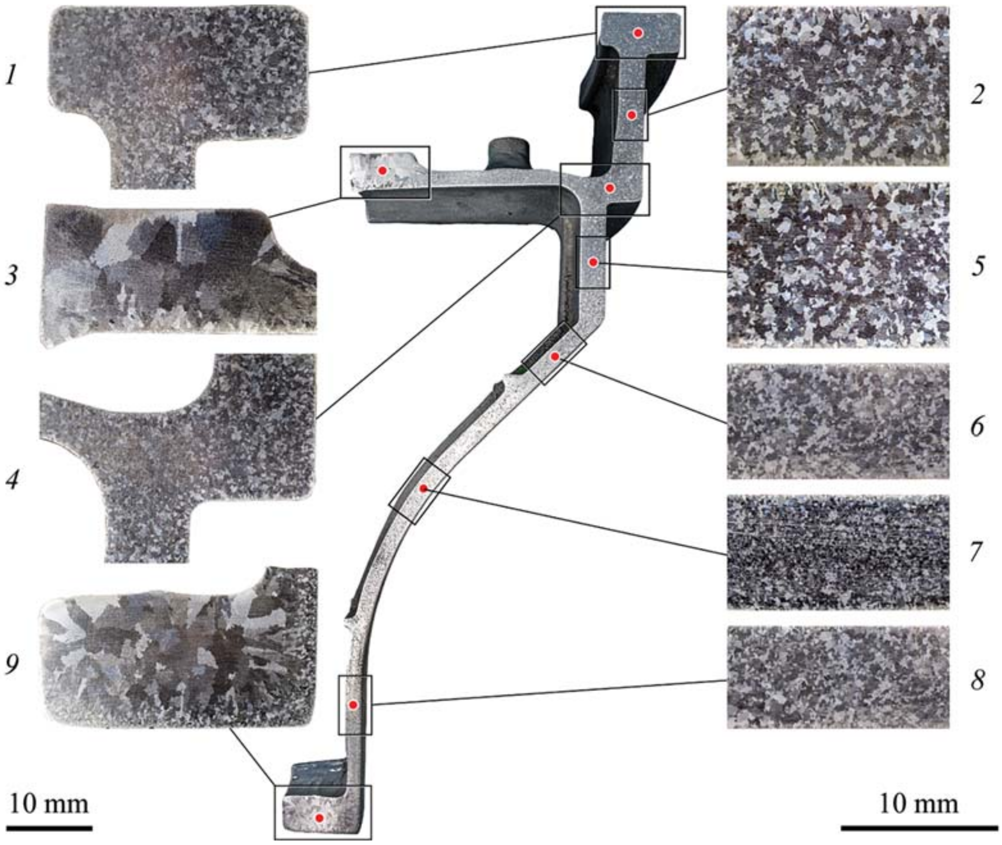

Fig. 2. Grain structure of the test casting wall (etched)
1–9 – grain size measurement areas

Рис. 2. Макроструктура стенки тестовой отливки (травлено)
1–9 – области определения размеров зерен

counted for in the simulation [13]. Fig. 4 presents the relationship between grain size and cooling rate within the solidification interval, based on simulation results at the locations where grain size measurements were performed, as shown in Fig. 2.

At constant wall thickness, higher cooling rates generally result in finer grain sizes. However, this trend is not observed in the relatively thick-walled areas corresponding to points *2* and *5* in Fig. 2: the grain sizes there are nearly identical despite differences in cooling rate. Fig. 5 presents the calculated thermal modulus (equivalent wall thickness) [12] and the temperature distribution across the cross-section of the casting at the moment of mold filling. It can be seen that the areas corresponding to points *2* and *5* had lower initial temperatures — close to the alloy's liquidus temperature — compared to neighboring areas. In addition, these areas exhibited a higher thermal modulus than the surrounding regions in the same cross-section.

These findings suggest that in castings with complex geometry, the relationship between grain size and wall thickness is not always clearly defined when comparing areas of different thicknesses. However, a consistent correlation between grain size and thermal modulus can be observed in areas with similar wall thickness. For example, in areas *1*, *9*, and *3* (see Fig. 2), the grain size increases progressively (see Fig. 4), which corresponds to an increase in the equivalent wall thickness (see Fig. 5). This correlation is logical, as the thermal modulus is defined as the ratio of the volume of a given casting region to its cooling surface area. A higher thermal modulus indicates slower heat removal and a more uniform temperature distribution in the solidifying casting. Therefore, grain size appears to depend not only on the cooling rate, but primarily on the degree of undercooling achieved in the molten alloy ahead of the solidification front [24; 25]. This principle underlies the grain size prediction model implemented in ProCast [20; 23].

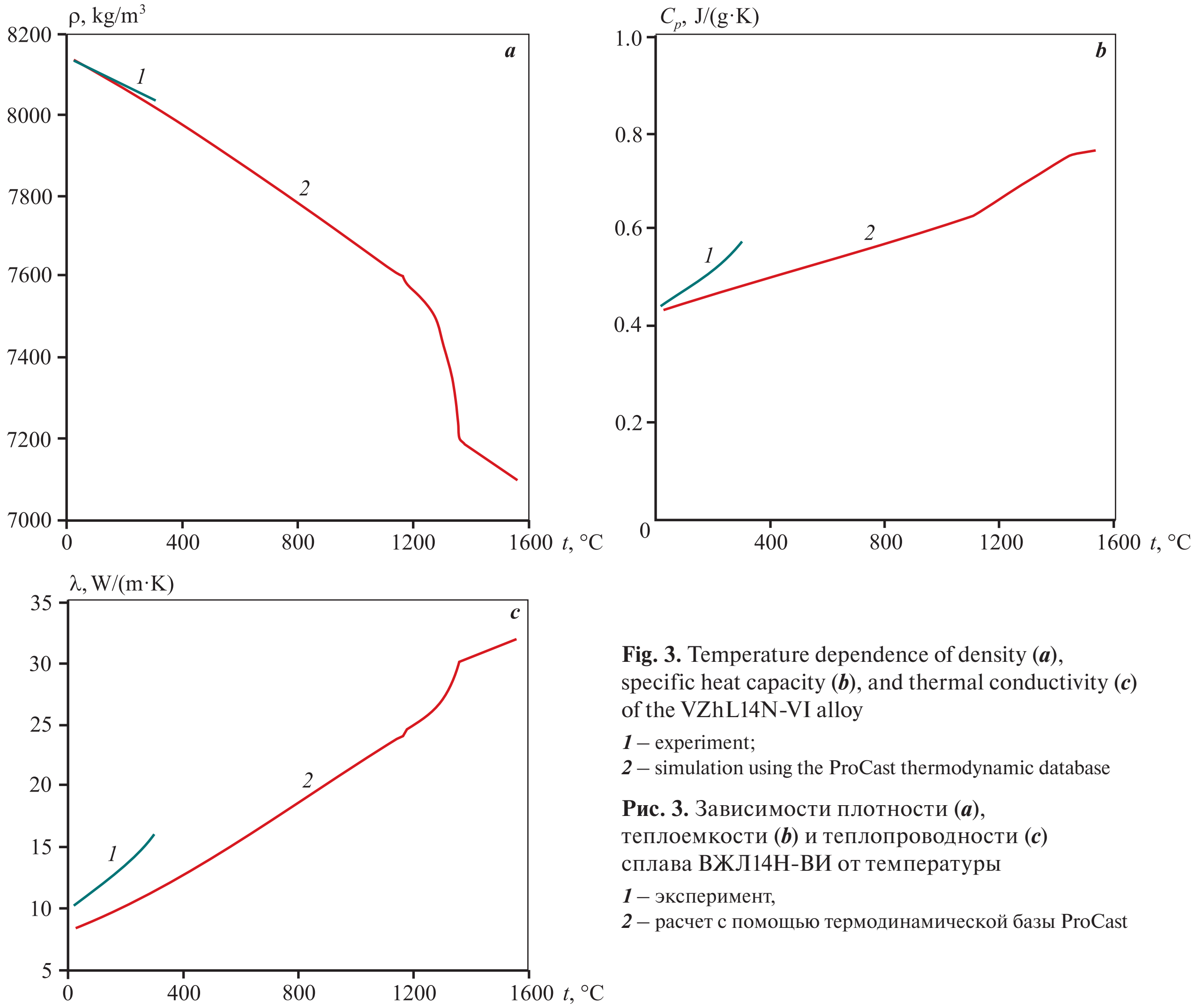

Fig. 3. Temperature dependence of density (***a***), specific heat capacity (***b***), and thermal conductivity (***c***) of the VZhL14N-VI alloy

1 – experiment;
2 – simulation using the ProCast thermodynamic database

Рис. 3. Зависимости плотности (***a***), теплоемкости (***b***) и теплопроводности (***c***) сплава ВЖЛ14Н-ВИ от температуры

1 – эксперимент,
2 – расчет с помощью термодинамической базы ProCast

Figure 6 shows the simulation results for the solid phase fraction in the casting at the beginning and just before the end of solidification. It can be seen that an isolated thermal node forms at the Y-shaped junction of the walls (position *4*), which leads to the formation of shrinkage porosity in this area, confirmed by metallographic examination. The presence of shrinkage defects does not affect the grain size in the corresponding areas (see Fig. 3). It should be noted that the revealed porosity zone was not identified during production using non-destructive testing methods and was discovered only after analyzing the simulation results. This demonstrates the great potential of computer-aided casting process simulation for improving the quality of castings.

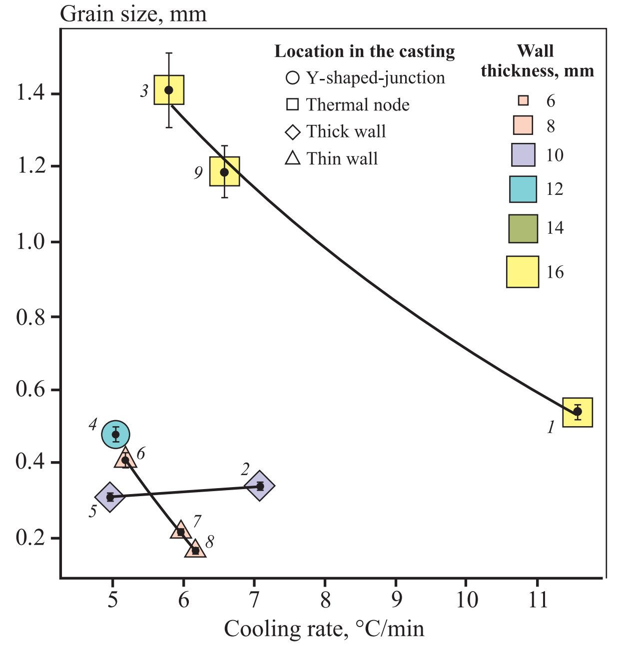

Fig. 4. Grain size vs. cooling rate in the solidification interval for the casing-shaped test component

Points *1*–*9* correspond to the locations shown in Fig. 2

Рис. 4. Зависимость размера зерна в отливке «корпус» от скорости охлаждения в интервале кристаллизации

Цифры *1*–*9* соответствуют точкам, обозначенным на рис. 2

The results of grain structure simulation using the CAFE module are shown in Fig. 7, with the input parameters listed in the accompanying table. The initial simulation (Fig. 7, *a*) was performed using parameter values proposed for the IN713C nickel-base superalloy [23]. However, since the VZhL14N-VI alloy has a different composition and was cast under conditions differing from those described in [23], the simulation parameters may vary significantly, and the simulation results may not correspond to the actual grain structure observed in the casting. Nevertheless, due to the lack of verified data for VZhL14N-VI, the parameters for IN713C superalloy were used as a starting point [23].

As shown in Fig. 7, *a*, the simulated grain sizes are significantly larger than those observed in the real casting. Nevertheless, the main trends are consistent with

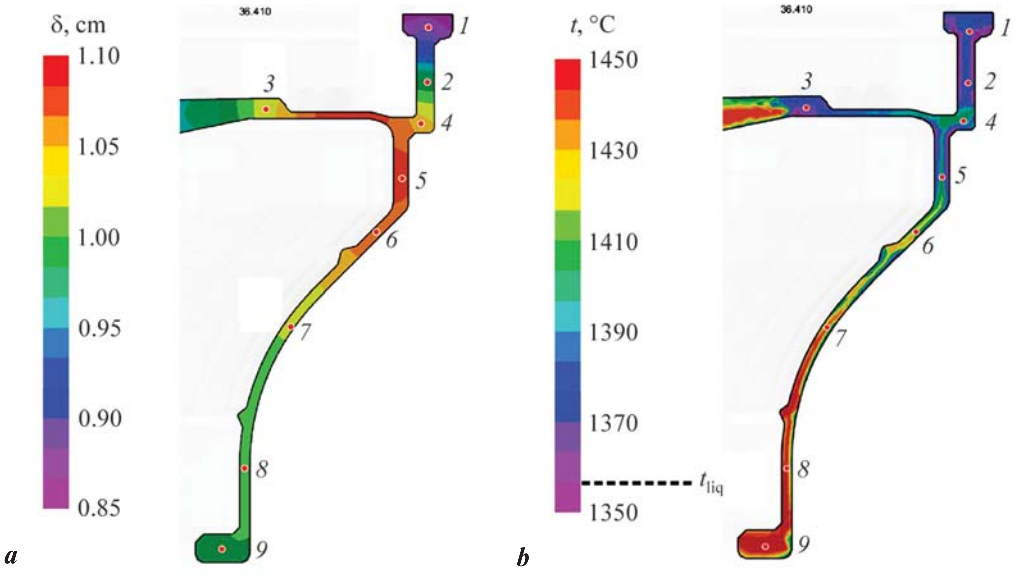

Fig. 5. Thermal modulus (δ) — equivalent wall thickness (***a***), and temperature at the moment of mold filling (***b***)

Рис. 5. Термический модуль отливки (δ) – приведенная толщина стенки (***a***) и температура в момент заполнения формы (***b***)

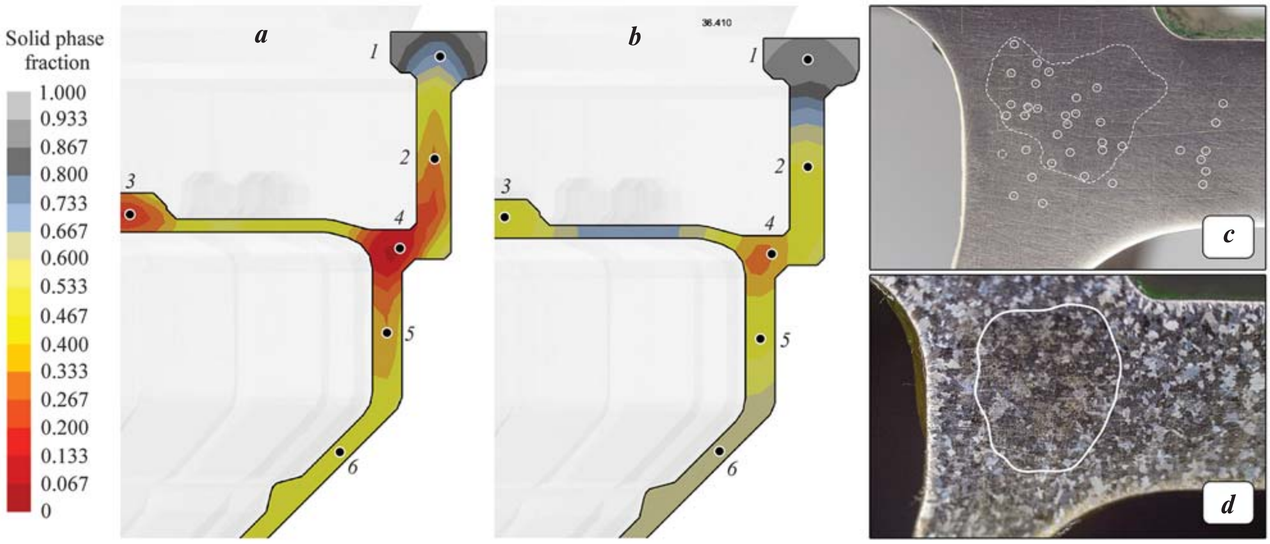

Fig. 6. Simulation results: solid phase fraction after 95 s (***a***) and 157 s (***b***) from the start of pouring; structure in area *4* on a polished sample (***c***) (dashed outline indicates the porous region; individual pores are marked with circles) and on an etched sample (***d***)

Рис. 6. Результаты моделирования: доля твердой фазы спустя 95 с (***a***) и 157 с (***b***) с начала заливки и структура в зоне *4* на полированном (пунктиром выделена область пористости, отдельными окружностями – визуально заметные поры) (***c***) и травленом (***d***) образцах

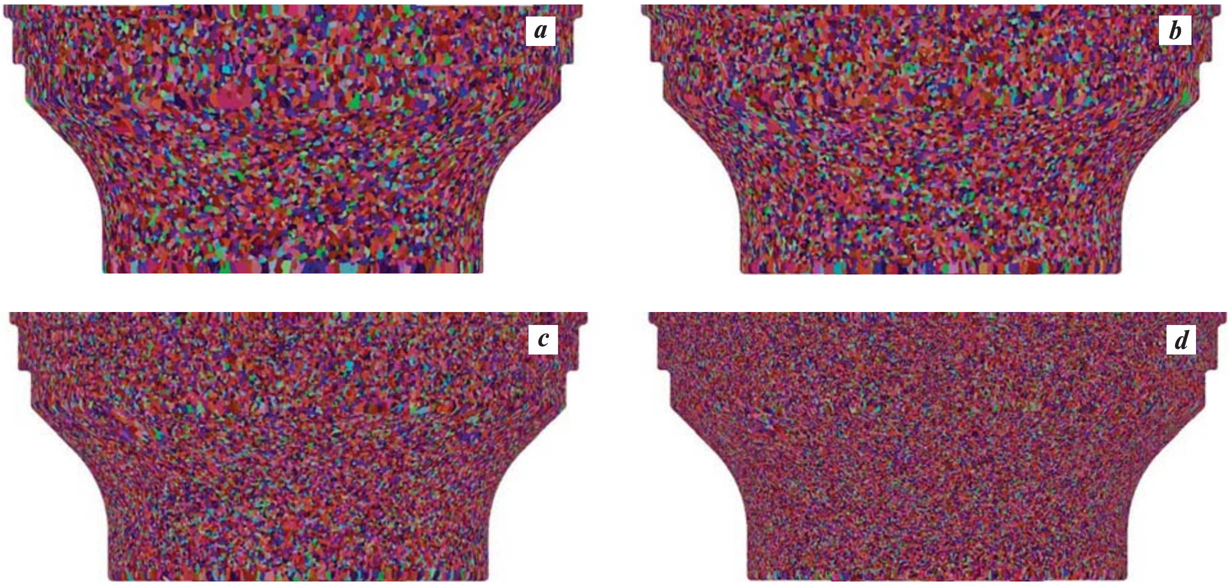

Fig. 7. Results of grain structure simulation using the CAFE module

Simulation cases: *1* (***a***), *2* (***b***), *3* (***c***), and *4* (***d***) (see table)

Рис. 7. Результаты моделирования зеренной структуры отливки с использованием модуля CAFE

Варианты моделирования *1* (***a***), *2* (***b***), *3* (***c***) и *4* (***d***) (см. таблицу)

the actual structure observed in the casting. The main parameters affecting the simulated grain size include the average undercooling (Δt_{avg}), its deviation (Δt_{dev}), and the number of grain nuclei in the melt ($n_{\max}$), which are defined separately for the casting volume and the mold-contacting surface layer [16].

Since the initial simulation produced grains larger than those found in the actual casting — while the overall

Key parameters in grain structure simulation with the CAFE module

Основные параметры моделирования зеренной структуры отливки с использованием модуля CAFE, применявшиеся в работе

Simulation case	Δt_{avg}, K		Δt_{dev}, K		$n_{\max}$, m^{-3}, m^{-2}	
	Volume	Surface	Volume	Surface	Volume	Surface
1 [23]	6.5	5.5	0.7	0.2	$5 \cdot 10^7$	$1 \cdot 10^4$
2					$1 \cdot 10^7$	$5 \cdot 10^4$
3					$5 \cdot 10^7$	$1 \cdot 10^5$
4					$1 \cdot 10^8$	$5 \cdot 10^5$

distribution pattern remained comparable — subsequent iterations retained the same undercooling parameters but increased the number of grain nuclei. In practice, it is extremely difficult to determine the actual number of grain nuclei present in the alloy under industrial casting conditions. Therefore, this number must be adjusted by comparing simulation results with experimentally observed grain structures. This approach requires a separate, resource-intensive study.

The results of the follow-up simulations are shown in Fig. 7, *b—d*. It is evident that increasing the number of grain nuclei in the alloy leads to grain refinement in the casting.

Thus, it is possible to select a combination of initial parameters that yields results correlating with data obtained from actual castings. These parameter values can subsequently be used in simulations to predict grain structure in castings. However, selecting such parameters requires additional studies on a series of castings followed by corresponding simulations. It should also be noted that grain structure simulation in large-scale castings is a highly resource-intensive and time-consuming process that requires the use of high-performance computing systems.

Conclusions

1. Grain size in large-scale castings made of nickel-base superalloys depends on the thermal conditions during solidification — primarily the cooling rate, equivalent wall thickness, and thermal gradient developed in the casting during solidification.

2. Computer simulation using the ProCast software enables the determination of cooling rates in various areas of the casting and helps identify their effect on grain size in walls of similar thickness. In cases of significant variation in wall thickness, grain size is influenced by multiple factors and does not always correlate directly with cooling rate.

3. The CAFE module can be used to simulate grain size in the walls of large-scale castings made of nickel-base superalloys; however, preliminary studies are required to determine key simulation parameters, especially the number of grain nuclei.

4. The ProCast simulation software can also be used to reliably predict shrinkage-related casting defects in large-scale castings made of nickel-base superalloys.

References

1. Logunov A.V., Shmotin Yu.N. Modern heat-resistant nickel-base superalloys for gas turbine disks (Materials and technologies). Moscow: Nauka i tekhnologii, 2013. 264 p. (In. Russ.).
Логунов А.В., Шмотин Ю.Н. Современные жаропрочные никелевые сплавы для дисков газовых турбин (материалы и технологии). М.: Наука и технологии, 2013. 264 с.
2. Hassan B., Corney J. Grain boundary precipitation in Inconel 718 and ATI 718Plus. *Materials Science and Technology*. 2017;33(16):1879—1889.
https://doi.org/10.1080/02670836.2017.1333222
3. Cemal M., Cevik S., Uzunonat Y., Diltemiz F. ALLVAC 718 Plus™ superalloy for aircraft engine applications. In: *Recent Advances in Aircraft Technology*. Agarwal R. (Ed.). 2012. P. 75—96.
https://doi.org/10.5772/38433
4. Kirchmayer A., Pröbstle M., Huenert D., Neumeier S., Göken M. Influence of grain size and volume fraction of η/δ precipitates on the dwell fatigue crack propagation rate and creep resistance of the nickel-base superalloy ATI 718Plus. *Metallurgical and Materials Transactions: A*. 2023;54:2219—2226.
https://doi.org/10.1007/s11661-023-07001-3

5. Donachie M.J., Donachie S.J. Superalloys: A technical guide. 2nd ed. Materials Park, Ohio: ASM International, 2002. 408 p.
6. Chen Y.T., Yeh A.C., Li M.Y., Kuo, S.M. Effects of processing routes on room temperature tensile strength and elongation for Inconel 718. *Materials & Design*. 2017;119:235—243.
https://doi.org/10.1016/j.matdes.2017.01.069
7. Geddes B., Leon H., Huang X. Superalloys: alloying and performance. Ohio, Materials Park: ASM International, 2010. 176 p.
8. Reed R.C. The superalloys: Fundamentals and applications. Cambridge: Cambridge University Press, 2006. 392 p.
9. Gadalov V.N., Vornacheva I.V., Pankov D.N., Bugorsky I.A., Zagidullin R.R., Sabitov L.S., Ivanov A.A. Study of the influence of the structure of nickelchromium superalloys on their mechanical properties. *Izvestiya Tul'skogo gosudarstvennogo universiteta. Tekhnicheskie nauki*. 2022;10:463—471. (In. Russ.).
https://doi.org/10.24412/2071-6168-2022-10-463-471
Гадалов В.Н., Ворначева И.В., Паньков Д.Н., Бугорский И.А., Загидуллин Р.Р., Сабитов Л.С., Иванов А.А. Изучение влияния структуры жаропрочных никельхромовых сплавов на их механические свойства. *Известия Тульского государственного университета. Технические науки*. 2022;10:463—471.
https://doi.org/10.24412/2071-6168-2022-10-463-471
10. Lv J. Effect of grain size on mechanical property and corrosion resistance of the Ni-based alloy 690. *Journal of Materials Science & Technology*. 2018;34:1685—1691.
https://doi.org/10.1016/j.jmst.2017.12.017
11. Cantor B., O'Reilly K. Solidification and casting. 1st ed. CRC Press. 2002. 428 p.
https://doi.org/10.1201/9781420033502
12. Pikunov M.V. Melting of metals. Solidification of alloys. Solidification of castings. Moscow: MISIS, 2005. 416 p. (In. Russ.).
Пикунов М.В. Плавка металлов. Кристаллизация сплавов. Затвердевание отливок. М.: МИСИС, 2005. 416 с.
13. Nikitina A.A., Bazhenov V.E., Koltygin A.V., Belov V.D. Effect of the temperature of the shell ceramic mold before pouring and the pouring temperature on defects in the casting "inner body of the combustion chamber" from nickel heat-resistant alloy VZhL14N-VI. *Tsvetnyye metally*. 2024;1:79—85. (In. Russ.).
https://doi.org/10.17580/tsm.2024.01.10
Никитина А.А., Баженов В.Е., Колтыгин А.В., Белов В.Д. Влияние температуры оболочковой керамической формы перед заливкой и температуры заливки на дефекты в отливке «корпус внутренний камеры сгорания» из никелевого жаропрочного сплава ВЖЛ14Н-ВИ. *Цветные металлы*. 2024;1:79—85.
https://doi.org/10.17580/tsm.2024.01.10
14. Gandin Ch.A., Rappaz M.A. 3D Cellular automaton algorithm for the prediction of dendritic grain growth. *Acta Materialia*. 1997;45(5):2187—2195.
https://doi.org/10.1016/S1359-6454(96)00303-5
15. Rappaz M., Gandin Ch.A. Probabilistic modelling of microstructure formation in solidification processes. *Acta Metallurgica et Materialia*. 1993;41(2):3450—3460.
https://doi.org/10.1016/0956-7151(93)90065-Z
16. Kavoosi V., Abbasi S.M., Mirsaed S.M. Ghazi, Mostafaei M. Influence of cooling rate on the solidification behavior and microstructure of IN738LC superalloy. *Journal of Alloys and Compounds*. 2016;680:291—300.
http://dx.doi.org/10.1016/j.jallcom.2016.04.099
17. Bekkert M., Klemm Kh. Methods of metallographic etching. 2nd ed., revised and enlarged. Moscow: Metallurgiya, 1988. 400 p. (In. Russ.).
Беккерт М., Клемм Х. Способы металлографического травления: Справ. изд.: Пер. с нем. 2-е изд., перераб. и доп. М.: Металлургия. 1988. 400 с.
18. Bazhenov V.E., Koltygin A.V., Fadeev A.V. The use of the ProCast software to simulate the process of investment casting of alloy based on titanium aluminide TNM-B1 into ceramic molds. *Russian Journal of Non-Ferrous Metals.* 2014;55(1):15—19.
https://doi.org/10.3103/S1067821214010039
Баженов В.Е., Колтыгин А.В., Фадеев А.В. Использование программы ProCast для моделирования процесса получения отливок из сплава TNM-B1 на основе алюминида титана литьем в керамические формы. *Известия вузов. Цветная металлургия.* 2013;(6):9—13.
https://doi.org/10.17073/0021-3438-2013-6-9-13
19. Yu J., Wang D., Li D., Tang D., Zhu G., Dong A., Shu D., Peng Y. Process parameter effects on solidification behavior of the superalloy during investment casting. *Materials and Manufacturing Processes*. 2019;34(15):1726—1736.
https://doi.org/10.1080/10426914.2019.1666989
20. Guo J., Beckermann C., Carlson K., Hirvo D., Bell K., Moreland T., Gu J., Clews J., Scott S., Couturier G., Backman D. Microporosity prediction and validation for Ni-based superalloy castings. *IOP Conference Series: Materials Science and Engineering*. 2015;84:012003.
https://doi.org/10.1088/1757-899X/84/1/012003

21. Xu M., Lekakh S.N., Richards V.L. Thermal property database for investment casting shells. International *Journal of Metalcasting*. 2016;10(3):329—337. https://doi.org/10.1007/s40962-016-0052-4
22. Torroba A.J., Koeser O., Calba L., Maestro L., Carreño-Morelli E., Rahimian M., Milenkovic S., Sabirov I., LLorca J. Investment casting of nozzle guide vanes from nickel-based superalloys: Part I. Thermal calibration and porosity prediction. *Integrating Materials and Manufacturing Innovation*. 2014;3(1): 344—368. https://doi.org/10.1186/s40192-014-0025-5
23. Szeliga D., Kubiak K., Burbelko A.A., Cygan R., Ziaja W. Modelling of grain microstructure of IN-713C castings. *Solid State Phenomena*. 2013;197:83—88. https://doi.org/10.4028/www.scientific.net/SSP.197.83
24. Kermanpur A., Rappaz M., Varahram N., Davami P. Thermal and grain-structure simulation in a land-based turbine blade directionally solidified with the liquid metal cooling process. *Metallurgical and Materials Transactions B*. 2000;31(6):1293—1304. https://doi.org/10.1007/s11663-000-0017-z
25. Dantzig J.A., Rappaz M. Solidification: Revised & Expanded. EPFL press, 2016. 700 p.

Information about the authors

Andrey V. Koltygin – Cand. Sci. (Eng.), Assistant Prof., Department of Foundry Technologies and Material Art Working (FT&MAW), National University of Science and Technology “MISIS” (NUST MISIS).
https://orcid.org/0000-0002-8376-0480
E-mail: misistlp@mail.ru

Anna A. Nikitina – Laboratory Assistant, Department of FT&MAW, NUST MISIS.
https://orcid.org/0000-0002-5399-0330
E-mail: nikitina.misis@gmail.com

Anastasia A. Belova – Postgraduate Student, Department of FT&MAW, NUST MISIS.
https://orcid.org/0000-0002-6679-7126
E-mail: belova@ic-ltm.ru

Viacheslav E. Bazhenov – Cand. Sci. (Eng.), Assistant Prof., Department of FT&MAW, NUST MISIS.
https://orcid.org/0000-0003-3214-1935
E-mail: V.E.Bagenov@gmail.com

Vladimir D. Belov – Dr. Sci. (Eng.), Prof., Head of the Department of FT&MAW, NUST MISIS.
https://orcid.org/0000-0003-3607-8144
E-mail: vdbelov@mail.ru

Eugene Yu. Shchedrin – Chief Metallurgist, Public Joint Stock Company “UEC-Kuznetsov”.
E-mail: ogmet@uec-kuznetsov.ru.

Информация об авторах

Андрей Вадимович Колтыгин – к.т.н., доцент кафедры литейных технологий и художественной обработки материалов (ЛТиХОМ), Национальный исследовательский технологический университет «МИСИС» (НИТУ МИСИС).
https://orcid.org/0000-0002-8376-0480
E-mail: misistlp@mail.ru

Анна Андреевна Никитина – учебный мастер 1-й категории кафедры ЛТиХОМ, НИТУ МИСИС.
https://orcid.org/0000-0002-5399-0330
E-mail: nikitina.misis@gmail.com

Анастасия Андреевна Белова – учебный мастер кафедры ЛТиХОМ, НИТУ МИСИС.
https://orcid.org/0000-0002-6679-7126
E-mail: belova@ic-ltm.ru

Вячеслав Евгеньевич Баженов – к.т.н., доцент кафедры ЛТиХОМ, НИТУ МИСИС.
https://orcid.org/0000-0003-3214-1935
E-mail: V.E.Bagenov@gmail.com

Владимир Дмитриевич Белов – д.т.н., профессор, зав. кафедрой ЛТиХОМ, НИТУ МИСИС.
https://orcid.org/0000-0003-3607-8144
E-mail: vdbelov@mail.ru

Евгений Юрьевич Щедрин – главный металлург ПАО ОДК «Кузнецов».
E-mail: ogmet@uec-kuznetsov.ru

Contribution of the authors

A.V. Koltygin – development of the main concept, data analysis, manuscript writing.

A.A. Nikitina – experimental work, data analysis.

A.A. Belova – experimental work, data analysis.

V.E. Bazhenov – scientific supervision, data analysis, manuscript editing.

V.D. Belov – overall supervision, manuscript editing.

E.Yu. Shchedrin – formulation of research objectives and tasks, provision of resources.

Вклад авторов

А.В. Колтыгин – формирование основной концепции, обработка результатов исследований, написание текста статьи.

А.А. Никитина – проведение экспериментов, обработка результатов исследований.

А.А. Белова – проведение экспериментов, обработка результатов исследований.

В.Е. Баженов – научное руководство, обработка результатов исследований, редактирование текста статьи.

В.Д. Белов – общее руководство, редактирование текста статьи.

Е.Ю. Щедрин – формулировка цели и задачи исследования, обеспечение ресурсами.

The article was submitted 10.09.2024, revised 17.12.2024, accepted for publication 19.12.2024

Статья поступила в редакцию 10.09.2024, доработана 17.12.2024, подписана в печать 19.12.2024

FOUNDRY / ЛИТЕЙНОЕ ПРОИЗВОДСТВО

UDC 669.35′6
https://doi.org/10.17073/0021-3438-2025-2-66-75

Research article
Научная статья

Structure and properties of C92900 antifriction bronze produced by upward continuous casting

L.D. Miteva, A.Yu. Titov, I.I. Baranov, T.A. Bazlova, A.A. Nikitina, V.D. Belov

National University of Science and Technology MISIS
1 Bld, 4 Leninskiy Prosp., Moscow 119334, Russia

✉ Ludmila D. Miteva (miteva.ld@misis.ru)

Abstract: Antifriction tin bronzes are used in the aerospace industry to manufacture components that operate in friction assemblies at elevated temperatures. This is due to the alloy's favorable combination of antifriction, mechanical, and corrosion properties. In particular, tin bronze C92900 (alloy Cu–10Sn–3Ni–2Pb (wt. %)) is widely used in such applications. It is employed in the production of braking system components and plunger pump parts. Currently, these parts are manufactured by machining ingots produced through casting with directional solidification. However, this method has a low material utilization rate, typically between 5 % and 15 %. The most promising method for producing C92900 ingots is upward continuous casting technology, which allows the ingot dimensions to closely match those of the finished part. This significantly reduces machining effort and increases metal utilization to 95 %. This study presents the results of process development for the upward continuous casting technology of 15 mm diameter C92900 ingots. The structure and properties of the castings were also investigated. It was shown that as the casting speed increased from 90 to 360 mm/min, the volume fraction of the γ-Cu_3Sn intermetallic phase increased, while the amount of tin-based solid solution remained nearly unchanged. At the same time, the phase distribution became more refined. The macrostructure consisted of columnar and equiaxed grains. As the casting speed increased, the columnar grains became more tilted relative to the direction of heat removal. The hardness increased from 127 ± 2.73 to 136 ± 4.25 HB, and the tensile strength and elongation slightly increased up to 250 mm/min, then decreased at 360 mm/min, which was associated with the macrostructure approaching a transcrystalline form. The study also examined shrinkage cavities and segregation defects in ingots cast at 150 mm/min and analyzed their causes. Finally, the paper provides recommendations for optimal casting parameters for 15 mm diameter ingots produced by upward continuous casting technology.

Keywords: upward continuous casting technology, antifriction bronze, C92900, mechanical properties, ingot defects.

For citation: Miteva L.D., Titov A.Yu., Baranov I.I., Bazlova T.A., Nikitina A.A., Belov V.D. Structure and properties of C92900 antifriction bronze produced by upward continuous casting. *Izvestiya. Non-Ferrous Metallurgy*. 2025;31(2):66–75.
https://doi.org/10.17073/0021-3438-2025-2-66-75

Исследование влияния режимов получения слитков методом непрерывно-пошагового литья вверх на структуру и свойства антифрикционной бронзы БрО10С2Н3

Л.Д. Митева, А.Ю. Титов, И.И. Баранов, Т.А. Базлова, А.А. Никитина, В.Д. Белов

Национальный исследовательский технологический университет «МИСИС»
Россия, 119049, г. Москва, Ленинский пр-т, 4, стр. 1

✉ Людмила Димитровна Митева (miteva.ld@misis.ru)

Аннотация: Антифрикционные оловянные бронзы используются в авиастроении для изготовления деталей, работающих в узлах трения при повышенных температурах. Это обусловлено хорошим сочетанием антифрикционных, механических и коррозионных свойств сплава. В частности, в таких изделиях широко используется оловянная бронза БрО10С2Н3. Из нее изготавливают узлы систем торможения и детали плунжерных насосов. В настоящее время детали из этой бронзы производят механической обработкой слитка, полученного наполнительным литьем с направленной кристаллизацией. Однако такой способ имеет низкий коэффициент использования материала, который составляет 5–15 %. Наиболее перспективным методом получения слитков из бронзы БрО10С2Н3 является непрерывно-пошаговое литье вверх, которое позволяет максимально приблизить размеры слитка к размеру детали, что значительно сокращает трудоемкость механической обработки и повышает коэффициент использования металла до 95 %. В настоящей работе приведены результаты отработки режимов литья слитков диаметром 15 мм из оловянной бронзы БрО10С2Н3 по этой технологии. Также исследованы их структура и свойства. Показано, что с увеличением скорости литья с 90 до 360 мм/мин в слитках возрастает объемная доля интерметаллидной фазы γ-Cu_3Sn, а количество твердого раствора на основе олова практически не изменяется. При этом распределение фаз в бронзе становится более дисперсным. Макроструктура бронзы состоит из столбчатых и равноосных кристаллов. С увеличением скорости литья столбчатые кристаллы меняют свой наклон относительно направления теплоотвода, твердость возрастает с 127 ± 2,73 до 136 ± 4,25 HB, а предел прочности и относительное удлинение незначительно повышаются при скорости литья до 250 мм/мин, а затем снижаются при 360 мм/мин, что связано с приближением макроструктуры к транскристаллитной форме. В работе также проанализированы дефекты (ужимины и ликваты) в слитках, полученных при скорости литья 150 мм/мин, и причины их возникновения. В заключение сформулированы рекомендации по режимам литья слитков диаметром 15 мм при непрерывно-пошаговом литье вверх.

Ключевые слова: непрерывно-пошаговое литье вверх, антифрикционная бронза, БрО10С2Н3, механические свойства, дефекты в слитках.

Для цитирования: Митева Л.Д., Титов А.Ю., Баранов И.И., Базлова Т.А., Никитина А.А., Белов В.Д. Исследование влияния режимов получения слитков методом непрерывно-пошагового литья вверх на структуру и свойства антифрикционной бронзы БрО10С2Н3. *Известия вузов. Цветная металлургия*. 2025;31(2):66–75. https://doi.org/10.17073/0021-3438-2025-2-66-75

Introduction

Tin bronze C92900 is widely used in the aerospace industry due to its advantageous combination of strength, corrosion resistance, and antifriction properties [1; 2]. It is most commonly used for manufacturing components that operate in friction assemblies under elevated temperatures [3; 4]. These parts are typically produced by machining ingots obtained through gravity casting with directional solidification of the alloy. However, this casting method has a low material utilization rate and requires the use of a large feeder head to compensate for solidification shrinkage [5]. This is due to the alloy's tendency to form shrinkage porosity, which results from the wide solidification temperature range of the alloy (70 to 200 °C) [6]. To reduce porosity, special water-cooled molds are used. These ensure a high cooling rate and create favourable conditions for directional solidification of the alloy [5].

The most promising and cost-effective method for producing C92900 blanks is upward continuous casting technology [5; 7]. This method enables the production of ingots with diameters ranging from 15 to 55 mm with minimal shrinkage porosity. This is achieved by promoting directional solidification and ensuring a high cooling rate during solidification. In addition, this casting method reduces the labour intensity of machining and increases material utilization to up to 95 % [8; 9].

It is known [8; 10] that the ingot casting speed during upward continuous casting significantly affects the alloy's micro- and macrostructure. This is due to the increasing intensity of heat removal through the lateral walls of the graphite sleeve of the mold. As shown in [5] for ingots produced by gravity casting, the cooling conditions during solidification influence the quantity, distribution, and size of the structural constituents in C92900 bronze, which in turn affects the mechanical properties of the ingots. However, no such data are available for C92900 ingots produced by upward continuous casting.

The aim of this study was to investigate the effect of casting speed on the structure and properties of C92900 bronze in 15 mm diameter ingots produced by upward continuous casting.

Experimental

To prepare the C92900 bronze samples, primary metals of industrial purity were used: copper grade M1, tin grade O1, nickel grade N-1, and lead grade S1. The alloy was melted in a high-frequency induction crucible furnace (RELTEK, Russia) with a 50 kg capacity, using a graphite-chamotte crucible. To protect the melt from oxidation and hydrogen absorption, the smelting process was carried out under a charcoal cover pre-dried at 120—150 °C. The full charge of nickel and copper was first placed into the crucible. The melt was then heated to 1150—1200 °C and held at this temperature to ensure complete dissolution of nickel. Deoxidation was performed using a copper—phosphorus master alloy (MF10). Tin and lead were introduced at 1150 °C, with the melt held for 3—5 min after each addition. Degassing and removal of non-metallic inclusions were per-

Table 1. Chemical composition of C92900 bronze

Таблица 1. Химический состав бронзы БрО10С2Н3

Composition	Elements, wt. %				Impurities, max wt. %						
	Cu	Ni	Sn	Pb	Fe	Zn	P	Si	Al	Sb	Bi
As per OST 1 90054-72	Balance	3–4	9–11	2–3.25	≤0.3	≤0.5	≤0.1	≤0.02	≤0.02	≤0.3	≤0.02
Actual	Balance	3.46	10.81	2.37	<0.01	<0.01	0.019	<0.005	<0.003	<0.01	<0.003

formed by argon purging (grade 5.6, high purity) for 5—7 min. The chemical composition of the C92900 alloy was determined using a Q4 Tasman optical emission spectrometer (Bruker Quantson, USA) and is presented in Table 1.

The casting process was carried out using the PUVL-450.PS portal-type upward continuous casting unit (NL-Engineering LLC, Belarus), which operates in a cycle of forward stroke — pause — reverse stroke. The working part of the mold (sleeve) was made of graphite grade MPG7. Before casting, the mold was immersed into the melt (temperature: 1100 ± 10 °C) to a depth of 115 ± 5 mm. The experiments were conducted by varying the forward stroke length and pause durations. The casting parameters are presented in Table 2.

To reveal the alloy's macrostructure, an etchant with the composition 5 g $FeCl_3$ + 15 mL HCl + 50 mL H_2O was used. The microstructure of the bronze was examined using a Vega SBH3 scanning electron microscope (Tescan, Czech Republic) equipped with an Oxford energy-dispersive spectroscopy (EDS) system. The phase fractions in the structure were determined using ImageJ 1.52a image analysis software (National Institutes of Health, USA).

Brinell hardness was measured using a NEMESIS 9001 universal hardness tester (INNOVATEST, Netherlands) under the following test parameters: 2.5 mm diameter steel ball, 187.5 kgf (≈1839 N) load, and a 10 s dwell time.

Table. 2. Casting modes of 15 mm diameter C92900 ingots produced by upward continuous casting

Таблица 2. Режимы литья слитков диаметром 15 мм из бронзы БрО10С2Н3
методом непрерывно-пошагового литья вверх

Mode No.	Forward stroke, mm	Pause duration, s	Reverse stroke, mm	Casting speed, mm/min
1	4	2	1	90
2	5	1	1	240
3	7	1	1	360

Tensile tests were performed using a 5569 universal testing machine (Instron, USA). The specimens were machined from the ingots with a gauge section diameter of 5 mm (specimen type Sh No. 7, in accordance with GOST 1497-84).

Phase composition calculations were carried out using the FactSage 8.0 thermochemical software package (Canada).

Results and discussion

The microstructure of C92900 bronze ingots produced by upward continuous casting is shown in Fig. 1. It consists of a copper-based solid solution, eutectic γ-Cu_3Sn intermetallic phase, and a lead-based solid solution [11; 12]. In addition, zonal segregation was observed, resulting in the formation of light regions of the copper-based solid solution with reduced nickel content (down to 2—3 %) and elevated tin content (up to 16.5 %), as well as dark regions containing up to 4 % of both Ni and Sn. The extent of dendritic segregation decreases as the ingot casting speed increases [13; 14]. This is due to enhanced heat removal from the ingot surface during solidification, which correlates with previously reported findings [15; 16]. As a result, the tin content dissolved in the copper-based solid solution in the light regions decreases to 12—14 %, while in the dark regions it remains unchanged at 4 %.

Fig. 2 presents an isothermal section of the Cu—2.5Pb—(9—11)Sn—(3—4)Ni system at 20 °C, constructed using the FactSage software package. It can be seen that in the region corresponding to the alloy's chemical composition (marked as a point on the diagram), in addition to the phases mentioned above, the Sn_4Ni_3Cu phase is also present. However, this phase could not be identified in the microstructure. It is likely that it forms as a result of eutectoid decomposition and occurs only in minor quantities at the examined casting speeds. Further studies are required to confirm this assumption.

---

[1] Unless otherwise stated, all compositions are given in wt. %.

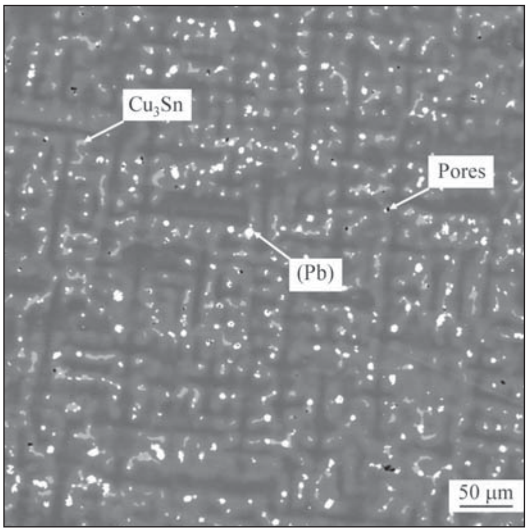

Fig. 1. Microstructure of C92900 bronze in ingots

Рис. 1. Микроструктура бронзы БрО10С2Н3 в слитках

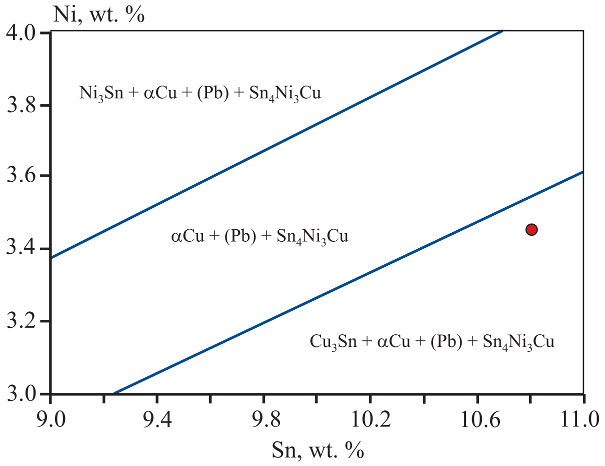

Fig. 2. Isothermal section of Cu–Ni–Sn–Pb phase diagram at 20 °C

Рис. 2. Изотермический разрез диаграммы Cu–Ni–Sn–Pb при $t = 20$ °C

Fig. 3 shows the dependence of the volume fraction and average size (*d*) of the structural components — lead phase (*a*) and γ-Cu_3Sn intermetallic phase (*b*) — on the литье (ν) of the ingots. It can be seen that as the casting speed increases, the volume fraction of the γ-Cu_3Sn phase rises from 3.5 ± 0.83 % to 4.7 ± 0.70 %, while the average grain size remains virtually unchanged. This is likely due to the increased cooling rate during solidification, which promotes the formation of more intermetallics in the alloy structure [7]. The volume fraction of the lead phase increases only slightly — up to 2.5 ± 0.19 %, and its average grain size remains stable. However, the lead inclusions become finer in shape, and their distribution becomes more dispersed. This can be attributed to the fact that lead crystallizes last, forming small globules in the interdendritic spaces [17; 18].

The macrostructure of C92900 bronze in the cross-section of ingots cast at different speeds is shown in Fig. 4. It can be observed that with increasing casting speed *d*, the columnar crystal zone becomes wider, and the inclination angle (α) of their growth relative to the direction of heat removal decreases. At a casting speed of 90 mm/min, the inclination angle is 52.86 ± ± 8.80° (Fig. 4, *a*), whereas at 360 mm/min the structure becomes close to transcrystalline, with an angle of $\alpha = 25.10 \pm 5.16°$ (Fig. 4, *c*). This is due to the increase in the temperature gradient along the graphite mold sleeve

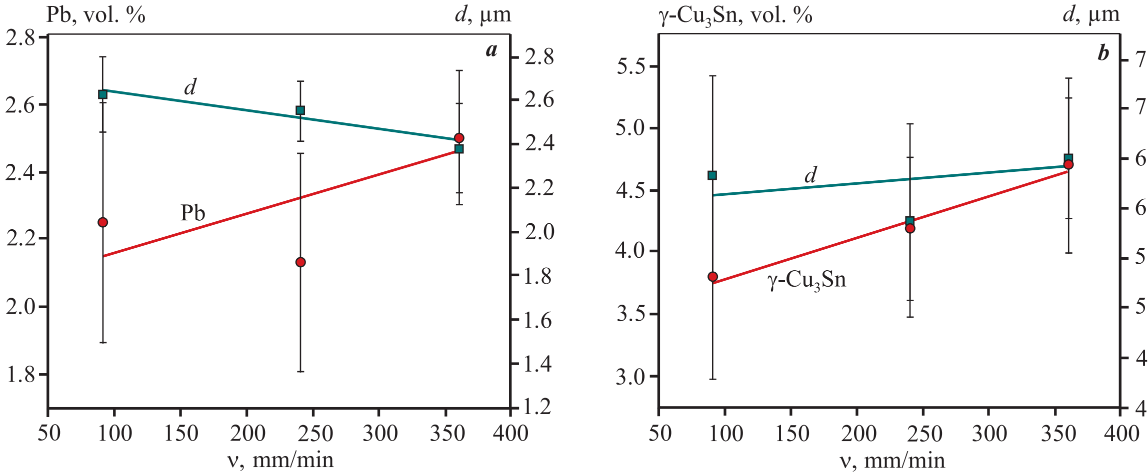

Fig. 3. Effect of casting speed on the phase fractions in the structure of 15 mm C92900 bronze ingots: lead phase (***a***), γ-Cu_3Sn phase (***b***)

Рис. 3. Влияние скорости литья слитков Ж15 мм из бронзы БрО10С2Н3 на долю фаз в структуре сплава: свинцовой (***a***) и γ-Cu_3Sn (***b***) and enhanced heat removal from the ingot surface. A similar pattern was reported by the authors of [8; 19] for C92900 bronze ingots with a diameter of 25 mm.

The effect of ingot casting speed on the mechanical properties of C92900 bronze is shown in Fig. 5. As previously established, an increase in casting speed (ν) leads to a higher volume fraction of the intermetallic phase in the bronze structure, which in turn causes an increase in hardness from 127 ± 2.73 to 136 ± 4.25 HB. At the same time, both ultimate tensile strength (σ_u)and elongation (δ) decrease. The increase in tensile strength at ν = = 240 mm/min is associated with refinement of the macrostructure, while the subsequent decline is attributed to changes in the growth direction of columnar crystals. As the macrostructure of the bronze approaches a transcrystalline form, the alloy strength decreases further due to the accumulation of insoluble impurities in the central part of the ingot [20].

During the development of casting parameters for 15 mm ingots, surface defects were observed on the outer surfaces of the ingots. These included uzhimina defects and segregation defects, as shown in Fig. 6. Uzhimina defects may appear as isolated features or form a ring-shaped pattern on the ingot surface.

Fig. 7 shows the macrostructure and microstructure of the alloy in the area of an uzhimina defect. For clarity, grain boundaries in the macrostructure image of the transverse section are outlined in yellow. Two distinct regions can be identified within the defect: the upper region, containing interdendritic porosity, and the

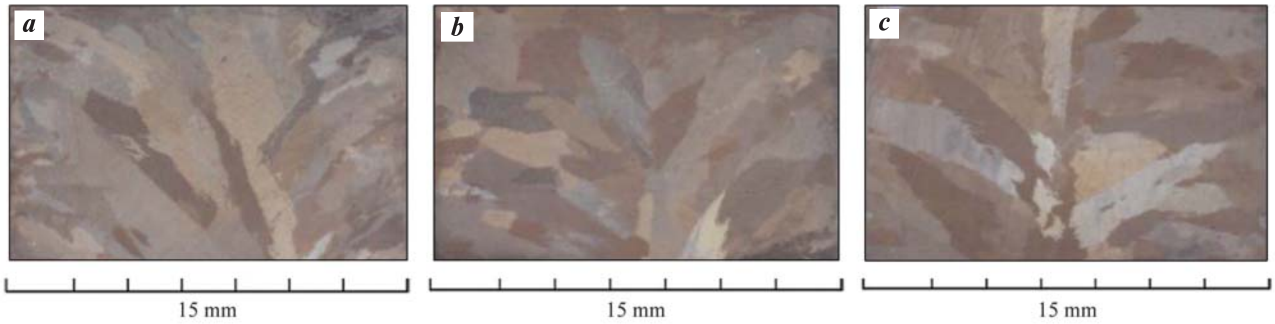

Fig. 4. Macrostructure of C92900 bronze in samples from 15 mm diameter ingots
a – ν = 90 mm/min, inclination angle α = 52.86° ± 8.80°; ***b*** – 240 mm/min, α = 43.71° ± 11.96°; ***c*** – 360 mm/min, α = 25.10° ± 5.16°

Рис. 4. Макроструктура бронзы БрО10С2Н3 в образцах из слитков диаметром 15 мм
a – ν = 90 мм/мин и угол α = 52,86° ± 8,80°; ***b*** – 240 мм/мин и α = 43,71° ± 11,96°; ***c*** – 360 мм/мин и α = 25,10° ± 5,16°

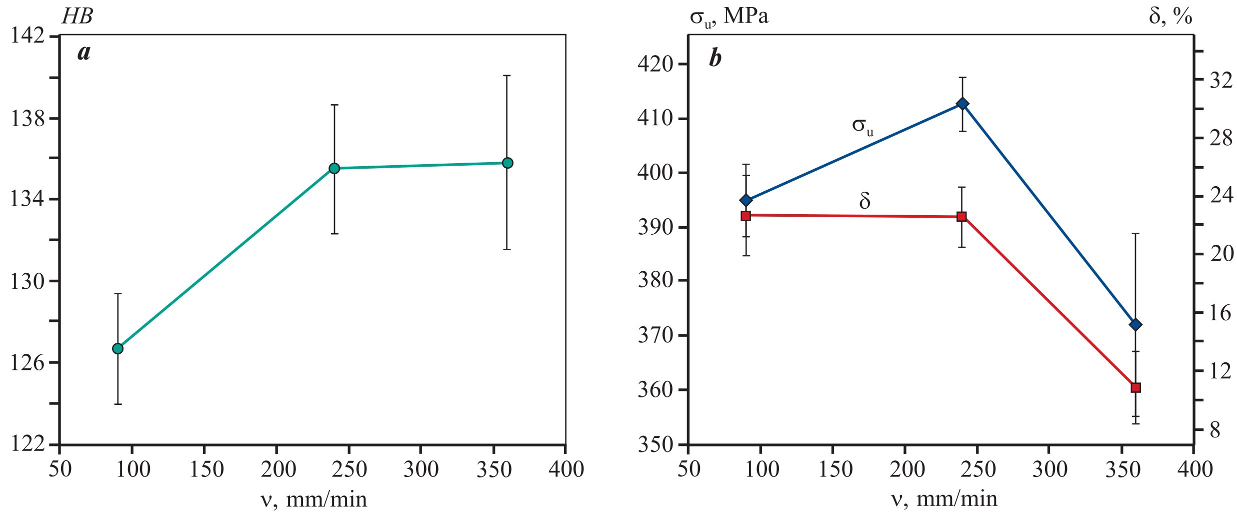

Fig. 5. Effect of ingot casting speed on the mechanical properties of C92900 bronze
a – hardness, ***b*** – ultimate tensile strength and elongation

Рис. 5. Влияние скорости литья слитков на механические свойства бронзы БрО10С2Н3
a – твердость, ***b*** – предел прочности и относительное удлинение

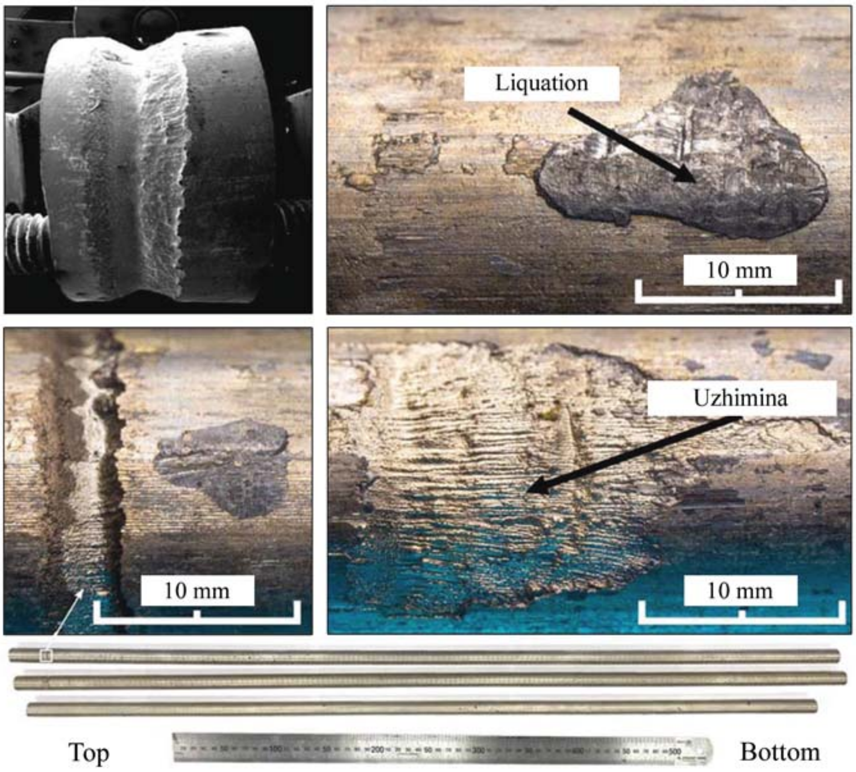

Fig. 6. Surface defects on C92900 bronze ingots

Рис. 6. Дефекты на поверхности слитков из бронзы БрО10С2Н3

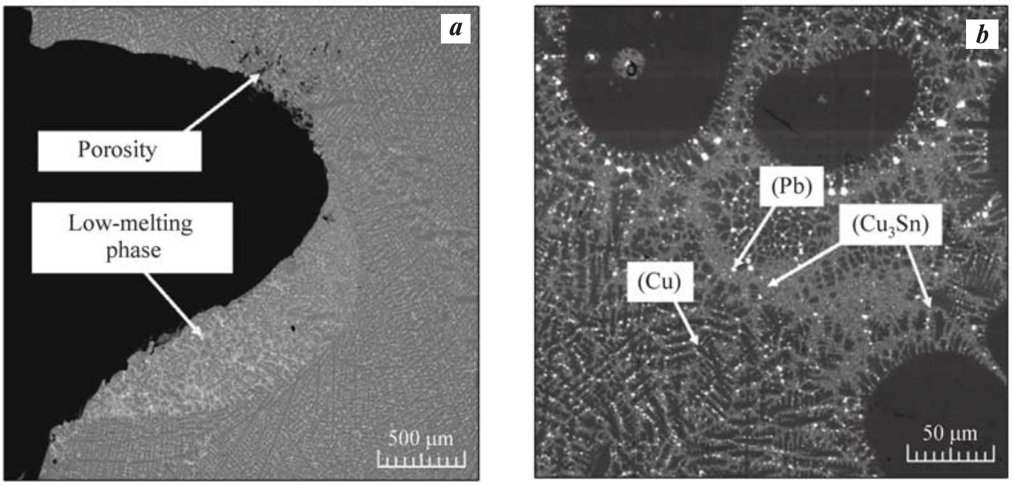

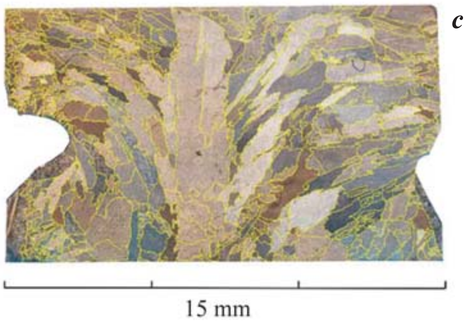

Fig. 7. Microstructure of the uzhimina defect on a C92900 bronze ingot at magnifications of $100^{\times}$ (***a***) and $1000^{\times}$ (***b***), and its macrostructure (***c***)

Рис. 7. Микроструктура дефекта «ужимина» на слитке бронзы БрО10С2Н3 при увеличениях $100^{\times}$ (***a***) и $1000^{\times}$ (***b***), а также его макроструктура (***c***) lower region, consisting mainly of eutectic phase, fine copper-based solid solution grains, and lead inclusions (Fig. 7). This structural pattern is typical for bronze quenched from a temperature within its solidification range. Additionally, traces of a phase enriched in low-melting components can be observed along the surface of the defect, in the direction opposite to the ingot's casting direction (see Fig. 7, *a*). The formation of uzhimina defects is likely associated with increased friction between the surface of the solidifying ingot and the graphite mold sleeve — a common cause of strand breakage and shell sticking during upward continuous casting [18; 21; 22].

As the graphite sleeve undergoes natural wear during operation, microroughness develops on its surface. This roughness becomes filled with molten bronze under static pressure. During the next stage of the casting cycle (forward or reverse stroke), the increased friction causes tearing of the solidifying surface layer, resulting in the formation of a uzhimina defect, which then solidifies without additional melt feeding. As the ingot shrinks, an air gap forms between the ingot surface and the graphite mold sleeve, significantly reducing heat extraction in that area. Under the combined effects of solidification shrinkage and capillary forces, low-melting phases (Pb and Cu3Sn) are squeezed out and accumulate at the base of the defect. As casting proceeds, lead is smeared along the ingot surface during its movement along the mold sleeve, forming segregation defects in the form of lead-enriched surface films. Meanwhile, the microroughness of the graphite surface is gradually polished by contact with the moving ingot. This mechanism accounts for the irregular appearance of such defects on the surface of 15 mm diameter C92900 bronze ingots during upward continuous casting.

Conclusions

1. With an increase in the casting speed of 15 mm diameter C92900 ingots by upward continuous casting from 90 to 240 mm/min, the inclination angle of columnar crystal growth relative to the direction of heat removal decreases from 52.86° ± 8.80° to 43.71° ± 11.96°, which leads to an increase in the alloy's strength to 412 ± 4.91 MPa. The elongation remains unchanged at 22 ± 2.07 %. Further increasing the casting speed to 360 mm/min reduces the inclination angle to 25.10° ± 5.16°, resulting in a decrease in strength and elongation to 372 ± 16.81 MPa and 11 ± 2.47 %, respectively.

2. The macrostructure of C92900 bronze in ingots cast at 360 mm/min approaches a transcrystalline form. It is likely that further increases in casting speed would lead to the formation of a fully transcrystalline structure and, consequently, a decline in both strength and elongation.

3. Increasing the casting speed of 15 mm C92900 ingots to 360 mm/min leads to an increase in the γ-Cu_3Sn phase fraction in the alloy structure from 3.5 ± 0.83 % to 4.7 ± 0.70 %, and in the lead phase fraction to 2.5 ± 0.19 %. The average particle size of γ-Cu_3Sn remains unchanged, while the lead inclusions become smaller and more finely dispersed. This is associated with the higher cooling rate during solidification.

4. The hardness of C92900 bronze ingots produced by upward continuous casting increases from 127 ± 2.73 to 135 ± 3.14 HB as the casting speed rises from 90 to 240 mm/min. This is likely due to the increase in γ-Cu_3Sn phase content in the alloy. Further increases in casting speed do not affect the hardness.

5. Surface defects such as uzhimina and liquation may form on 15 mm diameter C92900 bronze ingots. Their formation is associated with the natural cyclic variation in the surface roughness of the graphite mold sleeve during continuous casting.

6. The recommended casting speed for upward continuous casting of 15 mm C92900 bronze ingots is 240 mm/min. Ingots produced under these conditions exhibit high mechanical properties: ultimate tensile strength σ_u = 412 ± 4.91 MPa, elongation δ = = 22 ± 2.07 %.

References

1. Gruzdeva I.A., Sulitsyn A.V., Mysik R.K., Sokunov B.A. Effect of electromagnetic mixing on tin bronze structure and properties. *Liteishik Rossii.* 2006;(11):27—29. (In Russ.).

   Груздева И.А., Сулицин А.В., Мысик Р.К., Сокунов Б.А. Влияние электромагнитного перемешивания на структуру и свойства оловянных бронз. *Литейщик России*. 2006;(11):27—29.
2. Song K., Zhou Y., Zhao P., Zhang Y., Bai N. Cu—10Sn—4Ni—3Pb alloy prepared by crystallization under pressure: An experimental study. *Acta Metallurgica Sinica (English Letters).* 2013;26(2):199—205. https://doi.org/10.1007/s40195-012-0118-0
3. Gerasimenko E.A., Konovalov A.N., Belov V.D. On solidification of ingots from bronze C92900 when casting in bottom water-cooled casters. *Liteishchik Rossii.* 2013;(7):15-17.

   Герасименко Е.А., Коновалов А.Н., Белов В.Д. О затвердевании слитков из бронзы Бр010С2Н3 при литье в изложницы с донным водяным охлаждением. *Литейщик России*. 2013;(7):15–17.

4. Ozerdem M.S., Kolukisa S. Artificial neural network approach to predict the mechanical properties of Cu—Sn—Pb—Zn—Ni cast alloys. *Materials & Design*. 2009;30(3):764—769.
   https://doi.org/10.1016/j.matdes.2008.05.019
5. Belov V.D., Gerasimenko E.A., Guseva V.V., Konovalov A.N. Effect of solidification conditions for castings of BrO10S2N3 tin bronze on their structure. *Izvestiya. Non-Ferrous Metallurgy*. 2016;(2):26—33. (In Russ.).
   https://doi.org/10.17073/0021-3438-2016-2-26-33
   Белов В.Д., Герасименко Е.А., Гусева В.В., Коновалов А.Н. Влияние условий затвердевания заготовок из оловянистой бронзы БРО10С2Н3 на ее структуру. *Известия вузов. Цветная металлургия*. 2016;(2):26—33.
   https://doi.org/10.17073/0021-3438-2016-2-26-33
6. Ezhov Yu.A., Zheleznyak L.M. Improvement of quality of continuous cast ingots of complex-alloyed brasses and bronzes. In: Proceedings of XVII International Scientific and Technical Ural School-Seminar of Metallurgists-Young Scientists (December 5–9, 2016). Yekaterinburg: UrFU, 2016. Vol. 1. P. 19–23.
   Ежов Ю.А., Железняк Л.М. Улучшение качества непрерывнолитых слитков сложнолегированных латуней и бронз. В сб: *Сборник трудов XVII Международной научно-технической Уральской школы-семинара металловедов — молодых ученых* (5—9 декабря 2016 г.). Екатеринбург: Изд-во УрФУ, 2016. Ч. 1. С. 19—23.
7. Bazhenov V.E., Titov A.Yu., Shkalei I.V., Marukovich E.I., Plisetskaya I.V., Mezrin A.M., Koltygin A.V., Belov V.D., Yudin V.A. Investigation of effect of casting speed on structure and properties of bronze rods C92900 obtained by continuous casting upwards. *Metallurgist*. 2021;65(7-8):735—745.
   https://doi.org/10.52351/00260827_2021_07_44
   Баженов В.Е., Титов А.Ю.. Шкалей И.В., Марукович Е.И., Плисецкая И.В., Мезрин А.М., Колтыгин А.В., Белов В.Д. Юдин В.А. Исследование влияния скорости литья на структуру и свойства прутков из бронзы БрО10С2Н3. *Металлург*. 2021;(7):44—51.
8. Tavolzhanskiy S.A., Pashkov I.N. Features of the continuous casting of small-section billets from copper-based alloys. *Metallurgist*. 2021;64(9-10):1068—1076.
   https://doi.org/10.1007/s11015-021-01088-y
   Таволжанский С.А., Пашков И.Н. Особенности непрерывного литья заготовок малого сечения из сплавов на основе меди. *Металлург*. 2020;64(9-10): 74—80.
9. Tavolzhanskiy S.A., Pashkov I.N., Koletvinov K.F. Features of continuous casting of small-section billets from copper-based alloys. *Liteyshik Rossii*. 2020;(12): 18—23. (In Russ.).
   Таволжанский С.А., Пашков И.Н., Колетвинов К.Ф. Особенности непрерывного литья заготовок малого сечения из сплавов на основе меди *Литейщик России*. 2020;(12):18—23.
10. Yakubovich E.A. Peculiarities of two-phase ingot zone formation at continuous casting. *Sovremennye materialy, tehnika i tehnologii*. 2016;3(4):144—148. (In Russ.).
    Якубович Е.А. Особенности формирования двухфазной зоны слитка при непрерывном литье. *Современные материалы, техника и технологии*. 2016;3(4):144—148.
11. Gupta R., Srivastava S., Kumar N.K., Panthi S.K. High leaded tin bronze processing during multi-directional forging: Effect on microstructure and mechanical properties. *Materials Science and Engineering: A*. 2016;654:282—291.
    https://doi.org/10.1016/j.msea.2015.12.068
12. Potekhin B.A., Ilyushin V.V., Khristolyubov A.S., Zhilyakov A.Yu. Formation of structure and properties of composite bronzes reinforced by steel dendrites. *The Physics of Metals and Metallography*. 2014;115(4): 413—419.
    https://doi.org/10.1134/S0031918X14010128
13. Ludwig A., Gruber-Pretzler M., Wu M., Kuhn A., Riedle J. About the formation of macrosegregations during continuous casting of Sn-bronze. *Fluid Dynamics & Materials Processing*. 2005;1(4):285—300.
    https://doi.org/10.3970/fdmp.2005.001.285
14. Kreil A., Vosskühler H., Walter K. The continuous casting of copper and its alloys. *Metallurgical Reviews*. 1960;5(1):413—446.
    https://doi.org/10.1179/mtlr.1960.5.1.413
15. Korchmit A.V., Martyushev N.V., Drozdov Yu.Yu. The influence of the pouring temperature on the structure andproperties of copper metal alloys. *Key Engineering Materials*. 2016;685:450—454. https://doi.org/10.4028/www.scientific.net/KEM.685.450
16. Maltseva L.A., Grib S.V., Stolbovskiy A.V. Liquation in alloys. Ekaterinburg: UGTU-UPI, 2006. 21 p. (In Russ.).
    Мальцева Л.А., Гриб С.В., Столбовский А.В. Ликвация в сплавах. Екатеринбург: УГТУ—УПИ, 2006. 21 с.
17. Scott D.A., Schwab R. Metallography in archaeology and art. *The Structure of Metals and Alloys*. 2019:69—261.
    https://doi.org/10.1007/978-3-030-11265-3
18. Mysik R.K., Sulicin A.V., Brusnicyn S.V., Ozhgihin I.V. Problems of production of copper castings. *Zhurnal Sibirskogo federalnogo universiteta. Seriya: Tehnika i tehnologii*. 2014;7(4):394—399. (In Russ.).
    Мысик Р.К., Сулицин А.В., Брусницын С.В., Ожгихин И.В. Проблемы производства литых заготовок

из меди. *Журнал Сибирского федерального университета. Серия: Техника и технологии*. 2014;7(4):394—399.

19. Kim Y.-Y., Kim H.-S. Prediction of grain structure of thin bronze slab produced by horizontal continuous casting. *Metals and Materials International*. 2019;25:465—472. https://doi.org/10.1007/s12540-018-00231-w
20. Bazhenov V.E., Titov A.Yu., Shkalei I.V., Sannikov A.V., Tavolzhanskii S.A., Mezrin A.M., Koltygin A.V., Nikitina A.A., Plisetskaya I.V., Belov V.D., Yudin V.A. Investigation of C92900 bronze properties obtained by permanent mold casting, continuous upcasting and hot extrusion. *Izvestiya. Non-Ferrous Metallurgy*. 2021;(3):24—36. (In Russ.). https://doi.org/10.17073/0021-3438-2021-3-24-36
    Баженов В.Е., Титов А.Ю., Шкалей И.В., Санников А.В., Таволжанский С.А., Мезрин А.М., Колтыгин А.В., Никитина А.А., Плисецкая И.В., Белов В.Д., Юдин В.А. Исследование свойств бронзы БРО10С2Н3, полученной наполнительным литьем, непрерывным литьем вверх и горячей экструзией. *Известия вузов. Цветная металлургия*. 2021;27(3):24—36. https://doi.org/10.17073/0021-3438-2021-3-24-36
21. Sergejevs A., Kromanis A., Ozolins Ya., Gerins E. Influence of casting velocity on mechanical properties and macro-structure of tin bronzes. *Key Engineering Materials*. 2016;674:81—87. http://doi.org/10.4028/www.scientific.net/KEM.674.81
22. Koletvinov K.F., Tavolzhanskij S.A., Pashkov I.N. Obtaining copper-based high-temperature solder blanks by continuous up-casting method. *Liteyshik Rossii*. 2015;(11):29—31. (In Russ.).
    Колетвинов К.Ф., Таволжанский С.А., Пашков И.Н. Получение заготовок высокотемпературных припоев на медной основе методом непрерывного литья вверх. *Литейщик России*. 2015;(11):29—31.

Information about the authors

Ludmila D. Miteva – Postgraduate Student, Department of Foundry Technologies and Material Art Working (FT&MAW), National University of Science and Technology «MISIS» (NUST MISIS).
https://orcid.org/0009-0002-5289-9735
E-mail: miteva.ld@misis.ru

Andrey Yu. Titov – Cand. Sci. (Eng.), Assistant Professor, Department of FT&MAW, NUST MISIS.
https://orcid.org/0000-0002-3326-7778
E-mail: titov.ay@misis.ru

Ivan I. Baranov – Postgraduate Student, Department of FT&MAW, NUST MISIS.
https://orcid.org/0000-0002-0465-7865
E-mail: baranov.ii@misis.ru

Tatiana A. Bazlova – Cand. Sci. (Eng.), Docent, Associate Professor, Department of FT&MAW, NUST MISIS.
https://orcid.org/0000-0001-9517-5871
E-mail: bazlova.ta@misis.ru

Anna A. Nikitina – Laboratory Assistant, Department of FT&MAW, NUST MISIS.
https://orcid.org/0000-0002-5399-0330
E-mail: a.nikitina@misis.ru

Vladimir D. Belov – Dr. Sci. (Eng.), Prof., Head of the Department of FT&MAW, NUST MISIS.
https://orcid.org/0000-0003-3607-8144
E-mail: vdbelov@mail.ru

Информация об авторах

Людмила Димитровна Митева – аспирант кафедры литейных технологий и художественной обработки материалов (ЛТиХОМ), Национальный исследовательский технологический университет «МИСИС» (НИТУ МИСИС).
https://orcid.org/0009-0002-5289-9735
E-mail: miteva.ld@misis.ru

Андрей Юрьевич Титов – к.т.н., доцент кафедры ЛТиХОМ, НИТУ МИСИС.
https://orcid.org/0000-0002-3326-7778
E-mail: titov.ay@misis.ru

Иван Ильич Баранов – аспирант кафедры ЛТиХОМ, НИТУ МИСИС.
https://orcid.org/0000-0002-0465-7865
E-mail: baranov.ii@misis.ru

Татьяна Алексеевна Базлова – к.т.н., доцент кафедры ЛТиХОМ, НИТУ МИСИС.
https://orcid.org/0000-0001-9517-5871
E-mail: bazlova.ta@misis.ru

Анна Андреевна Никитина – учебный мастер 1-й категории кафедры ЛТиХОМ, НИТУ МИСИС.
https://orcid.org/0000-0002-5399-0330
E-mail: a.nikitina@misis.ru

Владимир Дмитриевич Белов – д.т.н., профессор, зав. кафедрой ЛТиХОМ, НИТУ МИСИС.
https://orcid.org/0000-0003-3607-8144
E-mail: vdbelov@mail.ru

Contribution of the authors

L.D. Miteva – conducted the experiments, prepared samples for micro-X-ray spectral analysis, processed the data, and drafted the manuscript.

A.Yu. Titov – defined the research objective, conducted the experiments, and contributed to manuscript writing.

I.I. Baranov – performed thermodynamic modeling in FactSage and participated in the discussion of the results.

T.A. Bazlova – carried out micro X-ray spectral analysis and participated in the discussion of the results.

A.A.Nikitina – conducted experiments and took part in the discussion of the results.

V.D. Belov – participated in the discussion of the results and contributed to manuscript writing.

Вклад авторов

Л.Д. Митева – проведение экспериментов, подготовка образцов для микрорентгеноспектрального анализа, обработка данных, написание статьи.

А.Ю. Титов – определение цели работы, проведение экспериментов, написание статьи.

И.И. Баранов – работа в программе FactSage, участие в обсуждении результатов.

Т.А. Базлова – проведение микрорентгеноспектрального анализа, участие в обсуждении результатов.

А.А. Никитина – проведение экспериментов, участие в обсуждении результатов.

В.Д. Белов – участие в обсуждении результатов, написание статьи.

The article was submitted 05.09.2024, revised 12.12.2024, accepted for publication 13.12.2024

Статья поступила в редакцию 05.09.2024, доработана 12.12.2024, подписана в печать 13.12.2024

ENERGY AND RESOURCE SAVING / ЭНЕРГО- И РЕСУРСОСБЕРЕЖЕНИЕ

UDC 666.774
https://doi.org/10.17073/0021-3438-2025-2-76-85

Research article
Научная статья

New technologies and compositions for recycling non-ferrous metallurgical waste into acid-resistant ceramics without using traditional natural raw materials

E.S. Abdrakhimova

Samara National Research University named after Academician S.P. Korolev (Samara University)
34 Moscow Ave., Samara, 443086, Russia

✉ Elena S. Abdrakhimova (3375892@mail.ru)

Abstract: This study investigates non-ferrous metallurgy waste – specifically, the clay fraction of zircon-ilmenite ore gravity separation tailings (ZIGT) – with the aim of using it as both a clay component and a non-plastic additive (chamotte derived from ZIGT) in the production of acid-resistant ceramic tiles. It was found that samples made solely from ZIGT (without any additives), fired at temperatures of 1250–1300 °C, do not meet regulatory requirements for acid resistance. Introducing 40 wt. % chamotte into the ceramic body was found to be optimal for producing acid-resistant tiles at 1300 °C that comply with all requirements of GOST 961-89 Acid-Resistant and Thermo-Acid-Resistant Ceramic Tiles, grade KSh (chamotte-based acid-resistant tiles). Increasing the chamotte content beyond 40 wt.% reduces the clay binder fraction, which in turn lowers the plasticity index (to below 11), causing cracks to form in the samples during shaping. The phase composition of four tile samples with varying ZIGT and chamotte contents was analyzed. *X*-ray diffraction patterns of the samples fired at 1300 °C revealed prominent peaks corresponding to mullite, cristobalite, quartz, and hematite, which were also confirmed by IR spectroscopy. The formation of mullite is crucial in the production of acid-resistant ceramics, as mullite is the primary phase determining the operational properties of the material. As a result, new ceramic compositions were developed and acid-resistant tiles were obtained from non-ferrous metallurgy waste without the use of conventional natural raw materials.

Keywords: clay fraction of zircon-ilmenite ore gravity tailings (ZIGT), chamotte, acid-resistant ceramic tiles, metallurgical waste, phase composition, mullite, cristobalite, quartz, hematite.

For citation: Abdrakhimova E.S. New technologies and compositions for recycling non-ferrous metallurgical waste into acid-resistant ceramics without using traditional natural raw materials. *Izvestiya. Non-Ferrous Metallurgy.* 2025;31(2):76–85.
https://doi.org/10.17073/0021-3438-2025-2-76-85

Новые технологии и составы по рециклингу отходов цветной металлургии в производство кислотоупоров без применения традиционного природного сырья

Е.С. Абдрахимова

Национальный исследовательский университет им. С.П. Королева (Самарский университет)
Россия, 443086, г. Самара, Московское шоссе, 34

✉ Елена Сергеевна Абдрахимова (3375892@mail.ru)

Аннотация: В работе исследованы отходы цветной металлургии – глинистая часть «хвостов» гравитации циркон-ильменитовых руд (ГЦИ), в целях ее использования в качестве глинистого компонента и отощителя – шамота из ГЦИ, для получения кислотоупорной плитки. Установлено, что образцы из ГЦИ (без применения отощителей), обожженные при температурах 1250–1300 °С, не соответствуют нормативным требованиям по кислотостойкости. Введение в керамическую массу 40 % шамота является оптимальным для получения обжигом при 1300 °С кислотоупоров, которые по всем показателям отвечают условиям ГОСТ 961-89 «Плитки кислотоупорные и термокислотоупорные керамические», марка КШ (кислотоупорные шамотные). Увеличение содержания шамота более 40 % способствует снижению доли глинистого связующего, в результате чего уменьшается число пластичности (до менее 11) керамической массы, и на образцах при формовании появляются трещины. Исследован фазовый состав 4 образцов плиток, отличающихся содержанием компонентов – ГЦИ и шамота. На рентгенограммах образцов, обожженных при температуре 1300 °С, основные интенсивные линии принадлежат муллиту, кристобалиту, кварцу и гематиту, что подтверждают ИК-спектры. «Муллитизация» при производстве кислотоупоров имеет важное значение, так как эксплуатационные показатели определяет именно муллит. Таким образом, разработаны составы и получены кислотоупоры из отходов цветной металлургии без употребления традиционного природного сырья.

Ключевые слова: глинистая часть «хвостов» гравитации циркон-ильменитовых руд (ГЦИ), шамот, кислотоупорная плитка, металлургические отходы, фазовый состав, муллит, кристобалит, кварц, гематит.

Для цитирования: Абдрахимова Е.С. Новые технологии и составы по рециклингу отходов цветной металлургии в производство кислотоупоров без применения традиционного природного сырья. *Известия вузов. Цветная металлургия*. 2025;31(2):76–85.
https://doi.org/10.17073/0021-3438-2025-2-76-85

Introduction

Physicochemical processes involving phase transformations play a critical role in the formation of stronger, acid-resistant minerals. These processes result in changes to morphological properties, crystalline phases, and texture, which together largely determine the performance characteristics of acid-resistant ceramics. For this reason, special attention is paid to these transformations during the thermal treatment of acid-resistant products. Industries such as chemical manufacturing, ferrous and non-ferrous metallurgy, and other environmentally hazardous sectors are increasingly focused on expanding the production of accessible acid- and heat-resistant materials. Accordingly, it is essential to develop such products not from expensive, conventional natural raw materials, but from low-cost industrial waste.

The expansion of metallurgical production has led to the transformation of vast areas into industrial zones, affecting not only densely populated regions but also agricultural land, designated residential construction sites, areas intended for industrial infrastructure, and even water protection zones [1—4]. As a result, the environmental situation in industrially urbanized areas has significantly deteriorated.

The specific nature of metallurgical enterprises contributes to the harmful interaction of industrial waste with the environment, adversely impacting the health of the local population. Additionally, the large volumes of metallurgical waste lead to soil contamination, pollution of nearby water bodies, and degradation of ecosystems [5; 6]. In terms of environmental pollution, metallurgical enterprises rank second only to the fuel and energy sector.

Some ecologists and researchers suggest that the growing environmental threat stems from a shortage of reducers — organisms known as decomposers — which can no longer effectively break down industrial waste into microcomponents, owing to the rapid accumulation of technogenic materials [7]. These waste materials differ significantly in chemical composition from natural substances, and the quantity of microorganisms (such as reducers) capable of decomposing them is clearly insufficient [7—9]. From the standpoint of integrated materials science, the development of zero-waste technologies is essential. These technologies regulate the reuse of industrial by-products in the manufacture of value-added products. Such recycling helps reduce subsidies for geological exploration and mining operations, while simultaneously freeing up large areas from the adverse effects of anthropogenic activity.

In the 21st century, metallurgy involves not only competitive, cutting-edge technologies, but also the generation of hazardous waste and the creation of aggressive industrial environments. In such conditions, acid-resistant materials (ARM) are used to protect personnel from direct exposure to toxic, corrosive agents and to prevent the degradation of wall and floor surfaces. These materials are most commonly represented by ceramic products — such as pipes, bricks, tiles, and various shaped components — that demonstrate exceptional resistance to a wide range of aggressive media.

In [10], the authors reported that replacing acid-resistant bricks with acid-resistant tiles reduces raw material consumption by a factor of 2.5—3.0. In addition, the thinner tile profile shortens both drying and firing operations. Acid-resistant tiles serve as a stable and long-lasting barrier, preventing contact between workers and harmful components of hostile industrial environments. These tiles can effectively replace expensive metal equipment and apparatus, as they are not only significantly more affordable but also corrosion-resistant [11].

The production of high-quality acid-resistant ceramics requires aluminosilicate raw materials rich in aluminum oxide — over 20 wt. % Al_2O_3 for clay components and over 25—30 wt. % Al_2O_3 for non-plastic additives. However, such materials are either scarce or depleted in many regions of Russia [6; 11]. Moreover, no funding is currently allocated for geological exploration aimed at discovering new raw material sources [6], which underscores the rationale for substituting natural resources with industrial waste. Additionally, recycling technogenic feedstock into value-added products contributes to achieving environmental safety goals, as outlined in EU Directive 2008/98/EC [6].

Thus, the depletion of key natural raw materials used in the manufacture of acid-resistant ceramics has prompted the rational substitution of conventional inputs with technogenic industrial waste. This not only facilitates the production of various ceramic goods, but also supports the protection of ecological systems.

The objective of this study is to investigate the feasibility of recycling and repurposing the clay fraction of zircon-ilmenite ore gravity separation tailings (ZIGT) — a technogenic by-product of non-ferrous metallurgy — as a clay binder in acid-resistant ceramic compositions, and to analyze the phase composition of ceramic tiles obtained by firing these materials.

Materials and methods

To analyze the elemental composition and microstructure of the raw materials, a JSM 6390A scanning electron microscope (Jeol, Japan) was used. Petrographic analysis was performed using immersion liquids, transparent thin sections, and polished sections, examined under MIN-8 and MIN-7 optical microscopes. The qualitative mineral (phase) compositions of the samples were determined using a Dron-3 automated *X*-ray diffractometer (Burevestnik, Russia) with CuK_α radiation and a β-filter, as well as a Spekord 75JR spectrophotometer (Carl Zeiss, Germany).

The basic physicochemical and technological properties of the ZIGT (zircon-ilmenite ore gravity separation tailings) were determined and analyzed in accordance with standard laboratory procedures and data from previous studies [12—15]. These properties included particle size distribution, plasticity, shrinkage, drying sensitivity, water permeability, sinterability, refractoriness, water absorption, mechanical strength, and others.

ZIGT, a by-product of non-ferrous metallurgy, was used as the clay binder in the production of acid-resistant ceramics, while chamotte derived from ZIGT, pre-fired at 1200 °C, was used as a non-plastic additive. Their oxide and elemental compositions are presented in Tables 1 and 2, while their microstructure and mineralogical composition are shown in Figs. 1 and 2.

The clay component (ZIGT) is formed as a homogeneous slurry with a moisture content of 37—45 % and a density of 2.36—2.42 g/cm^3 after screening and mechanical processing of the mined ore [6; 16]. A review of the literature and numerous studies have shown that ceramics shaped from homogeneous clay feedstock exhibit 10—15 % higher strength compared to those produced from clay taken directly from the quarry [16—19.

Based on its Al_2O_3 content, ZIGT is classified as a raw material with semi-acidic properties and an elevated content of colorant oxides (Fe_2O_3 > 3 %, see Table 1). According to its particle size distribution (58 % < < 0.001 mm, see Table 3), it is classified as a fine-grained (highly dispersed) material. In terms of plasticity, it is medium-plastic (plasticity index of 21—23); in terms of drying behavior, it is moderately sensitive; in terms of refractoriness, it is highly refractory (t = 1580 °C); and in terms of sintering behavior, it exhibits high sinterability, with a sintering interval of 120—150 °C.

Table 1. **Average oxide composition of the components**

Таблица 1. Усредненный оксидный химический состав компонентов

Material	Oxide content, wt. %							
	SiO_2	$Al_2O_3 + TiO_2$	Fe_2O_3	CaO	MgO	R_2O	ZrO_2	LOI*
ZIGT	58.77	22.43	6.74	1.28	1.54	1.58	0.82	7.04
Chamotte	61.02	25.18	7.58	1.54	1.89	1.93	0.86	–

* LOI – loss on ignition; $R_2O = Na_2O + K_2O$.

Table 2. **Elemental c™omposition of the components**

Таблица 2. Элементный химический состав компонентов

Material	Elemental composition, wt. %									
	C	O	Na	Mg	Al + Ti	Si	K	Zr	Ca	Fe
ZIGT	2.18	50.78	0.26	0.54	15.45	24.8	0.32	0.48	0.2	4.87
Chamotte	–	48.22	0.31	0.71	17.18	27.14	0.35	0.54	0.22	5.18

The main clay mineral in ZIGT is kaolinite (Fig. 2), which differs significantly from natural, kaolinite-rich clays. The elevated iron oxide content ($Fe_2O3 > 3\ \%$) promotes the formation of poorly crystalline kaolinite, as partial substitution of aluminum ions (Al^{3+}) by iron ions (Fe^{3+}) occurs within the mineral structure. This substitution leads to the formation of a solid solution in which iron ions are strongly retained in the crystal lattice and cannot be removed without structural degradation [16, 20—23]. Based on the kaolinite crystallinity index (0.68), ZIGT is classified as Class III. According to the author of monograph [20], the lower the structural order of kaolinite, the more it enhances the material's reactivity.

Thermal treatment of ZIGT at 1200 °C yielded chamotte, which is commonly used in ceramic materials as a non-plastic additive. Chamotte stabilizes firing shrinkage, helps establish a robust structural framework,

Table 3. **Particle size distribution of the clay component (ZIGT)**

Таблица 3. Фракционный состав глинистого компонента (ГЦИ)

Fraction content, wt. %	>0.063	0.063–0.01	0.01–0.005	0.005–0.001	<0.001
Particle size, mm	0.8	8.1	12.1	21.0	58

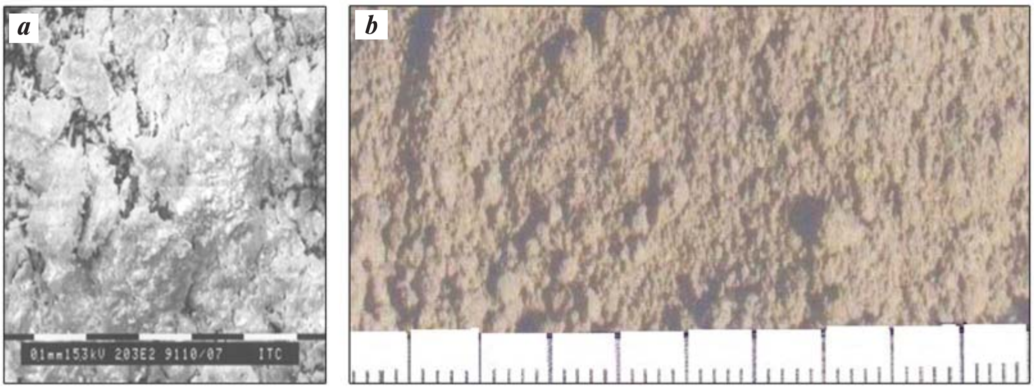

Fig. 1. Microstructure of raw materials: ZIGT (***a***) and chamotte derived from ZIGT (***b***)

Magnification: 1000$^\times$ (***a***), 10$^\times$ (***b***)

Рис. 1. Микроструктура сырьевых материалов: ГЦИ (***a***) и шамота из ГЦИ (***b***)

Увеличение 1000$^\times$ (***a***) и 10$^\times$ (***b***)

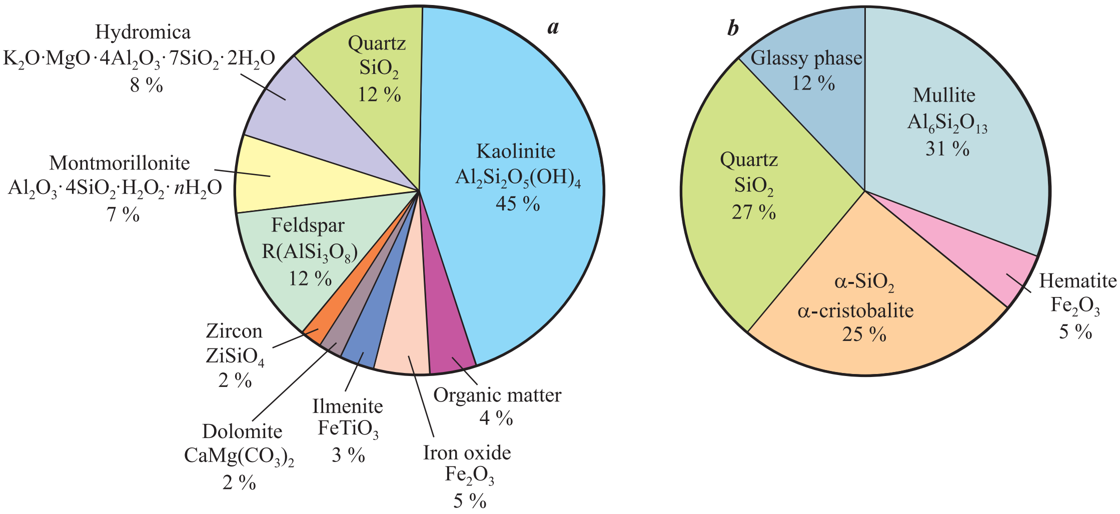

Fig. 2. Mineralogical composition of the raw materials: ZIGT (***a***) and chamotte derived from ZIGT (***b***)

Рис. 2. Минералогический состав сырьевых материалов: ГЦИ (***a***) и шамота из ГЦИ (***b***) and controls the plasticity of the ceramic body. As shown in Table 1, firing increased the aluminum oxide content of the clay material from 22.43 % to 25.18 %.

Production of acid-resistant tiles and their technical characteristics

Square acid-resistant tiles of type PK-1, measuring 100×100×20 mm, were produced using classical ceramic technology. ZIGT and chamotte were ground to a particle size of no more than 1 mm and thoroughly mixed (see Table 4). The ceramic samples were shaped by plastic forming at a charge moisture content of 22—24 %. After pressing, the tiles were dried to a moisture content below 5 %, and then fired at 1250 and 1300 °C. Their physical and mechanical (technical) properties are presented in Table 5.

Fig. 3 shows the *X*-ray diffraction (XRD) patterns of samples *1* and *4* fired at 1300 °C, while Fig. 4 presents their IR spectra. Sample *1* is included for comparison purposes, whereas sample *4* demonstrates optimal technical performance. It should be noted that potential impurities or poorly crystallized mineral phases, whose identification cannot be confirmed due to their low content, are not included in the diffractograms.

Results and discussion

The data presented in Table 5 show that samples based on composition *1*, when fired at 1250—1300 °C, do not meet the GOST acid resistance requirements. The addition of 20—40 wt. % chamotte to the ceramic body significantly improves the drying behavior of the semi-finished products (see table 4). However, after firing at 1300 °C, the samples comply with all GOST standards for acid-resistant tiles (see Table 5).

Composition *4*, which contains 40 wt. % chamotte, can be considered optimal, as it exhibits superior performance compared to samples *1—3* (Table 5). In selecting the optimal composition, it is also important to account for the plasticity of the clay binder, since its reduction causes the plasticity index of the ceramic body to drop below 11, resulting in cracking during forming..

X-ray diffraction analysis of samples *1* and *4* confirmed the presence of mullite, cristobalite, quartz, and hematite, which was further supported by IR spectroscopy (see Figs. 3 and 4). In the Al_2O_3—SiO_2 system, both mullite ($3A1_2O_3{\cdot}2SiO_2$) and sillimanite ($Al_2O_3{\cdot}SiO_2$) can form. These phases exhibit similar crystal structures, as mullite is regarded as a structurally disordered or defective form of sillimanite. Consequently, their XRD patterns are nearly indistinguishable, although they can be differentiated by their IR spectral signatures [17; 20; 23—26].

The crystallization of α-cristobalite typically originates from amorphous silica released during mullite formation. Due to its high thermal expansion, cristobalite increases the permeability of acid-resistant ceramics while simultaneously reducing their mechanical strength [12; 14—16; 19; 20].

Previous studies [2; 29; 30] have demonstrated that hematite promotes the formation of iron-rich glass phases in ceramic materials, which serve as a cementing matrix within the ceramic body. During firing, a glassy phase of variable composition forms in the samples, depending on the firing temperature, as confirmed by IR spectra (Fig. 4). This phase enhances structural disor-

Table 4. **Sample compositions, plasticity of the ceramic body, and characteristics of semi-finished products after drying**

Таблица 4. Составы образцов, пластичность шихты и показатели полуфабрикатов после сушки

Component	Component content, wt. %			
	Sample *1*	Sample *2*	Sample *3*	Sample *4*
ZIGT	100	80	70	60
Chamotte	–	20	30	40
Plasticity index of ceramic body	22	17	14	11
Characteristics of semi-finished products after drying				
Shrinkage of dried tile, %	6.8	6.1	5.3	4.8
Drying time to constant shrinkage at $t = 100{\div}120$ °C, h	1.2	1.1	1.0	0.8
Compressive strength of dried body at 5 % residual moisture, MPa	7.8	5.2	3.9	2.7
Water permeability, 10^{-4} m^2/h	1.80	2.89	3.50	4.30

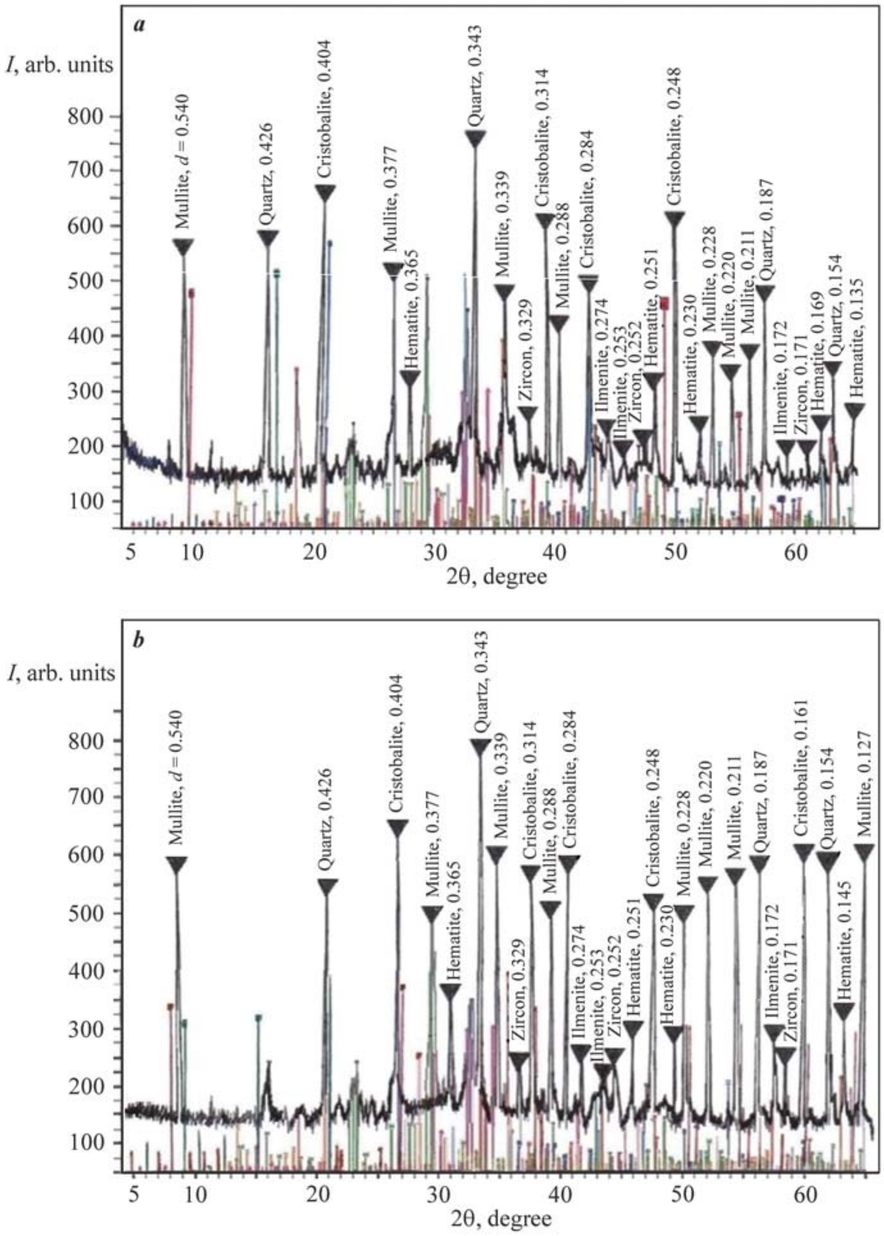

Fig. 3. *X*-ray diffraction patterns of samples *1* (***a***) and *4* (***b***)

d, nm – interplanar spacing between planes of the same family of parallel crystallographic planes

Рис. 3. Рентгенограммы образцов *1* (***a***) и *4* (***b***)

d, нм –межплоскостное расстояние между плоскостями одного семейства параллельных плоскостей

der during thermal treatment, elevates internal stresses, weakens the crystal lattices of individual mineral phases (and may even partially dissolve them), and can inhibit the development of specific phases such as mullite [11; 31]. The crystallization of structurally imperfect mullite is initiated at temperatures above 1100 °C.

Even in limited amounts, the glassy phase facilitates sintering of the ceramic body by promoting particle adhesion into a consolidated matrix, and may accelerate the overall densification and firing process.

Conclusions

1. The study revealed that fired samples made from the clay fraction of zircon-ilmenite ore gravity separation tailings (ZIGT) at temperatures of 1250—1300 °C did not meet the acid resistance requirements of GOST 961-89. The addition of 20—40 wt. % chamotte to the ceramic body significantly improves the drying behavior of the semi-finished product (except for strength), and after firing at 1300 °C, the resulting tiles

Table 5. **Physical and mechanical properties of acid-resistant tiles**

Таблица 5. Физико-механические показатели кислотоупорных плиток

Property	Sample *1*	Sample *2*	Sample *3*	Sample *4*	Regulatory requirements*
Firing temperature 1250 °C					
Water absorption, %	3.8	3.8	3.7	3.6	<5
Acid resistance, %	96.5	96.9	97.4	97.7	>98
Compressive strength, MPa	57.2	58.1	59.3	60.1	>50
Flexural strength (static), MPa	32.4	32.9	33.6	34.3	>25
Frost resistance, cycles	42	44	46	47	>20
Thermal shock resistance, thermal cycles	4	4	5	6	>5
Firing temperature 1300 °C					
Water absorption, %	2.3	2.3	2.2	2.2	<5
Acid resistance, %	97.8	98.2	98.5	98.7	>98
Compressive strength, MPa	63.8	65.4	67.8	69.4	>50
Flexural strength (static), MPa	38	39	41	42	>25
Frost resistance, cycles	58	63	67	69	>20
Thermal shock resistance, thermal cycles	6	6	8	9	>5

* According to GOST 961-89 “Acid-resistant and thermal acid-resistant ceramic tiles”, grade KSh (acid-resistant chamotte-based tiles).

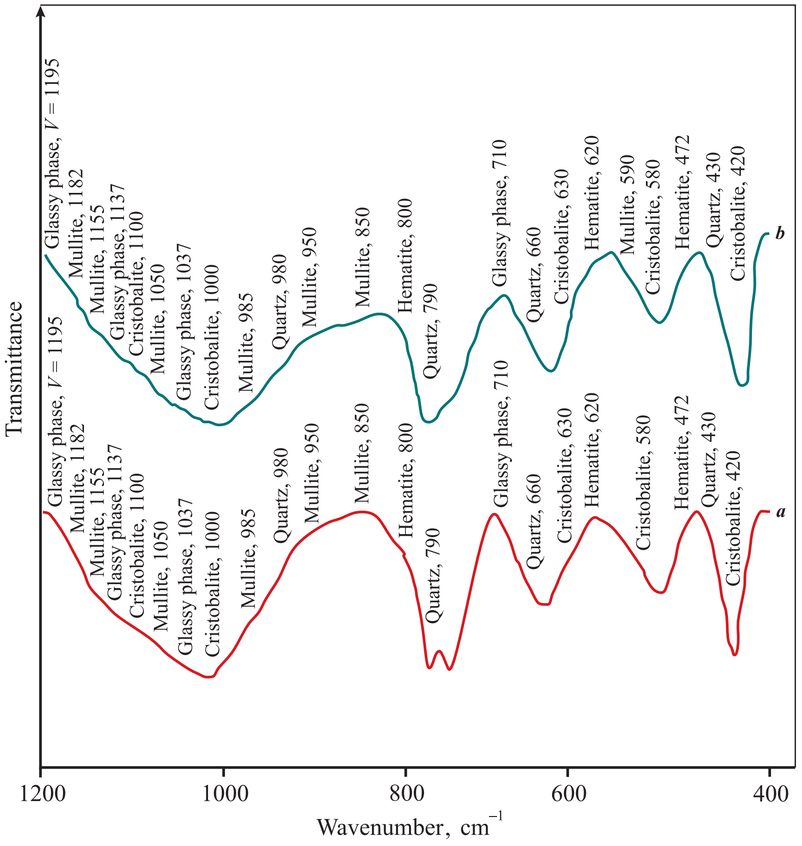

Fig. 4. IR spectra of samples *1* (***a***) and *4* (***b***)

Рис. 4. ИК-спектры исследуемых образцов *1* (***a***) и *4* (***b***) meet all regulatory standards for acid-resistant ceramic tiles.

2. Sample composition *4* was identified as optimal, as it fully complies with the GOST standards for acid-resistant tiles. The plasticity of the clay binder must also be taken into account, since its reduction causes the plasticity index of the ceramic body to drop below 11, resulting in cracking during forming.

3. *X*-ray diffraction analysis of compositions *1* and *4* revealed that the dominant peaks correspond to mullite, cristobalite, quartz, and hematite, which was confirmed by IR spectroscopy. The presence of a glassy phase was also detected in these samples, and it has a negative effect on the mineral structure.

References

1. Koryakov V.E., Shishkina A.A., Shishkina P.A. The influence of metallurgical industry enterprises on the environment and human health. *Izvestiya Tul'skogo gosudarstvennogo universiteta. Tekhnicheskie nauki.* 2019;(4):275—278. (In Russ.).
   Коряков В.Е., Шишкина А.А., Шишкина П.А. Влияние предприятий металлургической промышленности на окружающую среду и здоровье человека. *Известия Тульского государственного университета. Технические науки*. 2019;(4):275—278.
2. Patel A., Enman J., Gulkova A., Guntoro P.I., Dutkiewicz A., Ghorbani Y., Matsakas L. Integrating biometallurgical recovery of metals with biogenic synthesis of nanoparticles. *Chemosphere*. 2020;263(12):1—23.
   http://doi.org/10.1016/j. chemosphere.2020.128306
3. Zhang Y., Xiong Z., Yang L., Ren Z., Shao P., Shi H., Luo X. Successful isolation of a tolerant co-flocculating microalgae towards highly efficient nitrogen removal in harsh rare earth element tailings (REEs) wastewater. *Water Research*. 2019;166 (8):18—24.
   http://doi.org/10.1016/j.watres.2019.115076
4. Politaeva N.A., Smyatskaya Y.A., Dolbnya I.V., Sobgaida D.S. Microalgae biotechnology multiple use of chlorella sorokiniana. In: *Advances in Raw Material Industries for Sustainable Development Goals.* (November 27—29, 2020) Saint Petersburg, 2020. P. 252—261.
5. Abdrakhimov D.V., Abdrakhimova E.S., Abdrakhimov V.Z. The influence of some waste products of nonferrous metallurgy on the physical and mechanical properties of bricks. *Izvestiya. Non-Ferrous Metallurgy.* 2004;(2):4—9. (In Russ.).
   Абдрахимов Д.В., Абдрахимова Е.С., Абдрахимов В.З. Влияние некоторых отходов производств цветной металлургии на физические и механические свойства кирпича *Известия вузов. Цветная металлургия*. 2004;(2):4—9.
6. Pasmurtseva N.N. Main trends and problems of innovative development of the metallurgical industry of the Russian Federation. *Vestnik Tyumenskogo gosudarstvennogo universiteta. Sotsial'no-ekonomicheskie i pravovye issledovaniya.* 2018;4:219—231. (In Russ.).
   http://doi.org/10.21684/2411-7897-2018-4-4-219-231
   Пасмурцева Н.Н. Основные тенденции и проблемы инновационного развития металлургической промышленности Российской Федерации. *Вестник Тюменского государственного университета. Социально-экономические и правовые исследования.* 2018;(4): 219—231.
   http://doi.org/10.21684/2411-7897-2018-4-4-219-231
7. Medvedeva I. V., Amirova E.V., Studentok G.A., Tseitlin E.M., Medvedeva O.M. Environmental impact of mining and metallurgical enterprises in the Sverdlovsk region and ways to reduce it. *Izvestiya UGGU.* 2023;4(72): 116—126. (In Russ.).
   http://doi.org/10.21440/2307-2091-2023-4-116-126
   Медведева И. В., Амирова Е.В., Студенток Г.А., Цейтлин Е.М., Медведева О.М. Воздействие предприятий горно-металлургического комплекса Свердловской области на окружающую среду и направления его снижения. *Известия УГГУ.* 2023;4(72): 116—126.
   http://doi.org/10.21440/2307-2091-2023-4-116-126
8. Kalner V.D. Ecologically oriented habitat — an integral criterion of quality of life. *Ekologiya i promyshlennost' Rossii.* 2019;11:50—54. (In Russ.).
   http://doi.org/10.18412/1816-0395-2019-10-50-55
   Кальнер В.Д. Экологически ориентированная среда обитания — интегральный критерий качества жизни. *Экология и промышленность России.* 2019;11:50—54.
   http://doi.org/10.18412/1816-0395-2019-10-50-55
9. Kryazhev A.M. Gusev T.V., Tikhonova I.O., Ocheretenko D.P., Almgren R. Pulp and paper production: sustainable development and formation of a closed-cycle economy. *Ekologiya i promyshlennost' Rossii*. 2020;11: 48—53. (In Russ.).
   http://doi.org/10.18412/1816-0395-2020-11-48-53
   Кряжев А.М., Гусев Т.В., Тихонова И.О., Очеретенко Д.П., Алмгрен Р. Целлюлозно-бумажное производство: устойчивое развитие и формирование экономики замкнутого цикла. *Экология и промышленность России.* 2020;11:48—53.
   http://doi.org/10.18412/1816-0395-2020-11-48-53
10. Gaprindashvili G.P., Kekeladze M.K. Acid-resistant ceramic materials using industrial waste. *Steklo i keramika*. 1988;(1):21—23. (In Russ.).

Гаприндашвили Г.П., Кекеладзе М.К. Кислотоупорные керамические материалы с применением промышленных отходов. *Стекло и керамика.* 1988;(1):21—23.

11. Abdrakhimova E.S., Abdrakhimov V.Z. Physico-chemical processes during the firing of acid-resistant materials. Saint Petersburg: Nedra, 2003. 273 p. (In Russ.).
Абдрахимова Е.С., Абдрахимов В.З. Физико-химические процессы при обжиге кислотоупоров. СПб.: Недра, 2003. 273 с.

12. Zhenzhurist I.A. Structure, properties and technologies of ceramic materials: From 87 workshop. Kazan: Kazan State Power Engineering University, 2021. 47 p. (In Russ.).
Женжурист И.А. Структура, свойства и технологии керамических материалов: С 87 практикум. Казань: Казанский государственный энергетический университет, 2021. 47 с.

13. Abdrakhimov V.Z., Abdrakhimov A.V., Vdovina E.V., Abdrakhimova E.S. Technology of ceramic products production. Educational and methodical manual for laboratory work. Samara: Samara State University of Architecture and Civil Engineering, 2007. 120 p. (In Russ.).
Абдрахимов В.З., Абдрахимов А.В., Вдовина Е.В., Абдрахимова Е.С. Технология производства керамических изделий. Учебно-методическое пособие для лабораторных работ. Самара: Самарский государственный архитектурно-строительный университет, 2007. 120 с.

14. Ushnitskaya N.N., Mestnikov A.E. Investigation of the properties of clay raw materials by methods of physicochemical analysis. *Vestnik Belgorodskogo tekhnologicheskogo universiteta im. V.G. Shukhova*. 2024;(4):16—25. http://doi.org/10.17513/use.37919
Ушницкая Н.Н., Местников А.Е. Исследование свойств глинистого сырья методами физико-химического анализа. *Вестник Белгородского технологического университета им. В.Г. Шухова*. 2024;(4):16—25. http://doi.org/10.17513/use.37919

15. Suleimenov S.T., Ralko A.V., Saibulatov S.Z., Nurbaturov K.A. Moisture conductivity of zologlin mixtures. *Stroitel'nye materialy i konstruktsii.* 1981;(3):31—35. (In Russ.).
Сулейменов С.Т., Ралко А.В., Сайбулатов С.З., Нурбатуров К.А. Влагопроводность зологлиняной смесей. *Строительные материалы и конструкции.* 1981;(3):31—35.

16. Abdrakhimova E.S., Abdrakhimov V.Z. The use of non-ferrous metallurgy waste in the production of acid-resistant. *Izestiya. Non-Ferrous Metallurgy.* 2004;(4): 13—18. (In Russ.).
Абдрахимова Е.С., Абдрахимов В.З. Использование отходов цветной металлургии в производстве кислотоупоров. *Известия вузов. Цветная металлургия*. 2004;(4):13—18.

17. Kingery U.D. Introduction to ceramics. Moscow: Nauka, 1964. 529 p. (In Russ.).
Кингери У.Д. Введение в керамику. М.: Наука, 1964. 529 с.

18. Tursukova I.I., Baymetova M.G. Methodological approach to assessing the effectiveness of a metallurgical enterprise in the context of environmental risks. *Ekonomika, predprinimatel'stvo i pravo.* 2024;14(2):277—288. (In Russ.). http://doi.org/10.18334/epp.14.2.120551
Турсукова И.И., Байметова М.Г. Методический подход к оценке эффективности деятельности металлургического предприятия в условиях экологических рисков. *Экономика, предпринимательство и право.* 2024;14 (2):277—288. http://doi.org/10.18334/epp.14.2.120551

19. Chen J., Min Fan-fei, Liu Ling-yun, Jia Fei-fei. Adsorption of methylamine cations on kaolinite basal surfaces: A DFT study. *Physicochemical Problems of Mineral Processing.* 2020; 56(2):338—349. http://doi.org/10.37190/ppmp/117769

20. Augustinik A.I. Ceramics. Leningrad: Lenizdat, 1975. 591 p. (In Russ.).
Августиник А.И. Керамика. Л.: Лениздат, 1975. 591 с.

21. Chetverikova A.G., Makarov V.N., Kanygina O.N., Seregin M.M., Stroganova E.A. Correction of the structural formula of kaolinite of the Orenburg region by spectroscopic methods. *Kondensirovannye sredy i mezhfaznye granitsy.* 2023;25(2):277—291. (In Russ.). https://doi.org/10.17308/kcmf.2023.25/11108
Четверикова А. Г., Макаров В.Н., Каныгина О.Н., Серегин М.М., Строганова Е.А. Коррекция структурной формулы каолинита Оренбургской области спектроскопическими методами. *Конденсированные среды и межфазные границы.* 2023;25(2):277—291. https://doi.org/10.17308/kcmf.2023.25/11108

22. Liu Y., Huang Q., Zhao L., Lei S. Influence of kaolinite crystallinity and calcination conditions on the pozzolanic activity of metakaolin. *Gospodarka Surowcami Mineralnymi-Mineral Resources Management.* 2021:39—56. https://doi.org/10.24425/gsm.2021.136295

23. Abdrakhimova E.S., Abdrakhimov V.Z. Synthesis of mullite from technogenic raw materials. *Zhurnal neorganicheskoi khimii*. 2007;52(3):395—400. (In Russ.).
Абдрахимова Е.С., Абдрахимов В.З. Синтез муллита из техногенного сырья. *Журнал неорганической химии.* 2007;52(3):395—400.

24. Biswal B., Mishra D.K., Das S.N., Bhuyan S. Structural, micro-structural, optical and dielectric behavior of

mullite ceramics. *Ceramics International.* 2021;47(22): 32252—32263.
https://doi.org/10.1016/j.ceramint.2021.08.120

25. Weiquan Yuan, Jingzhong Kuang, Zheyu Huang, Mingming Yu. Effect of aluminum source on the kinetics and mechanism of mullite preparation from kaolinite. *Chemical Physics Letters.* 2022;787:139—242.
https://doi.org/10.1016/j.cplett.2021.139242
26. Yarotskaya E.G., Fedorov P.P. Mullite and its isomorphic substitutions. *Kondensirovannye sredy i mezhfaznye granitsy.* 2018;20(4):573—544. (In Russ.).
https://doi.org/10.17308/kcmf.2018.20/626
Яроцкая Е.Г., Федоров П.П. Муллит и его изоморфные замещения. *Конденсированные среды и межфазные границы.* 2018; 20(4):573—54.
https://doi.org/10.17308/kcmf.2018.20/626
27. Moshnyaga M.A., Grinberg E.E., Pochitalkna I.A. Obtaining high-purity cristobalite using sol-gel -alcoholic technology. *Uspekhi khimii i khimicheskoi tekhnologii.* 2021;35(6):75—76. (In Russ.).
Мощняга М.А., Гринберг Е.Е., Почиталкна И.А. Получение высокочистого кристобалита с использованием «золь-гель»-алкоголятной технологии. *Успехи химии и химической технологии.* 2021;35(6):75—76.
28. Kotlyar V.D., Terekhina Yu.V. Mineralogical, chemical and structural features of opiate opal-cristobalite rocks as raw materials for the construction industry. *Izvestiya Tomskogo politekhnicheskogo universiteta. Inzhiniring georesursov.* 2023;334(1):145—155. (In Russ.).
https://doi.org/10.18799/24131830/2023/1/3852
Котляр В.Д., Терёхина Ю.В. Минералого-химические и структурные особенности опоковидных опал-кристобалитовых пород как сырья для стройиндустрии. *Известия Томского политехнического университета. Инжиниринг георесурсов.* 2023;334(1):145—155.
https://doi.org/10.18799/24131830/2023/1/3852
29. Pavlov V.F., Meshcheryakova I.V. The role of iron oxide in the formation of the structure of acid-resistant porcelain. In: Proceedings of the Research Institute “Stroykeramika”. Scientific research in the field of mechanization of technological processes, development of new compositions of masses and glazes. 1982. P. 48—56. (In Russ.).
Павлов В.Ф., Мещерякова И.В. Роль оксида железа в формировании структуры кислотоупорного фарфора. В сб.: *Труды НИИ «Стройкерамика». Научные исследования в области механизации технологических процессов, разработки новых составов масс и глазурей.* 1982. С. 48—56.
30. Pavlov V.F., Meshcheryakova I.V. The effect of the addition of iron-containing low-melting clays on the change in the phase composition and properties of acid-resistant materials. In: Proceedings of the Research Institute “Stroykeramika”. Improvement of technology in the production of building ceramics.1981. P. 109—115. (In Russ.).
Павлов В.Ф., Мещерякова И.В. Влияние добавки железосодержащих легкоплавких глин на изменение фазового состава и свойств кислотоупоров. В сб.: *Труды НИИ «Стройкерамика». Совершенствование технологии в производстве строительной керамики.* 1981. С. 109—115.
31. Pavlov V.F. Influence of the composition and structure of the liquid phase of ceramic masses on the formation of the structure of products made of them during firing. In: Proceedings of the Research Institute “Stroykeramika”. 1977. № 42. P. 123—154. (In Russ.).
Павлов В.Ф. Влияние состава и строения жидкой фазы керамических масс на формирование структуры изделий из них при обжиге. В сб.: *Труды НИИ «Стройкерамика».* 1977. № 42. С. 123—154.

Information about the author

Elena S. Abdrakhimova – Cand. Sci. (Eng.), Associate Professor of the Department “Chemistry”, Samara National Research University named after Academician S.P. Korolev (Samara University).
https://orcid.org/0009-0009-0001-5941
E-mail:3375892@mail.ru

Информация об авторе

Елена Сергеевна Абдрахимова – к.т.н., доцент кафедры «Химия» Национального исследовательского университета им. С.П. Королева (Самарского университета).
https://orcid.org/0009-0009-0001-5941
E-mail: 3375892@mail.ru

The article was submitted 07.08.2024, revised 07.10.2024, accepted for publication 14.10.2024

Статья поступила в редакцию 07.08.2024, доработана 07.10.2024, подписана в печать 14.10.2024